The Dissertation Committee for Jacqueline Lee Norrie Certifies that this is the approved version of the following dissertation:

Mechanisms directing chondrocyte specification in the developing limb

Committee:

Steven Vokes, Supervisor

John Wallingford

Jeff Gross

Paul Macdonald

Lauren Ehrlich

Mechanisms directing chondrocyte specification in the developing limb

by

Jacqueline Lee Norrie, B.S., B.S.

Dissertation

Presented to the Faculty of the Graduate School of

The University of Texas at Austin

in Partial Fulfillment

of the Requirements

for the Degree of

Doctor of Philosophy

The University of Texas at Austin

May 2016

Dedication

To my mom and dad

For a lifetime of support

Acknowledgements

First and foremost, I would like to express my sincere gratitude to my mentor Steve Vokes. I have considered it an absolute privilege to have done my graduate studies in the Vokes lab and learn from Steve. He has been an incredibly supportive, constructive, and motivating mentor and I am extremely grateful for his guidance. Secondly, I would like to thank my committee, John Wallingford, Lauren Ehrlich, Jeff Gross, and Paul Macdonald. Their support and scientific input have been essential for both my projects and my professional development. I would like to thank the developmental biology community at UT for their encouragement and collaborations. I would especially like to thank Jordan Lewandowski and Jacqui Tabler for being great role models and for their support in every aspect of my graduate career. Additionally, I would like thank Qiang Li, Rachel Lex, Kristin Falkenstein, Swanie Co, and other past and present members of the Vokes lab for creating a fun and engaging scientific environment. Lastly, I would like to thank my family; my mom, dad, and brother, my friends, and I would especially like to thank my husband for his support in everything I do.

Mechanisms directing chondrocyte specification in the developing limb

Jacqueline Lee Norrie, Ph.D.

The University of Texas at Austin, 2016

Supervisor: Steven A. Vokes

During limb development, skeletal elements originate from highly proliferative mesodermal progenitor cells that differentiate into chondrocytes. While this process must be tightly regulated to ensure proper size and specialization of cartilage elements, the mechanisms behind the maintenance of mesodermal progenitor cells and the initiation of differentiation is poorly understood. Bone morphogenetic proteins (BMPs) are early drivers of chondrogenesis, promoting compaction and the initiation of differentiation, but their biological role in limb development remains controversial. To address both the mechanism and timing of BMPs role in chondrogenesis we created a new mouse model to inhibit overall BMP signaling in the limb. With reduced BMP signaling during a precise 24-hour time window there is increased proliferation and delayed differentiation leading to polydactyly. Additionally, in an effort to identify regulators of chondroprogenitor cell maintenance, we found that PRMT5, a protein arginine methytransferase essential for stem cell pluripotency, is dynamically expressed in the distal undifferentiated limb. We found that loss of PRMT5 in the limb results in apoptosis of distal chondroprogenitor cells leading to severe limb truncations and unique autopod defects. We show that PRMT5 is essential for the maintenance of chondroprogenitor cells in the limb.

Table of Contents

List of Tables

List of Figures

Chapter 1: Chondrogenic differentiation

1.1: Chondrogenic differentiation in the developing limb

Throughout development, embryos need to maintain a precise balance between cell proliferation and differentiation in order to form tissues of the right size and specialization. The importance and complexity of this balance is exemplified in appendicular skeletal formation during mouse limb development (Barna and Niswander, 2007; Bi et al., 1999; Goldring, 2012). During chondrogenic differentiation in the limb, there is a distal, highly proliferative population of chondroprogenitor cells that contribute cells to the differentiating chondrocytes of the proximal limb (Boehm et al., 2010; Suzuki et al., 2008). How these chondroprogenitor cells are maintained and how differentiation signals initiate their fate decisions are still not fully understood.

1.2: Limb development

Limb development begins as an out-pocketing of cells from lateral plate mesoderm. These mesenchymal cells are surrounded by a thin layer of ectoderm which, at the distal tip of the limb, forms a structure known as the apical ectodermal ridge (AER). The AER is a signaling center for growth factors, such as FGFs, that are important for cell survival and proliferation (Ahn et al., 2001; Bénazet et al., 2009; Khokha et al., 2003; Lewandoski et al., 2000; Martin, 1998; Verheyden and Sun, 2008). Together FGFs, sonic hedgehog (SHH), and Gremlin1 (GREM1) form a signaling loop which drives limb outgrowth and

inhibits differentiation, driven by Bone Morphogenetic Proteins (BMPs) (Bastida et al., 2009; Buckland et al., 1998; Norrie et al., 2014; Pajni-Underwood et al., 2007).

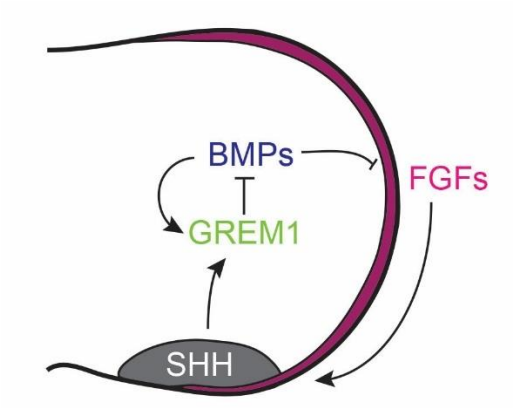

Figure 1.1: FGF-SHH feedback loop. FGFs from the AER (pink) activates SHH in the posterior limb, which in turn signals to GREM1, a BMP inhibitor.

Eventually, BMPs become upregulated and cells in the proximal limb will begin to differentiate (Badugu et al., 2012; Bandyopadhyay et al., 2006; Norrie et al., 2014; Robert, 2007; Yoon and Lyons, 2004). These cells begin expressing Sox9, the earliest marker of chondrogenesis, condense, and differentiate into chondrocytes (Bell et al., 1997; Bi et al., 1999; Wright, 1995).

1.3: BMP SIGNALING IN LIMB DEVELOPMENT

BMPs are secreted ligands that, in canonical BMP signaling, bind to an extracellular BMP receptor and initiate the phosphorylation of Smads 1, 5, and 8. Together with co-Smad4, phospho-Smad1,5,8 will enter the nucleus and activate transcriptional targets (Derynck and Zhang, 2003; Suzuki et al., 2008). While it is known that BMPs can

drive cellular compaction and chondrogenic differentiation (Barna and Niswander, 2007), there are several complexities concerning BMP signaling that have made fully understanding the early roles for BMPs in initiating chondrogenic differentiation within the developing limb difficult.

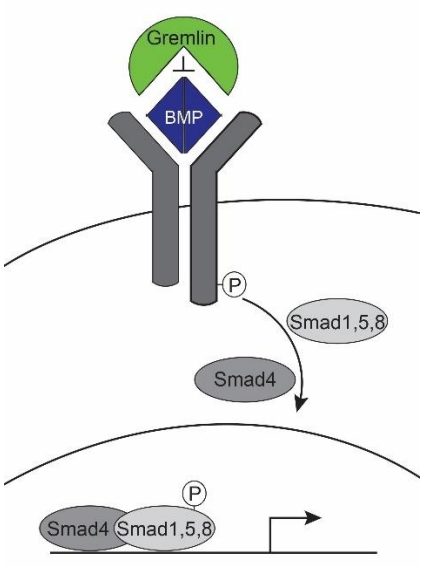

Figure 1.2: Canonical BMP signaling. BMP ligand binds the BMP receptor which phosphorylates Smad 1/5/8. Together with Smad4, pSmad 1/5/8 enters the nucleus to activate transcriptional targets.

There are three partially redundant BMPs (BMP 2, 4, 7) in the limb that are necessary for multiple functions at several timepoints during limb development (Bandyopadhyay et al., 2006; Choi et al., 2012; Pignatti et al., 2014). For this reason, it has been difficult to perform genetic analyses to tease out the underlying principles of BMP signaling and differentiation of the limb. Due to these challenges, there is conflicting evidence supporting the role of BMPs in digit formation. Loss of different combinations

of the 3 BMPs or downstream factors has led to opposing phenotypes, ranging from polydactyly to severe limb truncations (Bandyopadhyay et al., 2006; Selever et al., 2004). These contradictory results demonstrate that the precise role of BMP signaling in limb differentiation is still unclear. To define precisely the mechanisms of BMP activity in the limb, we generated a novel mouse model that revealed a critical developmental time window in which BMPs are necessary to regulate differentiation (Chapter 2).

1.4: CHONDROPROGENITOR CELL MAINTENANCE

In contrast with differentiating cells, mesenchymal progenitor cells at the distal region of the limb are important for driving continued growth and proliferation (Fallon, 1994; Rowe and Fallon, 1982; Suzuki et al., 2008). These cells have been shown to have both a higher rate of proliferation and a shorter cell cycle than the more proximal limb (Boehm et al., 2010). As limb development continues it is thought that these progenitor cells become further restricted to the distal tips of the developing digit rays. A study in chick embryos showed that cells just proximal to the AER at the top of each digit ray contribute to ray growth in a proximal to distal fashion (Suzuki et al., 2008). This area, known as the phalanx-forming regions (PFR), has been identified as an important progenitor population directing proper growth of the digits (Suzuki et al., 2008). Still, factors that regulate and maintain this population remain elusive.

PRMT5, a protein arginine methyltransferase, is known to play essential roles in stem cell and progenitor cell populations throughout development and adult homeostatis (Ancelin et al., 2006; Kim et al., 2014; Liu et al., 2015; Nagamatsu et al., 2011; Tee et al.,

2010; Wang et al., 2015a; Wang et al., 2015b). Specifically, PRMT5 regulates cell proliferation and inhibits differentiation via methylation of histones on H4R3 and H3R8 (Di Lorenzo and Bedford, 2011; Pal et al., 2007; Tarighat et al., 2015; Zhao et al., 2009). However, due to its essential roles in stem cells and primordial germ cells, complete knockout of *Prmt5* is early embryonic lethal and its function in later embryogenesis has yet to be explored. We have found that it is highly expressed in many progenitor cell populations during embryogenesis including the brain, presomitic mesoderm, and the limb bud (Fig. 3.1). Specifically, in the limb bud, its expression pattern overlaps with the progenitor cell population in the distal limb. Using a conditional *Prmt5* knockout we have discovered a novel role for PRMT5 in the essential maintenance of limb chondroprogenitor cells (Chapter 3).

1.5: CONCLUDING REMARKS

Chondrogenesis depends on the maintenance of the progenitor cell population in the distal limb and differentiation in the proximal limb, but the mechanisms underlying these processes are still unclear. Here, we will identify the mechanism through which BMP activity controls digit number and differentiation (Chapter 2) and the role PRMT5 plays in maintaining undifferentiated chondroprogentitor cells in the distal limb (Chapter 3).

Chapter 2: The dynamics of BMP signaling in limb mesenchyme and polydactyly

Portions of this chapter are modified with the permission from the authors. Norrie, J.L., Lewandowski, J.P., Bouldin, C.M., Amarnath, S., Li, Q., Vokes, M.S., Ehrlich, L.I.R., Harfe, B.D., Vokes, S.A. Dynamics of BMP signaling in limb bud mesenchyme and polydactyly. Developmental Biology (2014) 393(2):270-281

Jacqueline Norrie, under the advisement of Steven Vokes, completed all experiments and quantification unless otherwise stated here. Jordan Lewandowski completed the limb mesenchymal cultures in Figure 2.14 and qPCR in Figures 2.11 and 2.12. Cortney Bouldin and Brian Harfe created the $Rosa^{Gremlin}$ stem cells. Qiang Li made the $Rosa^{Gremlin}$ mouse line and assisted with breeding. Smita Amarnath assisted with the immunostaining in Figure 2.10. Martha Vokes quantified the mitotic index in Figure 2.10. Lauren Ehrlich assisted with the flow cytometry protocol and analysis in figures 2.10 and 2.11.

2.1: INTRODUCTION

Digit specification occurs within a complicated milieu of signaling pathways. Ultimately, the formation of digits is the product of regulated growth and patterning that initiate and modulate chondrogenic regulatory networks (Lopez-Rios et al., 2012; Sheth et al., 2012; Towers et al., 2008). Mutations in a surprisingly large number of genes cause the formation of extra digits (polydactyly) (Biesecker, 2011). Most of these genes likely

perturb the activity or output of a core signaling network that regulates proliferation and patterning in the limb bud. One of the defining features of the network is a set of iterative interactions between the limb mesenchyme and apical ectodermal ridge (AER) (Rabinowitz and Vokes, 2012).

The AER, a structure formed at the distal intersection of the dorsal and ventral ectoderm, expresses four FGF genes (*Fgf4*, *Fgf8*, *Fgf9*, *Fgf17*). These genes are redundant but Fgf8 is the most important, as it is widely expressed and can maintain relatively normal limb development even in the absence of the other three genes (Lewandoski et al., 2000; Mariani et al., 2008). AER FGFs are involved in promoting distal fates as well as in mediating several processes during limb development: sculpting morphology, promoting cell survival, and regulating cell velocity (Cooper et al., 2011; Gros et al., 2010a; Mariani et al., 2008; Rosello-Diez et al., 2014; Sun et al., 2002; Verheyden, 2005).

In contrast to the actions of FGF proteins, BMP ligands are required for differentiation, where they promote exit from the cell cycle and, in the digits, chondrogenic fates (Benazet et al., 2012; Lopez-Rios et al., 2012). Three BMP proteins (BMP2, 4 and 7) are expressed in the limb with BMP4 exhibiting the most central role in digit patterning (Bandyopadhyay et al., 2006; Benazet et al., 2009; Selever et al., 2004). BMPs work in part by promoting compaction of mesodermal cells into cartilage elements (Barna and Niswander, 2007). In the complete absence of BMP activity, cartilage cells do not form in the autopod, resulting in a lack of digit formation (Benazet et al., 2012). Limb buds containing reduced levels of BMP activity often have varying degrees of digit loss, suggesting that BMP activity promotes digit formation (Badugu et al., 2012;

Bandyopadhyay et al., 2006; Ovchinnikov et al., 2006). On the other hand, conditional inactivation of *Bmp4* after the limb bud has initiated results in polydactylous limbs (Benazet et al., 2009; Selever et al., 2004). One proposed explanation for these contradictory phenotypes is that BMP4 mutations result in a feedback loop triggering upregulation of overall BMP (Badugu et al., 2012). Alternatively, lowered BMP4 signaling downregulated total BMP levels, suggesting that reductions in BMPs actually promote the formation of extra digits.

Not surprisingly, BMP activity within the limb bud is tightly regulated. Posteriorly expressed Sonic hedgehog (SHH) causes the upregulation of the BMP inhibitor Gremlin (GREM1) (Hsu et al., 1998). In the absence of GREM1 activity, BMP signaling is prematurely upregulated in the limb bud, resulting in the formation of fewer digits (Benazet et al., 2009; Khokha et al., 2003; Michos et al., 2004). Conversely, introduction of a GREM1-expressing virus in chick limb buds, results in the increased limb growth and a lack of cartilage formation (Harfe et al., 2004).

Given the central role that GREM1 plays in regulating BMP activity, it is not surprising that the correct temporal termination of *Grem1* is critical for terminating digit growth and initiating chondrogenesis. *Grem1* is normally down-regulated in the distal limb by high levels of AER-derived FGFs (Verheyden and Sun, 2008). In addition, the descendants of SHH-producing cells do not express *Grem1* (Harfe et al., 2004). *Grem1* is also repressed by direct transcriptional inputs from GLI3 and TBX2 in the anterior and posterior margins of the limb, respectively (Farin et al., 2013; Li et al., 2014; Litingtung et al., 2002; te Welscher, 2002; Vokes et al., 2008).

In this study, we have generated a Cre-inducible allele of *Grem1* and used it to temporally inhibit BMP activity in the developing limb bud. Reduced levels of mesodermal BMPs over a defined time interval result in polydactylous hindlimbs. The polydactyly is preceded by enhanced rates of proliferation that correlate with persistent FGF activity. Although the first digit rays initiate normally, they have reduced levels of SOX9 and delayed differentiation. This results in persistent populations of undifferentiated chondrocytes at the anterior and posterior margins of the limb bud. We suggest that the delayed differentiation of these populations is likely due to the combined influences of reduced BMP activity along with upregulated FGF activity.

2.2: ACTIVATION OF AN INDUCIBLE *GREMLIN* ALLELE RESULTS IN POLYDACTYLY

In order to inhibit overall BMP signaling within the limb we decided to generate a Cre-inducible knock-in allele that would allow us to misexpress Gremlin, a secreted protein that has previously been shown to inhibit all limb BMPs (BMP2, 4 and 7) (Eimon and Harland, 1999; Hsu et al., 1998). Mice containing the $Rosa^{Gremlin}$ allele (hereafter referred to as RG) were crossed with a limb specific Cre, *Prx1Cre* (Logan et al., 2002), to induce ectopic *Gremlin* expression throughout the limb mesenchyme. *Gremlin* is endogenously expressed in a distinct crescent in the limb bud (Fig. 2.1A) while $PrxCre^{+/-};Rosa^{Gremlin/+}$ (henceforth referred to as 'Prx-RG') embryos expressed *Gremlin* broadly throughout the mesenchyme in a pattern superimposed on the endogenous domain (Fig. 2.1B). Prx-RG embryos activate *Gremlin* in the limb mesenchyme but not in the overlying AER, which also expresses BMPs.

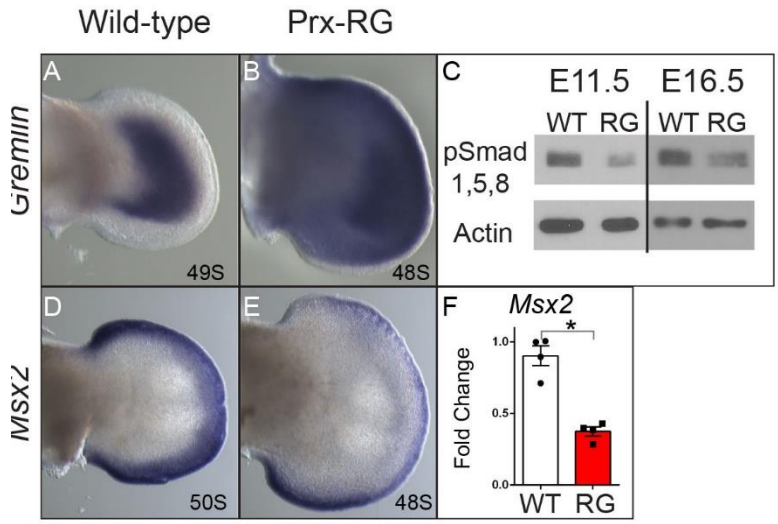

Figure 2.1: Ectopic Gremlin inhibits BMP signaling. *In-situ* hybridization for *Gremlin* at E11.75 (A-B). Note *Gremlin* expression throughout the limb mesenchyme in the Prx-RG (B). Prx-RG hindlimbs have reduced *pSMAD*1/5/8 levels on Western blots at 11.5 (53% reduction P=.0001) and continue to have reduced levels in E16.5 autopods (29% reduction P=0.04; normalized to beta-actin levels). *In-situ* hybridization for *Msx2* at E11.75 showing decreased expression in Prx-RG limb mesenchyme (D, E). There is a corresponding ~70% decrease in *Msx2* levels (P<0.05) Error bars indicate the standard error of mean (F).

By E11.5, Prx-RG limb buds had significantly reduced levels of phosphorylated SMAD 1/5/8 proteins, and this inhibition persisted at least until E16.5 (Fig. 2.1 C). Expression of the BMP target gene *Msx2* (Lallemand, 2005; Pizette et al., 2001) was reduced by approximately 70% at E11.75 when quantified by qRT-PCR (Fig. 2.1 F). When visualized by in situ hybridization, *Msx2* was strongly reduced in the mesenchyme with some expression persisting in the AER (Fig. 2.1D-E). BMPs have previously been shown to auto-regulate their expression in the limb bud (Khokha et al., 2003; Michos et al., 2004).

Consistent with these reports, *Bmp4* and *Bmp7* have significantly increased expression in Prx-RG limb buds (Fig. 2.2). We conclude that the Prx-RG allele has significant reductions in BMP signaling activity in the hindlimb mesoderm.

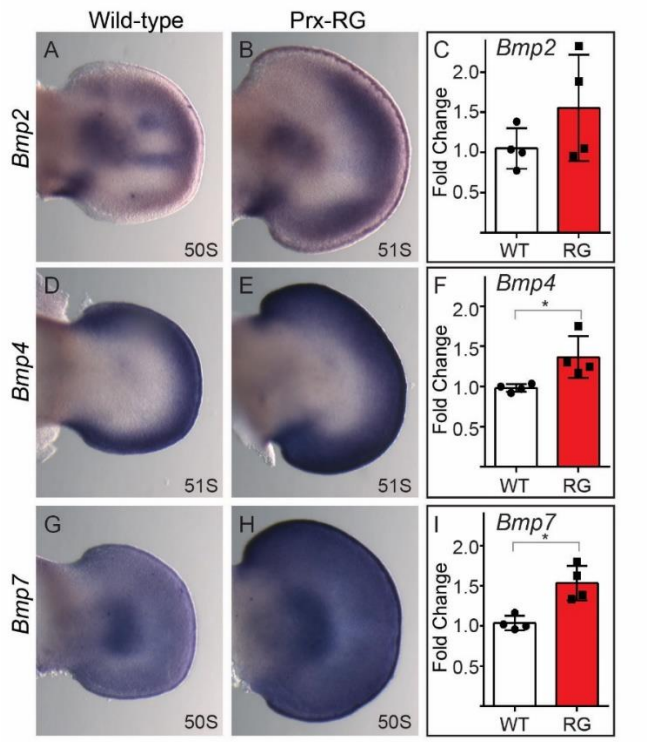

Figure 2.2: Ectopic expression of Gremlin causes an upregulation in BMP transcription. *In-situ* hybridization with somite stages indicated in the bottom right for *Bmp2* (A,B), *Bmp4* (D,E), and *Bmp7* (G,H) show increased BMP expression in Prx-RG hindlimbs compared to sibling wild-type controls. Quantification by qRT-PCR showing a significant increase in both *Bmp4* and *Bmp7* expression in Prx-RG hindlimbs ($P<0.05$) (F,I). Error bars indicate the standard error of mean (C,F,I).

To determine the result of reduced BMP levels, we examined Prx-RG skeletal preparations. The majority of Prx-RG embryos lacked forelimbs, containing only some residual cartilage attached to the scapula (7/10 embryos; Fig. 2.3). Of the remaining

embryos, two had reduced numbers of digits on both forelimbs while the third had polydactyly on both forelimbs (Appendix A, Table 1).

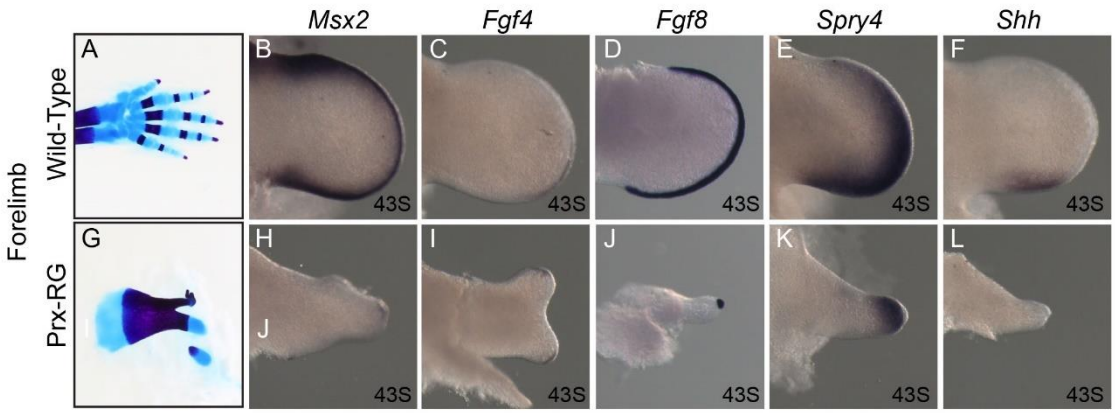

Figure 2.3: Loss of BMP in Prx-RG results in severe limb truncations. E18.5 skeletal preparations for WT and Prx-RG forelimbs. Most Prx-RG embryos lack forelimbs except for pieces of cartilage attached to the scapula (A, G). In situ hybridization for *Msx2*, *Fgf4*, *Fgf8*, *Spry4*, and *Shh* (B-F, H-L). Note the dramatic size reductions within the limb and AER.

The forelimb phenotype was grossly evident at E11.5, with shriveled limb buds containing only small patches of AER and an absence of *Shh* expression (Fig. 2.3 F-J, L-P). These phenotypes are consistent with previous reports indicating a transient early role for BMP signaling in AER formation (Ahn et al., 2001; Benazet and Zeller, 2013; Pajni-Underwood et al., 2007; Pignatti et al., 2014). We speculate that there is variability in the onset of *Prx-Cre* activity, as a later onset would explain why 3 embryos formed digits in the forelimbs.

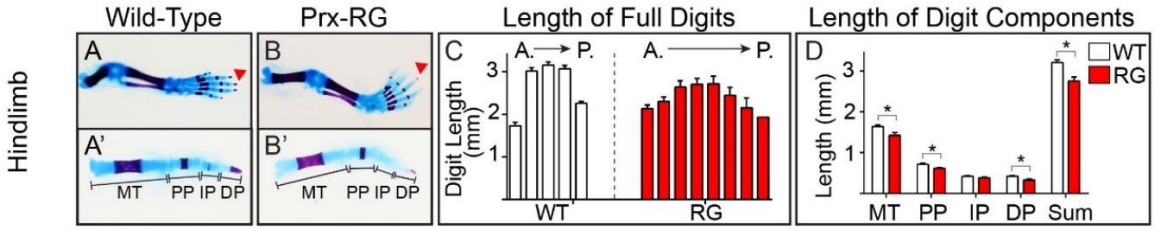

Figure 2.4: Loss of BMP in Prx-RG results in decreased digit length. Skeletal preparations of E18.5 hindlimbs (A,B). The corresponding middle digit (arrowheads) for each hindlimb is also shown in a dissected, magnified view (A',B'). RG hindlimb digits are shorter and more uniform. Digit length was measured from the proximal end of the MT to the tip of the DP. The average length of each digit is shown starting with the most anterior digit, regardless of total digit number, and ending with the posterior most digit (WT, n=7; RG, n=6)(C). Individual digit elements are uniformly shorter in Prx-RG digits compared to wild-type siblings. 'Sum' indicates the sum of the average measurements for the MT, PP, IP and DP elements (asterisk indicates that a statistically significant difference ($P<0.05$; WT, n=6; RG, n=5) (D). Error bars indicate the standard error of mean (C,D). Abbreviations: MT, metatarsal; PP, proximal phalange; IP, intermediate phalange; DP, distal phalange.

In contrast, the hindlimbs were completely formed with normally patterned stylopod and zeugopod elements (Fig. 2.4 A, B). The difference in phenotypes between the forelimb and hindlimb is likely caused by the earlier activation of the *Prx-Cre* transgene in the forelimb relative to the hindlimb (Logan et al., 2002). This would in turn inhibit BMP signaling at an earlier stage in forelimb development when the AER still requires BMPs.

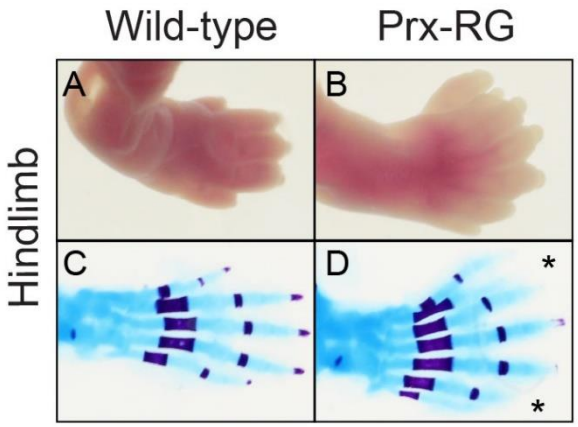

Figure 2.5: Loss of BMP signaling results in polydactyly. E18.5 hindlimbs (A-B) and skeletal preparations (C,D). Prx-RG hindlimbs have fully penetrant polydactylous hindlimbs along with soft tissue syndactyly (B,D).

The autopods had fully penetrant soft tissue syndactyly and polydactyly that ranged from 6-9 digits (mean=7.2; SD=0.92, n=10 embryos; Fig. 2.4 A,B; 2.5 A-D; Table 1). All embryos had a transformation of digit 1 ('big toe') from a shorter digit with 2 phalanges to a longer digit with 3 phalanges. Digits from RG embryos were significantly shorter than their wild type counterparts and they were also more uniform in length (Fig. 2.4 C, D). Each of the individual metatarsal and phalange elements comprising the shortened digits were proportionally reduced, indicating that this is a general shortening of the digit (Fig. 2.4 D). Compared to sibling controls, the phalanges had delays in ossification that were most pronounced at the digit tips (Fig. 2.5 C,D). Similar delays were noted in the posterior regions of *ShhCre*$^{+/-}$;RG digits (Fig. 2.6 A-D; Appendix A, Table 2), indicating that polydactyly can occur in both the anterior and posterior margins.

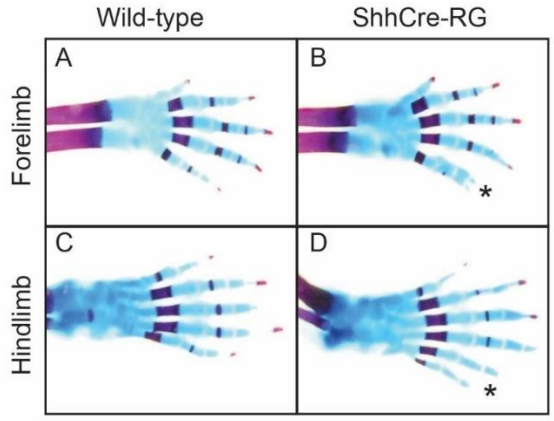

Figure 2.6: Activation of Gremlin in the Shh domain causes posterior polydactyly. Skeletal preparations of E18.5 embryos (A-D). ShhCre-RG embryos have posterior polydactyly. The ShhCre-RG forelimbs (B) have either a preaxial polydactyly (n=1/4) or large nubs in the posterior (n=3/4). The ShhCre-RG hindlimbs (D) had posterior polydactyly (n=3/4) or multiple posterior distal bifurcations.

2.3: TEMPORAL WINDOW FOR BMP-DEPENDENT REGULATION OF DIGIT NUMBER

Inhibiting BMPs could potentially cause polydactyly during a wide developmental time window. To determine the temporal range, we analyzed RG embryos containing *HoxB6CreER*, a tamoxifen-inducible Cre that has activity throughout hindlimb mesoderm (Nguyen et al., 2009). This approach allowed us to assay embryos expressing either one or two copies of RG (abbreviated as HoxB6CreER-RG or HoxB6CreER-RG/G, respectively). As a control, we established that siblings that did not contain HoxB6CreER (but also received tamoxifen) had normal, pentadactylous limbs. While we report phenotypes for the forelimb skeletal preparations (Fig. 2.7; Appendix A, Table 3), we focused on the hindlimb because HoxB6CreER is only active in the posterior portion of the forelimb (Nguyen et al., 2009).

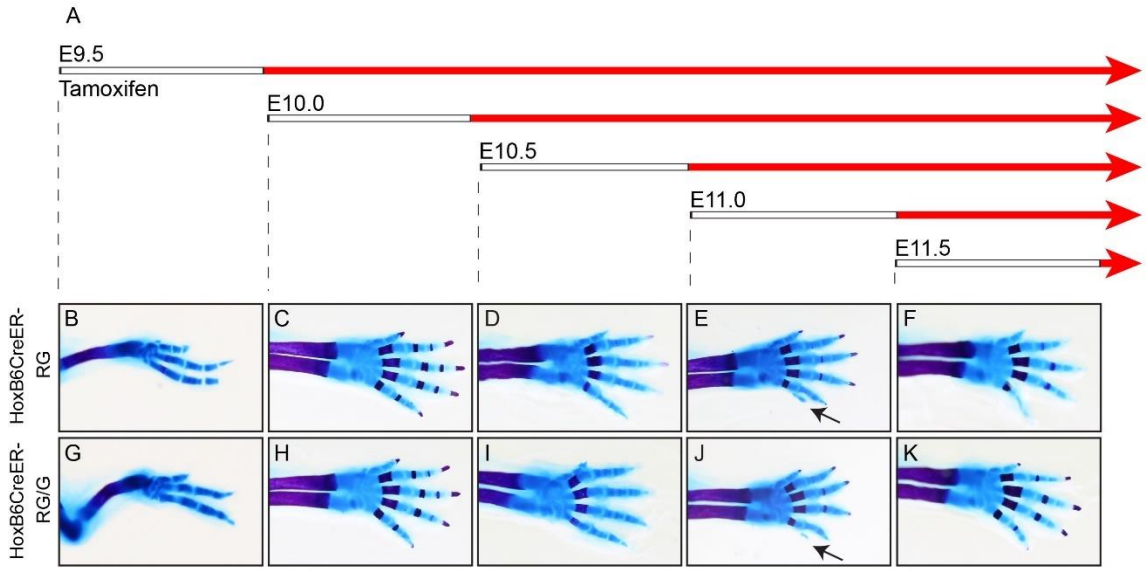

Figure 2.7: Temporal inhibition of BMP in forelimbs. Pregnant mice were injected with tamoxifen (A) at intervals between E9.5 and E11.5 (white bars). Effective activation of ectopic Gremlin (red bars) occurs approximately 8-12 hours later (white bars). Embryos were analyzed by skeletal preparation at E18.5 (B-K).

To determine the range over which BMPs regulate digit number, we injected pregnant mice at 12-hour intervals between E9.5 and E11.5. The *HoxB6CreER* mouse line causes efficient recombination at the *Rosa26* locus between 8-12 hours after Tamoxifen injection (Nguyen et al., 2009; Zhu et al., 2008); the interval between tamoxifen injection and the onset of BMP inhibition is represented by the white bars in Fig. 2.8 A. Overall, hindlimbs from embryos containing two copies of RG had more severe phenotypes than those with one copy, indicating that the phenotype is dose-responsive. When tamoxifen was injected at E9.5, HoxB6CreER-RG/G hindlimbs were either normal (2/5; Appendix A, Table 3) or had a loss of nearly the entire limb, containing only a few digit-like elements

(3/5; Fig. 2.8 B,G; Appendix A, Table 3). The loss of hindlimbs in these embryos was similar to the loss of forelimbs in Prx-RG embryos (Fig. 2.3 G), suggesting that this defect was caused by inhibiting BMPs during their early role in AER formation. As administration of tamoxifen at later stages resulted in polydactyly, it is not clear why a subset of these hindlimbs were normal at this stage. When injections were performed at E10.0 and E10.5, all HoxB6CreER-RG/G embryos had polydactyly (Appendix A, Table 3; Fig. 2.8 H,I). As observed in Prx-RG, this included a transformation of digit one from two phalanges to three phalanges. Some HoxB6CreER-RG/G embryos from E10 (5/8) and E10.5 (2/3) injections also had bowed femurs and tibia with a reduced or absent fibula (Fig. 2I, arrowhead). When injected at E11, HoxB6CreER-RG/G embryos had multiple bifurcated digits (n=3/3) but there were no completely formed extra digits. HoxB6CreER-RG embryos contained nubs or, in one case, bifurcated digits (Fig. 2.8 E,J; Appendix A; Table 3). Embryos injected at E11.5 contained a posterior skin nub that was smaller than nubs observed at when the transgene was activated earlier in development. The *HoxB6CreER* transgene is no longer expressed throughout the hindlimb after E11.5 but additional experiments using the ubiquitous $Rosa^{Cre\text{-}ERT2}$ (Ventura et al., 2007), which is expressed ubiquitously upon tamoxifen activation, indicated that $Rosa^{Cre\text{-}ERT2/Gremlin}$ embryos did not form nubs or polydactyly after E11.5 (Appendix A, Table 4). Because of the ~12 hour delay between injection and activation, we conclude that BMPs regulate digit number between E10.5-11.5.

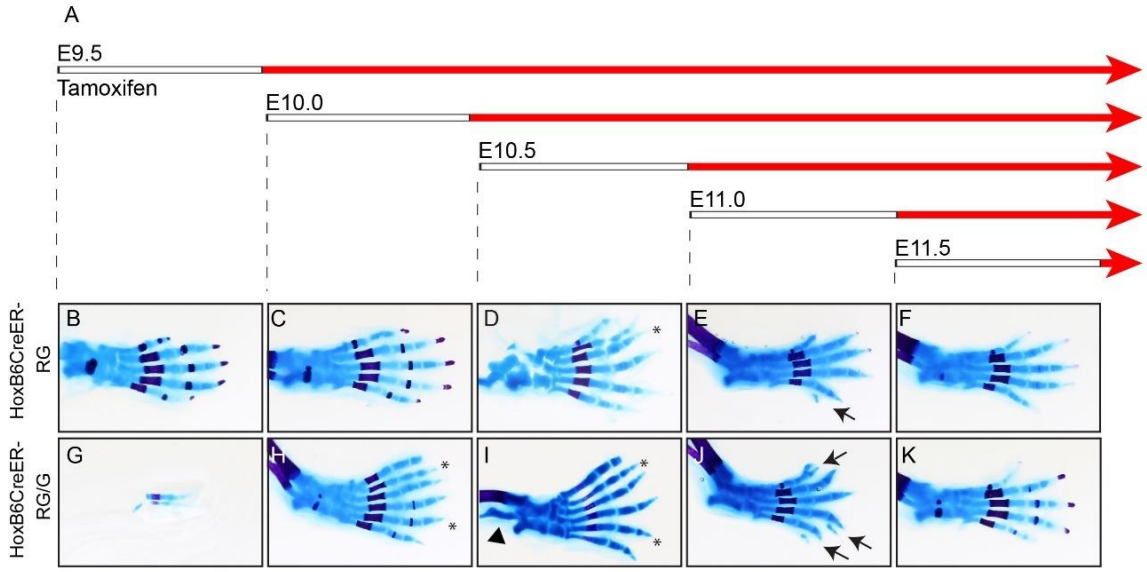

Figure 2.8: Mesodermal BMP signaling regulates digit number between E10.5 and E11.5. (A) Pregnant mice were injected with tamoxifen when embryos were at the specified time-points (white bars). Effective activation of ectopic *Gremlin* occurs approximately 8-12 hours later (red bars). Embryos were analyzed by skeletal preparation at E18.5 (B-K). Asterisks indicate polydactylous digits, arrows indicate nubs, and the arrowhead in I indicates defects in the tibia and fibula. The tibia and fibula were removed from the autopod in D prior to imaging. Images are representative of the most common phenotype with a minimum of three embryos per condition (Appendix A, Table 3) except for panel C (n=1). At all time-points, wild type siblings (containing RG or RG/G but no HoxB6CreER) from tamoxifen-injected litters had normal limbs and digits (Appendix A, Table 3).

2.4. BMP INHIBITION RESULTS IN PERSISTENT, AMPLIFIED FGF SIGNALING

To determine how *Gremlin* mis-expression and BMP inhibition affected early limb patterning, we determined the expression patterns for *Shh* and FGF response. At E11.5, Prx-RG hindlimbs have expanded anterior and posterior expression of *Fgf4* and *Fgf8* (Fig. 2.9 A, B, E, F). There also appears to be a slight increase in expression of the FGF target gene *Spry4* (Fig. 2.9 I,J). The domain of Shh expression is also expanded along the proximal to distal axis, consistent with previously described roles for BMPs in negatively regulating *Shh* (Bastida et al., 2009) (Fig. 2.9 M-N). By E12.5, wild type hindlimbs have normally lost *Fgf4* and *Shh* but their expression persists in Prx-RG hindlimbs (Fig. 2.9 C,D,O,P). In addition, *Fgf8* and *Spry4* are expressed at higher levels than control embryos (Fig. 2.9 G,H,K,L). To quantify these observations, we assayed gene expression in E11.75 limb buds by quantitative RT-PCR (Fig. 2.9 Q-T). Consistent with the expression data, there are significant increases in *Shh*, *Fgf8* and the FGF responsive genes *Dusp6* and *Spry4* (Kawakami et al., 2003; Mariani et al., 2008; Minowada et al., 1999b; Verheyden and Sun, 2008). We conclude that Prx-RG hindlimbs have elevated, sustained levels of FGF signaling.

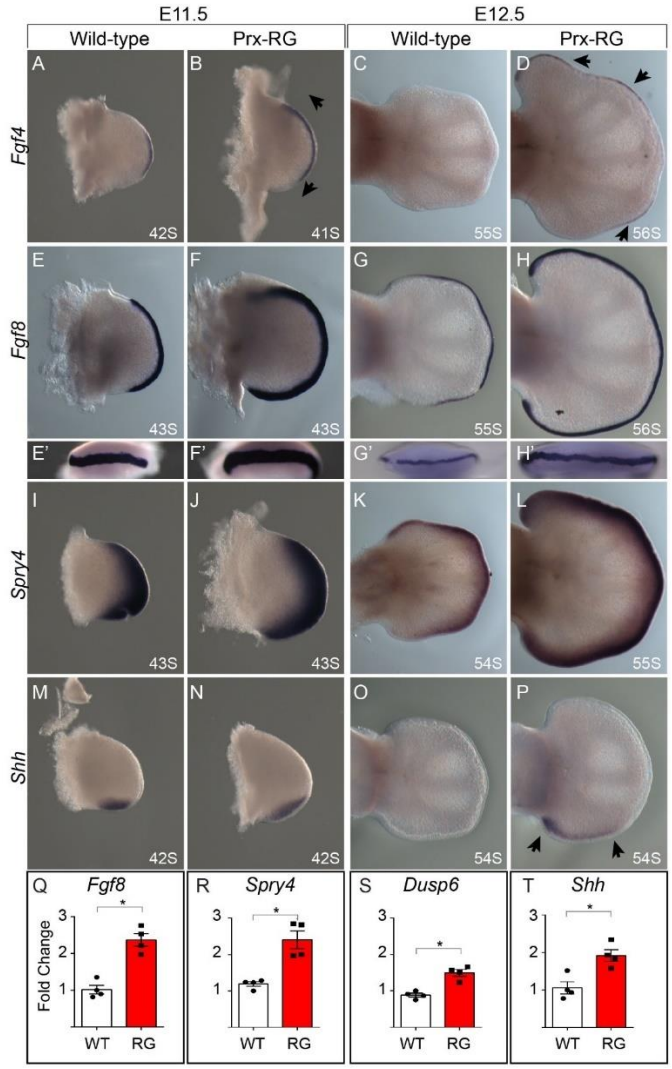

Figure 2.9: RG hindlimbs have elevated, persistent FGF signaling. *In-situ* hybridizations with the somite stage indicated at bottom right (A-P) for *Fgf4* (A-D), *Fgf8* (E-H'), *Spry4* (I-L) and *Shh* (M-P) at E11.5 and E12.5. *Fgf4* is expanded in both the anterior and posterior domains at E11.5 (B, arrows) with persistent and ectopic expression at E12.5 after expression is absent from wild type controls (D, arrow heads). Similar expression is seen for *Fgf8* (E-H') and for the FGF responsive gene *Spry4* levels (I-L). *Shh* is expanded in the proximal to distal domain at E11.5 and its expression is sustained at E12.5 in an expanded proximal/distal domain (arrows). Quantitative RT-PCR analysis of *Fgf8*, *Spry4*, *Dusp6,* and *Shh* at E11.75 indicate significant increases (asterisk indicates $P<0.05$) in expression levels in Prx-RG hindlimbs. Error bars indicate the standard error of mean (Q-T).

2.5: INHIBITING BMPS RESULTS IN ENHANCED PROLIFERATION AND REDUCED APOPTOSIS

The increased size of Prx-RG was initially apparent by E11.5 (Fig. 2.9) while there is a large difference by E12.5. This increased size could be caused by increased proliferation rates and/or reduced levels of apoptosis. To determine if there were changes in proliferation, we first examined the percentage of cells in mitosis using an antibody against phosphohistone H3 that recognizes cells in late G2 and mitosis (Hendzel et al., 1997). We focused our analysis to embryos between 45-47 somites, shortly after size differences between wild type and Prx-RG hindlimbs are apparent (Fig. 2.9). Autopods from Prx-RG hindlimbs had a 20% increase in their mitotic index (8.6% in sibling controls compared to 10.4% in Prx-RG $P<0.002$) (Fig. 2.10 A-C) indicating an increase in the percentage of proliferating cells.

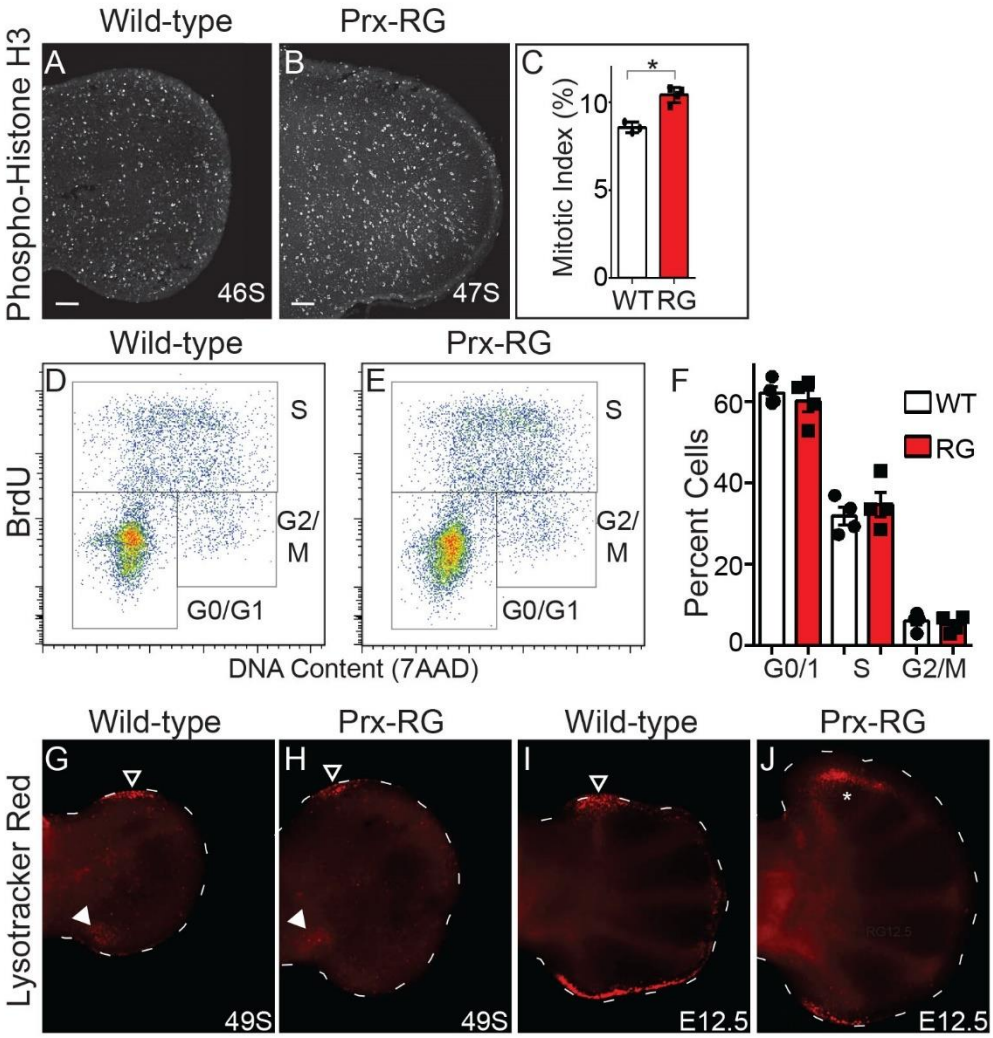

Figure 2.10: BMP inhibition results in increased proliferation and cell survival. Sections were immunostained for the presence of phosphohistone H3 (PHH3) on dorsal-ventral sections through the hindlimb autopod of E11.5 embryos (A, B). There is a significant increase in the percentage of PHH3 positive cells in RG ($P<0.05$) (C). Cell cycle analysis of WT and Prx-RG hindlimbs at E11.75 by flow cytometry gated into G0/G1, S, and G2,M phases (D,E). The average percentages of cells for each population (n=4) (F) are unchanged between WT and Prx-RG. Whole-mount staining for Lysotracker Red on hindlimbs at E11.75 (G,H) and E12.5 (I,J). Staging in somites (S) or embryonic day (E) is indicated on bottom right. Scale bars on images A,B indicate 100µM. Error bars indicate the standard error of mean (C,F).

We then measured proliferation by flow cytometry using hindlimb autopods from 45-49 somites. There was no difference in the percentage of cells in G0/1, S or G2/M (Fig. 2.10 D-F). At E12.5, the percentage of cells in G0/1, S or G2/M was comparable in percentage to the E11.75 (45-49 somite) sample (Fig. 2.11 C-E). Prx-RG hindlimbs did not have upregulated *Cdk6* expression as has previously been noted in *Gli3*$^{-/-}$ forelimbs (Lopez-Rios et al., 2012). Similarly, Prx-RG hindlimbs did not have upregulated *Axin2* expression, suggesting that canonical Wnt signaling was not elevated (Fig. 2.11 A,B). The discrepancy between these results and the increase observed in the mitotic index are discussed in the Discussion.

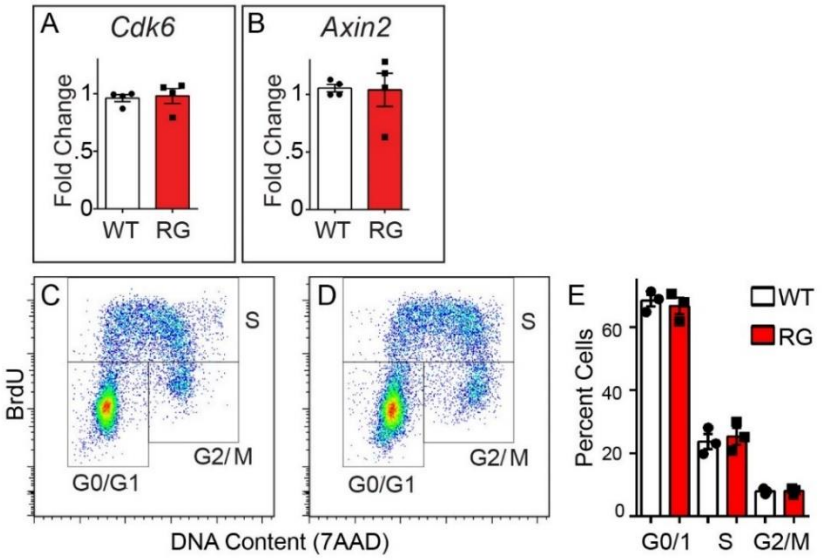

Figure 2.11: Loss of BMP signaling does not change cell cycle at E12.5. Quantitative real time PCR analysis of *Cdk6* and *Axin2* indicate no difference in expression levels between WT and Prx-RG in E11.75 hindlimbs (A,B). FACS data showing comparable levels of G0/1, S and G2/M cells between WT and Prx-RG hindlimbs at E12.5 (n=3). Error bars indicate the standard error of mean (A,B,E).

We examined changes in apoptosis using Lysotracker Red, an established marker of apoptotic cells in the limb bud (Fogel et al., 2012; Zhu et al., 2008). At E11.75, Prx-RG autopods have reduced levels apoptosis in the anterior AER and mesoderm (n=6) compared to sibling controls (Fig. 2.10 G,H; n=3). By E12.5, many apoptotic cells are present in the posterior AER and the anterior necrotic zone in control hindlimbs (Fig. 2.10 I; n=6). Apoptotic cells in the posterior zone are strongly reduced in Prx-RG limb buds. In addition the normal anterior necrotic zone (outlined arrowhead in 2.10 I) is completely absent with a new apoptotic domain expressed in a more proximal anterior position (asterisk in Fig. 2.10 J; n=3). We conclude that Prx-RG hindlimbs have enhanced levels of proliferation while having reduced levels of apoptosis.

2.6. REDUCED BMP LEVELS RESULT IN DELATED DIGIT FORMATION

To determine the onset of digit formation in Prx-RG hindlimbs, we examined the expression of *Sox9*, the earliest known marker of future chondrocytes, and *Col2a1*, a marker of differentiated chondrocytes that is a direct transcriptional target of SOX9 (Bell et al., 1997; Oh et al., 2010). At E12.5, wild type embryos expressed both *Sox9* and *Col2a1* in all five digit rays in contralateral hindlimbs (Fig. 2.12 A,B). At this stage, Prx-RG embryos had an average of 4.6 *Col2a1*-expressing rays while they had an average of 5.8 *Sox9* expressing rays in their contralateral hindlimbs ($P<0.05$ Paired T-Test). In addition to having a delayed onset in *Col2a1* expression in some digits, digit ray formation was still

ongoing in Prx-RG embryos at this stage, as they ultimately formed an average of 7.2 polydactylous digits (Fig. 2.12 C,D). The persistence of forming digits could be the result of developmental delay. To address this, we examined digit formation at earlier stages of development. Wild type hindlimbs at E11.75 had three fully resolved *Sox9*-expressing digit rays as did similarly staged Prx-RG embryos (Fig. 2.12 E,F), suggesting that initial digit ray formation was not delayed. However, Prx-RG hindlimbs had reduced levels of *Sox9* mRNA and SOX9 protein expression (Fig. 2.12 G, 2.13 D) and *Sox9*-expressing digit rays were significantly restricted from the most distal autopod in Prx-RG embryos (Fig 2.12 E,F). Sibling control embryos had an average domain of 112 μm between the boundary of *Sox9* expression and the AER while Prx-RG embryos had an average boundary of 144 μm ($P<0.05$). Together, these experiments suggested that Prx-RG embryos formed digit rays at a comparable rate to wild type controls albeit with more truncated domains. They also suggest that digit development persisted for a longer in the anterior and posterior margins that gave rise to most polydactylous digits.

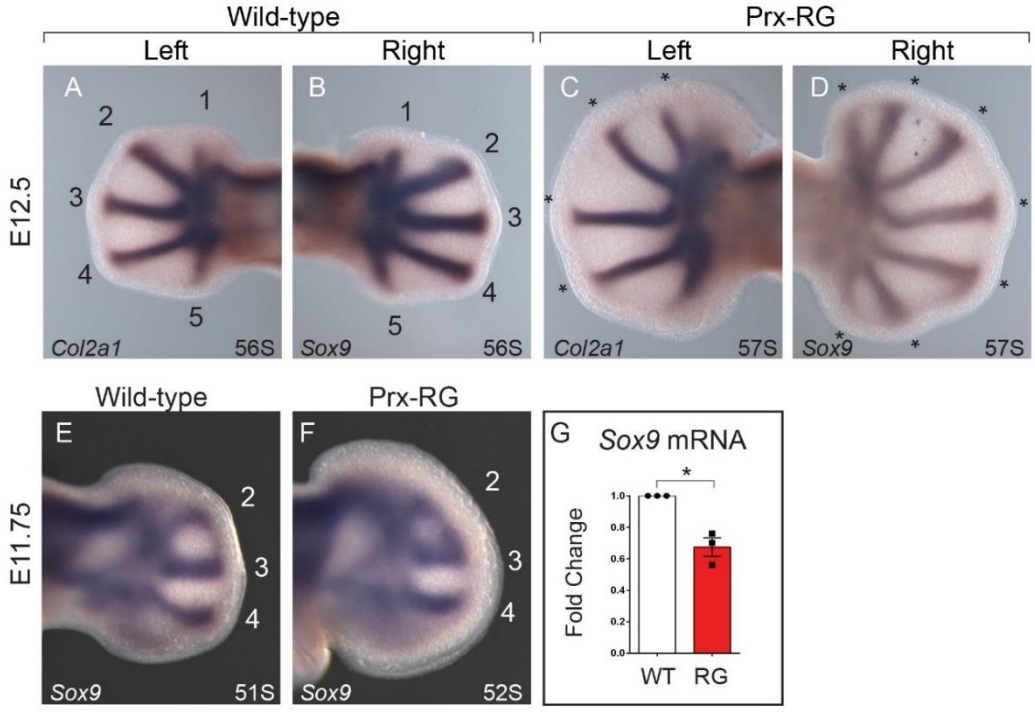

Figure 2.12: BMP inhibition delays chondrogenesis and reduces *Sox9*. *In-situ* hybridization for *Col2a1* and *Sox9* on contralateral hindlimbs from the same embryo (A-D). The wild type embryo has 5 condensed *Col2a1* positive digits as well as 5 *Sox9* positive digit rays while the RG embryo has more *Sox9* expressing rays than *Col2a1* expressing rays (asterisks indicate polydactylous digit rays – the posterior *Col2a1* domain (D) is not considered a digit because it has not yet fully expanded distally). *In-situ* hybridization for *Sox9* at E11.75 (E-F). Quantitative RT-PCR for *Sox9* normalized to *Gapdh* (G) shows a 33% decrease in expression in Prx-RG hindlimbs at E11.75 ($P<0.05$). Data points on graphs indicate measurements from independent embryos. Where applicable, somite stages are indicated in the bottom right. Error bars indicate the standard error of mean (G).

To examine this phenotype more closely, we examined SOX9 protein expression by immunostaining in sectioned RG hindlimbs. Consistent with the reduced levels of *Sox9* mRNA, SOX9 expression levels were significantly reduced both in fully resolved digit rays and pre-condensed regions (Fig. 2.13 B-D,F,G). At this stage, wild type digit rays

have more densely packed chondrocytes than Prx-RG rays (Fig. 2.13 B, F, H) while chondrocytes that have not yet formed rays appear to have similar densities in wild type and Prx-RG embryos (Fig. 2.13 C, G, H). The reduced levels of SOX9 and delayed compaction in Prx-RG embryos suggest that they have delays in later chondrogenesis although they initially form digit rays at a rate that is comparable to wild type embryos.

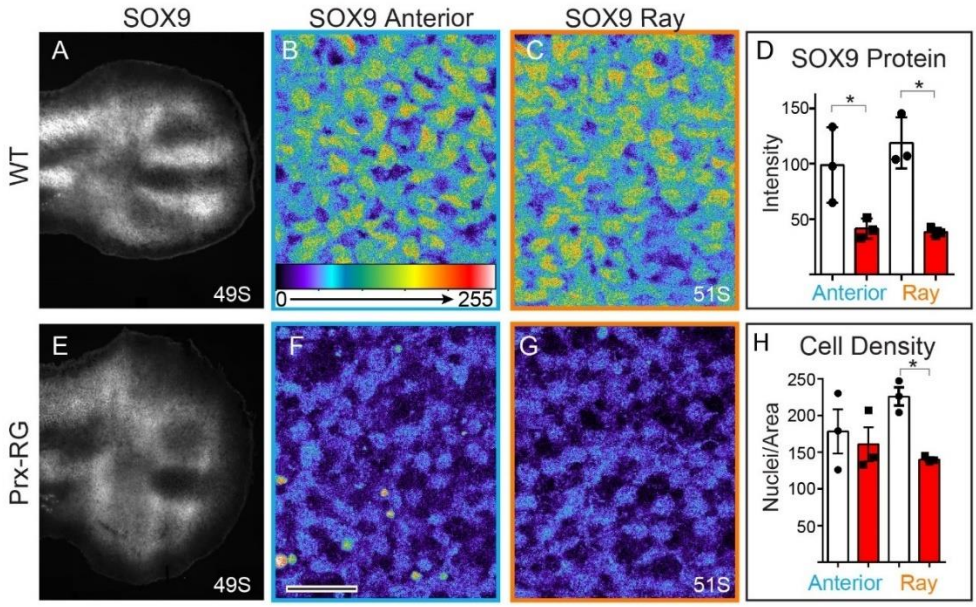

Figure 2.13: BMP inhibition reduces SOX9 and compaction. Sections immunostained for SOX9 and visualized epifluorescent light microscope (A, E). Additional 40x single plane confocal images (B, C, F and G; Scale bar= 20μm) show SOX9 positive cells with intensity indicated on a scale of 0-255 on comparable regions of WT and RG hindlimbs. The blue box (B, F) shows the anterior, uncondensed portion of the limb bud while the orange box (C, G) shows the condensing middle digit ray (sections in B, C, F, G are from different embryos than A, E). As reflected in the images, there is a significant reduction in SOX9 fluorescent intensity (D). There is also a significant reduction in nuclear density in the middle digit ray in Prx-RG limbs ($P<0.05$) while there is no difference in the density of uncondensed Sox9 expressing cells in the anterior limb (H). Data points on graphs indicate measurements from independent embryos. Where applicable, somite stages are indicated in the bottom right. Error bars indicate the standard error of mean (D, H).

2.7: REDUCED BMP AND ENHANCED FGF SIGNALING DELAY CHONDROGENIC DIFFERENTIATION

The preceding experiments suggested that Prx-RG hindlimbs digit rays were specified normally but might have delays in chondrocyte differentiation. This delay could be caused by threshold reductions in BMP signaling required to promote digit chondrogenesis; alternatively, the persistently elevated levels of FGF signaling present in Prx-RG hindlimbs (Fig. 2.9) could inhibit chondrogenesis as has been shown in cultured limb bud mesenchyme (Cooper et al., 2011; Lewandowski et al., 2014; ten Berge et al., 2008). This possibility is consistent with the distal truncations in *Sox9* expressing digits observed above. To test the roles of BMP and FGFs in more detail, we cultured wild type and Prx-RG hindlimb autopods under micromass-like conditions in control media or in media containing FGF8, BMP4, or both (Fig. 2.14). After 24 hours of culture under control conditions, Prx-RG had a 51% reduction in the BMP target gene *Msx2* and a 35% reduction in *Sox9* compared to wild type cultures (Fig. 2.14 B,C). In addition, Prx-RG cultures also had reductions in the chondrocyte differentiation markers *Agc1* and *Col9a1* (Fig. 2.14 D,E) (Bi et al., 1999; Derynck and Zhang, 2003; Sekiya, 2000). These results are consistent with the reduced levels of chondrogenic markers and delayed differentiation observed in embryonic limb buds (Figs. 2.12 D, G).

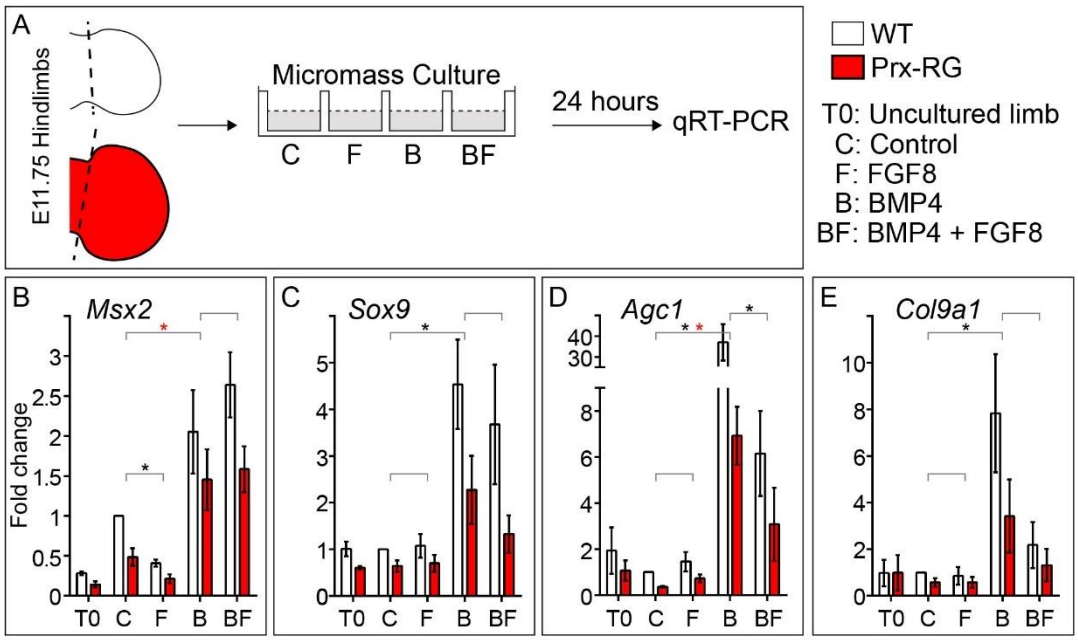

Figure 2.14: Limb bud cultures show a delay in differentiation of cells lacking BMP. Hindlimb autopods from WT and Prx-RG embryos were dissected and dissociated for a micromass culture (A) in either control media or media supplemented with Fgf8, BMP4, or Fgf8 and BMP4. Cultures were analyzed after 24 hours by qRT-PCR (B-E) for *Msx2* (n=5), *Sox9* (n=5), *Agc1* (n=5) and *Col9a1* (n=4). All samples were normalized to *Gapdh*. Brackets indicate pairs that were compared by statistical analysis. Statistical significance ($P<0.05$) is indicated by a black asterisk between WT samples and a red asterisk between RG samples. Analysis of WT and RG *Sox9* at T0 depicts that same data shown in Figure 5G. Error bars indicate the standard error of mean (B-E).

The addition of FGF8 to the media caused significant reductions in *Msx2* expression while *Sox9*, *Agc1* and *Col9a1* were not significantly changed in Prx-RG hindlimb cell cultures when compared to control conditions (Fig. 2.14 B-E). As expected, the addition of BMP4 to the media caused significant increases in *Msx2* as well as *Sox9*, *Agc1* and *Col9a1*. Conversely, these same markers are all reduced in the lowered BMP

environment present in cultured Prx-RG samples compared to wild type samples. These results are consistent with the in vivo results (Fig. 2.12) and suggest that BMP regulates *Sox9* in the autopod. Compared to the addition of BMP4 alone, cultures of wild type hindlimbs treated with BMP4 and FGF8 had comparable levels of *Msx2* and *Sox9* but strongly reduced levels of *Agc1* and *Col9a1* (Fig. 2.14 B-E). In this set of conditions, co-administration of FGF8 did not significantly inhibit Sox9 or BMP response (as measured by *Msx2*) yet strongly inhibited the activation of differentiation markers. This raises the possibility that an FGF-responsive protein could inhibit transcription of chondrocyte differentiation genes through a SOX9-independent mechanism (see Discussion, Fig. 2.15). In summary, these experiments suggest that both the reduced BMP signaling levels as well as increased FGF levels contribute to delays in chondrogenesis.

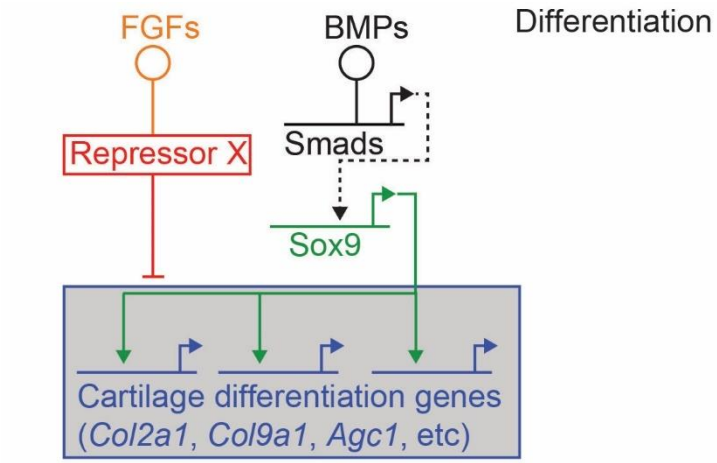

Figure 2.15: Gene regulatory network underlying digit chondrogenesis. Threshold levels of BMPs activate *Sox9* in a dose-dependent fashion through Smads in a direct or indirect fashion (dashed lines). SOX9, in turn, activates markers of differentiated chondrocytes. Amplified FGFs inhibit chondrogenesis both repressing differentiation genes in a parallel pathway by regulating a repressor.

2.8: DISCUSSION

In this study we have examined the effect of reducing BMP levels in the limb mesenchyme using a Cre-inducible construct that activates *Gremlin* (Fig. 2.1 A-F). We show that BMPs act in a dose and time dependent manner in which early or complete loss of BMPs result in digit loss, but inhibiting overall BMP signaling between E10.5 and E11.5 causes polydactylous digit formation (Fig. 2.8). RG hindlimbs have many phenotypes consistent with a loss of BMP signaling including ectopic *Fgf4* expression, expanded *Shh* expression and delayed AER regression (Bandyopadhyay et al., 2006; Bastida et al., 2009; Benazet et al., 2012; Pizette and Niswander, 1999; Verheyden and Sun, 2008). We were initially surprised that RG embryos ultimately form digits, as previous studies overexpressing BMP inhibitors resulted in an absence of cartilage formation (Capdevila et al., 1999b; Harfe et al., 2004; Lopez-Rios et al., 2012; Pizette et al., 2001). The most likely explanation is that in the RG allele BMP levels are reduced but not below a threshold level required for digit specification. Consistent with the idea the RG activation results in sustained inhibition of BMP signaling, BMP-specific pSMAD levels are decreased by ~50% in E11.5 Prx-RG hindlimbs and by ~30% in E16.5 autopods (Fig. 2.1 C). While the E16.5 autopod contains multiple differentiated cell types, the decrease in pSMAD inhibition suggests that BMP signaling has partially compensated for the presence of a steady-state inhibitor. If there is feedback compensation, BMP signaling might transiently be reduced to greater levels than indicated by overall protein levels on western blots.

In addition to their mesodermal roles, BMPs are also expressed in the AER where they are transiently required for its formation (Ahn et al., 2001; Barrow, 2003; Benazet and

Zeller, 2013; Benazet et al., 2012; Choi et al., 2012; Pizette et al., 2001). The mesodermal activation of *Gremlin* prior to ~E10.5 leads to severe reductions in limb growth and digit number that are consistent with this secreted protein providing localized disruption to the AER (Figs. 2.3, 2.8). While some conditional mutations in BMP result in digit reductions, mutations in BMP4 are polydactylous (Benazet et al., 2009; Dunn et al., 1997; Selever et al., 2004). Our results strongly suggest that the polydactyly seen in conditional deletions of BMP4 in the mesoderm are caused by overall reductions in BMP signaling levels and not by compensatory upregulation of other BMPs (Badugu et al., 2012).

2.8.1: Increased proliferation and reduced apoptosis in RG hindlimbs

At E11.5, near the onset of appreciable size difference between RG hindlimbs and controls, the mitotic index had a 20% overall increase in rate in RG hindlimbs (Fig 2.10 A-C). We do not detect any difference in G0/1, S or G2/M in similarly staged limb buds by FACS at either E11.75 or E12.5 (Figs. 2.10 D-F; 2.11 C-E). The mitotic index is likely a more sensitive method of detecting small changes in the G2/M phase while the lack of accompanying changes in the percentage of S-phase cells suggests that there could be changes in cell cycle rate. Consistent with this possibility, the most distal limb bud cells are reported to have decreased cell cycle times compared to the rest of the limb in wild type embryos (Boehm et al., 2010).

FGF8 does not cause increased proliferation in cultured limb bud mesenchyme, which is devoid of most or all ectoderm, but it does enhance proliferation when co-cultured

with either Wnt3a or Hedgehog activators (Lewandowski et al., 2014; ten Berge et al., 2008). Wnt ligands are expressed in the ectoderm where they act as mitogens on the adjacent mesoderm (ten Berge et al., 2008). If FGF8 plays a similar enhancing role *in vivo*, this effect should be most pronounced between E11.5-12.5 when there is normally a sharp reduction in FGF activity (Fig. 2.9 I,K). This correlates with period when there is an increase in size in the autopods of RG hindlimbs compared to controls (Fig. 2.9), and is consistent with the idea that persistent FGFs are causing an increase in proliferation. The increase in mitotic index in our study (Fig 2.10 A-C) but unchanged percentage of S-phase cells in RG limb buds contrasts with the enhanced anterior proliferation associated with anterior polydactyly in *Gli3*$^{-/-}$ limb buds, in which an enhanced G1-S transition is likely mediated by elevated CDK6 with no change in mitotic index (Lopez-Rios et al., 2012). Supporting the notion that RG limb buds have different drivers of proliferation, we also do not observe a change in *Cdk6* levels (Fig. 2.11 A).

An alternative interpretation of our data is that despite the increased mitotic index, proliferation is not a major driver of the increased size seen in RG limb buds. Computational simulations by Boehm et al suggest that increased proliferation rates do not play a role in normal distal limb development. Instead, they propose that limb growth is caused by directional cell behaviors(Boehm et al., 2010). FGF signaling has been shown to promote cell velocity in the early limb bud (Gros et al., 2010a) and could potentially continue to promote increased velocity this later phase of limb bud growth that could affect the increased size of the digit paddle. In addition to increased proliferation, RG hindlimbs have reduced apoptosis that is most pronounced in the anterior mesoderm (Fig. 2.10 G-J).

Apoptosis plays important roles in sculpting the autopod domain and reduced levels have classically been associated with polydactyly (Kimura and Shiota, 1996; Milaire and Rooze, 1983). Although we did not quantify apoptosis within the inter-digit mesenchyme of later limb buds, the webbing present in RG hindlimbs (Fig. 2.1 H) indicates a loss of apoptosis in this domain as well. This is consistent with other studies that have shown that persistent, elevated FGF signaling in the AER counteracts BMP-induced apoptosis (Lu, 2006; Pajni-Underwood et al., 2007).

2.8.2: The role of BMP signaling in digit specification

In the absence of Smad4 within the autopod, digit rays fail to form and *Sox9* is not expressed, implying a requirement for BMP signaling (Benazet et al., 2012). Based on this data, BMPs could either act upstream of *Sox9* to initiate transcription or they could provide a permissive environment in which *Sox9* would subsequently be activated. By reducing BMP activity, we do not observe significant delays in the onset of *Sox9*-expressing digit rays (Fig. 2.12 E,F) but there are significant reductions the levels of *Sox9* mRNA and protein (Fig. 2.12 G,K). This suggests that once BMP has reached a previously hypothesized threshold necessary for *Sox9* activation (Bandyopadhyay et al., 2006), it then regulates its expression in a dose-dependent fashion. In cultured limb bud mesenchyme we observe a similar trend with BMP4 causing a significant upregulation of *Sox9* that is dampened in RG cultures (Fig. 2.14 C). Although we do not observe delays in the onset of *Sox9* expression in the autopod, the reduced levels of SOX9 protein likely result in the

observed delay in activating the SOX9 target gene *Col2a1*. The delay suggests that SOX9 activity in RG embryos must reach threshold levels of activity before activating differentiation markers.

2.8.3: FGFs inhibit chondrogenic differentiation

Because RG limb buds have high levels of FGF signaling, we sought to determine how it influences chondrogenesis. Previous studies have shown that FGF signaling delays chondrogenesis in cultured limb bud mesenchyme (Cooper et al., 2011; Lewandowski et al., 2014; ten Berge et al., 2008). FGF signaling activity is highest in the distal mesoderm, suggesting that the truncated digit rays in RG embryos are caused by direct or indirect repression of *Sox9* (Fig 2.12 F). Interestingly, autopod cultures containing both BMP4 and FGF8 had significant reductions in the transcription of the cartilage differentiation marker *Agc1* compared to cultures treated only with BMP4. These cultures did not have significant reductions in the BMP-responsive gene *Msx2* or *Sox9*, which is already expressed in limb buds when they are dissected (Fig. 2.14 B-E). Moreover, FGF8 did not have a proliferative effect on cultures treated under identical conditions (Lewandowski et al., 2014). We speculate that FGF signaling represses *Sox9* activation by maintaining cells in a proliferative state as well as providing an independent repressive effect on the activation of chondrocyte differentiation markers that occurs in parallel to BMP-dependent activation of Sox9 (Fig 2.15).

2.8.4: Opposing actions of BMP and FGF on digit chondrogenesis

We have summarized the opposing roles for BMPs and FGFs in Fig. 2.16. The persistent FGF signaling in RG limb buds acts as a permissive factor to enhance cell proliferation and also provides increased cell survival in the anterior and posterior margins of the limb bud. Although BMP signaling is reduced in RG hindlimbs, it does not fall below threshold levels necessary to activate *Sox9* in the autopod. Nonetheless, *Sox9* expression is reduced within nascent chondrocytes, suggesting BMP acts as a dose dependent transcriptional regulator of *Sox9.* FGF signaling also negatively regulates chondrogenesis both by promoting cell proliferation and inhibiting differentiation of SOX9-expressing chondrocytes.

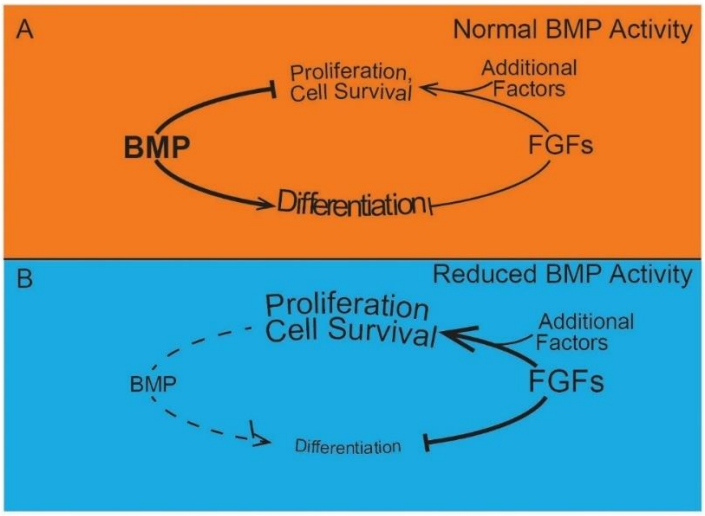

Figure 2.16: Model depicting the roles for BMP in digit chondrogenesis. (A) Under wild type conditions, increasing levels of BMP activity over development promote differentiation (chondrogenesis) and suppress proliferation. During this time, normal levels of FGFs promote proliferation by amplifying Shh and Wnt signaling (represented as 'additional factors'), until their downregulation at the end of limb specification. (B) When BMP levels are reduced in RG hindlimbs, there is a delay in chondrogenic differentiation. FGF levels persist after they are normally downregulated. This maintains the high level of proliferation seen in earlier limb mesoderm and inhibits normal apoptotic domains. Maintaining proliferation inhibits Sox9 expression and entry into a chondrogenic pathway and independently inhibits later chondrogenic differentiation.

We speculate that persistent FGF signaling in nascent chondrocytes upregulates a repressor of chondrogenic differentiation, depicted as "Repressor" in Fig. 2.15. The HOXD13 and HOXA13 paralogues are plausible repressor candidates, as FGFs promote the activation of these distal Hox genes (Rosello-Diez et al., 2014; Vargesson et al., 2001). While HOXA13 and HOXD13 are jointly required for normal digit condensation, the overexpression of HOXD13 negatively regulates chondrogenic differentiation (Fromental-Ramain et al., 1996; Kuss et al., 2008; Stadler et al., 2001). Moreover, *Sox9* is still expressed in *HoxA13*$^{-/-}$ digits (Perez et al., 2010), consistent with our finding that the repressor seems to act in a parallel pathway. As persistent FGF signaling from the AER is a common feature of many disparate polydactylies, we propose that this model will be more generally relevant to understanding how extra digits are generated.

Chapter 3: *Prmt5* is essential for the maintenance of chondrogenic progenitor cells in the limb bud

Portions of this chapter are modified with the permission from the authors. Norrie, J.L., Li, Q., Co, S., Huang, B., Mackem, S., Ding, D., Ji, Z., Bedford, M.T., Galli, A., Ji, H., Vokes, S.A. Prmt5 is essential for the maintenance of chondrogenic progenitor cells in the limb bud. Manuscript submitted.

Jacqueline Norrie, under the advisement of Steven Vokes, completed all experiments and quantification unless otherwise stated here. Qiang Li assisted with breeding and collecting mouse embryos. Swanie Co assisted with the in-situ hybridizations, skeletal preparations and quantification in Figures 3.4, 3.5, and 3.7. Bau-Lin Huang and Susan Mackem did the pSMAD immunostaining in Figure 3.13. Ding Ding, Zhicheng Ji and Hongkai Ji completed the intron retention analysis in Figure 3.6. Mark Bedford supplied the SDMA antibody in Figure 3.1. Antonella Galli made the Prmt5$^{tm2c(EUCOMM)Wtsi}$ mice.

3.1 INTRODUCTION

Differentiating cartilage elements are specified from a highly proliferative mesodermal progenitor population that is specified early in limb development. After specification, progenitor cells coalesce into condensates, activate *Sox9,* exit the cell cycle, and subsequently acquire the distinct morphology of chondrocytes (Akiyama et al., 2005; Barna and Niswander, 2007; Benazet et al., 2012; Boehm et al., 2010; Dudley et al., 2002; Pizette and Niswander, 2000). Early condensate growth is not well characterized but includes both localized chondrocyte proliferation as well as the recruitment of

undifferentiated cells onto their distal ends (Shubin and Alberch, 1986; Stark and Searls, 1973; ten Berge et al., 2008; Thorogood and Hinchliffe, 1975).

Mesodermal progenitor cells are regulated by multiple extrinsic signals. Sonic hedgehog (SHH) signaling regulates proliferation, inhibits differentiation and acts as a survival factor (Lopez-Rios et al., 2012; te Welscher, 2002; Zhu et al., 2008). Fibroblast growth factors (FGFs), in addition to acting as specification agents, survival factors, and motility agents, work in concert with WNT proteins to inhibit differentiation (Cooper et al., 2011; Gros et al., 2010b; Lewandowski et al., 2014; Mariani et al., 2008; ten Berge et al., 2008). In contrast, bone morphogenetic proteins (BMPs) drive chondrogenic differentiation (Bandyopadhyay et al., 2006; Barna and Niswander, 2007; Capdevila et al., 1999b; Lopez-Rios et al., 2012; Pizette et al., 2001). BMP signaling promotes apoptosis both in the anterior and posterior margins during limb outgrowth and later within the inter-digit mesenchyme (Kaltcheva et al., 2016; Macias et al., 1997; Pajni-Underwood et al., 2007). Unsurprisingly, BMP activity is tightly regulated by multiple inhibitory proteins, including GREM1 (GREMLIN) and NOGGIN (Bénazet et al., 2009; Brunet et al., 1998; Khokha et al., 2003; Macias et al., 1997; Michos et al., 2004; Norrie et al., 2014).

In contrast to the well-described roles for secreted signaling pathways in regulating limb differentiation, the internal mechanisms by which mesodermal cells maintain a progenitor state are poorly characterized. Progenitor populations must balance renewal and differentiation in a manner that controls the expansion of differentiated skeletal elements (Suzuki et al., 2008). This dynamic process is analogous to adult stem

cell homeostasis but differs in that the developmental progenitor population is ultimately depleted, regulating the size of the differentiated tissue.

Given the similarities between progenitor cells and stem cells, we hypothesized that limb bud mesodermal cells maintain progenitor-states through stem cell-like pluripotency genes. *Prmt5*, which we find is expressed at high levels in the distal limb, is an attractive candidate for mediating mesodermal progenitor maintenance in the limb. It is essential for maintaining mouse embryonic stem cell pluripotency and is also required *in-vivo* for mouse inner cell mass development (Tee et al., 2010). Moreover, in combination with OCT3/4 and KLF4, it can reprogram mouse embryonic fibroblasts into induced pluripotent stem cells (Nagamatsu et al., 2011). It also has essential functions in a host of stem cell populations, including hematopoietic cells, muscle stem cells, primordial germ cells and male germ cells (Ancelin et al., 2006; Kim et al., 2014; Liu et al., 2015; Wang et al., 2015a; Wang et al., 2015b; Zhang et al., 2015b).

PRMT5 is an arginine methyltransferase that symmetrically dimethylates arginine residues on a diverse set of proteins (reviewed in (Stopa et al., 2015)). It can methylate specific Sm proteins that facilitate their assembly into a core complex of spliceosomal snRNPs (Chari et al., 2008; Meister and Fischer, 2002; Neuenkirchen et al., 2015; Pelz et al., 2015). Additionally, PRMT5 can regulate gene expression by methylation of histones H2A/H4 and H3 (specifically H2A/H4R3 and H3R8), which are generally associated with transcriptional repression (Ancelin et al., 2006; Di Lorenzo and Bedford, 2011; Lee and Bedford, 2002; Tee et al., 2010; Zhang et al., 2015a; Zhao et al., 2009).

Based on the important roles PRMT5 plays in adult stem and progenitor cell populations, it has the potential to regulate many important events during embryogenesis. However, due to its early embryonic lethality (Tee et al., 2010), it has not been explored during organogenesis. Here, we show that *Prmt5* is expressed in mesodermal progenitor cells in the limb bud and is essential for their maintenance. Embryos lacking *Prmt5* in their limb buds develop striking defects in skeletal morphogenesis that are caused by early defects in cartilage formation. These defects are caused by widespread apoptosis and precocious differentiation of mesodermal progenitor cells as consequence of elevated BMP activity. These findings establish an intrinsic mechanism for regulating chondrogenic progenitor cells in the embryo and suggest that a stem cell pluripotency factor may have analogous roles in regulating progenitor cell populations during embryonic development.

3.2: PRMT5 EXPRESSION IS RESTRICTED TO THE DISTAL LIMB

To gain insight on the effects of *Prmt5* on limb development we first examined its expression pattern. At E11.5, *Prmt5* is dynamically expressed, with high levels of expression in the presomitic mesoderm, craniofacial primordia and, prominently, the limb buds (Fig. 3.1A). *Prmt5* is uniformly expressed throughout the forelimb and hindlimb buds at E10.5 (Fig. 3.1B, E) but becomes restricted to the distal mesenchyme at E11.5 (Fig. 3.1C, F). At E12.5 the expression domain is restricted to the distal tip of the developing digit rays (Fig. 3.1D arrowheads, G), in a region corresponding to the proposed phalanx

forming region (PFR) that provides a progenitor population for the elongating digit condensates (Suzuki et al., 2008).

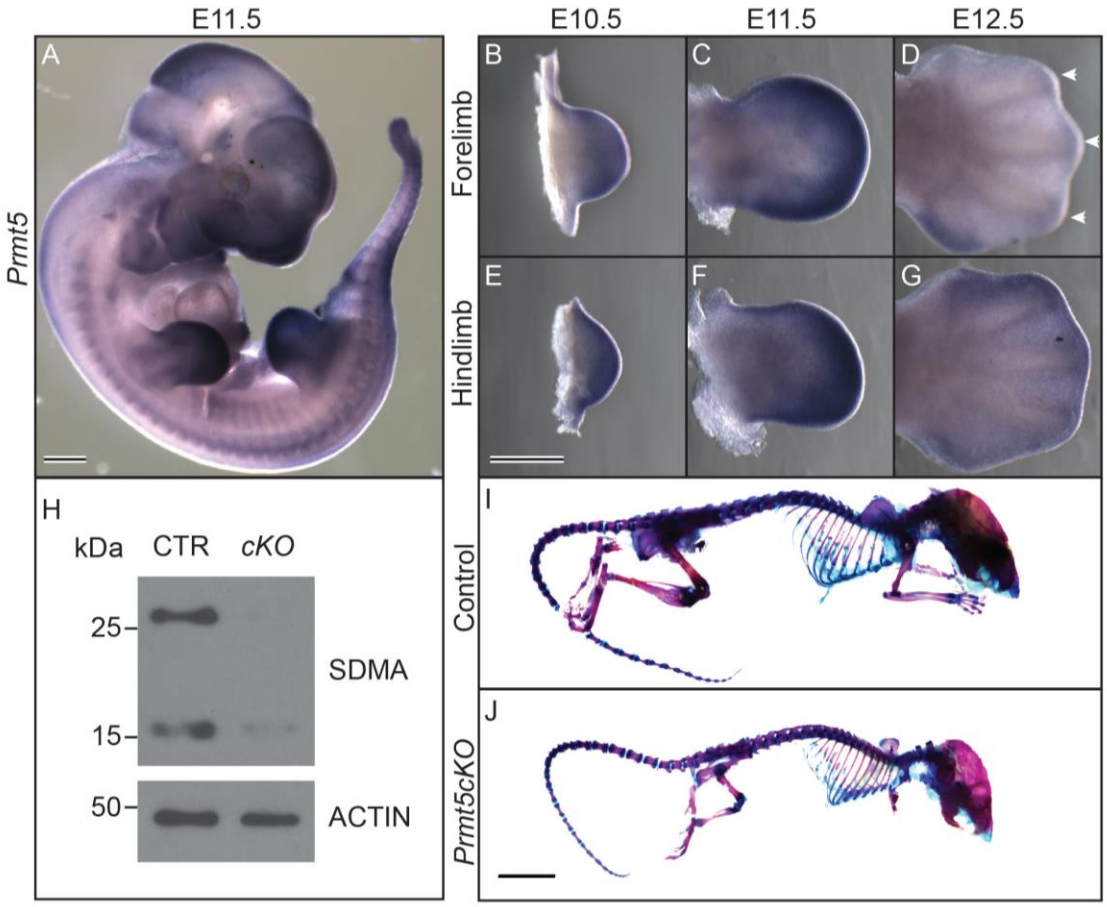

Figure 3.1: *Prmt5* is dynamically expressed in undifferentiated limb buds and is essential for their development. (A) Whole mount *in-situ* hybridization for *Prmt5* in an E11.5 embryo showing dynamic regional expression. *In-situ* hybridization for *Prmt5* in (B-D) forelimbs and (E-G) hindlimbs. Note the distal expression at the tip of the digit condensates at E12.5 (D, arrowheads). (H) Western blot with a SDMA antibody that recognizes proteins that contain symmetrically dimethylated arginines showing expression in forelimbs of E11.5 control (CTR) and *Prmt5cKO* (*cKO*) embryos. (I, J) Skeletal preparations of control and *Prmt5cKO* mice at P21. Scale bars in A and E indicated 500 μm. Scale bar in J indicates 1 cm.

The progressive distalization of *Prmt5* expression and its absence from chondrogenic condensates indicates that *Prmt5* is largely restricted to undifferentiated limb bud mesoderm. We noted a similar trend for the expression domain of *Mep50*, a co-factor that regulates the function of PRMT5 (Antonysamy et al., 2012; Burgos et al., 2015; Saha et al., 2016) (Fig. 3.2).

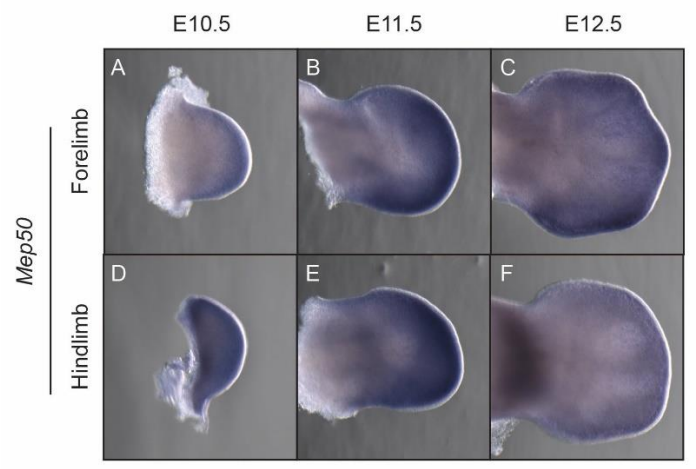

Figure 3.2: *Mep50* expression in forelimbs and hindlimbs. *In-situ* hybridization *Mep50* in control forelimbs (A-C) and hindlimbs (D-F) at E10.5, E11.5 and E12.5.

3.3: *PRMT5* CONDITIONAL MUTANTS HAVE TRUNCATED SKELETAL ELEMENTS AND ABNORMAL DIGITS

Because *Prmt5* null embryos fail to develop past the blastocyst stage (Tee et al., 2010), we conditionally knocked out *Prmt5* in limb buds using a floxed allele along with the limb bud specific *Prx1Cre* (Logan et al., 2002; Martin and Olson, 2000). There was a

substantial reduction of PRMT5 protein levels in E11.5 limb buds (Fig. 3.3), as well as a reduction of proteins with symmetrically dimethylated arginine residues in *Prmt5cKO* forelimbs (Fig. 3.1H) (Dhar et al., 2013). While *Prx1Cre*$^{+/-}$*; Prmt5*$^{c/+}$ littermates appeared normal, *Prx1Cre*$^{+/-}$*; Prmt5*$^{c/c}$ mice (hereafter referred to as *Prmt5cKO*) had severe, distinctive forelimb defects (Fig. 3.1I, J), suggesting an essential role for *Prmt5* during limb development.

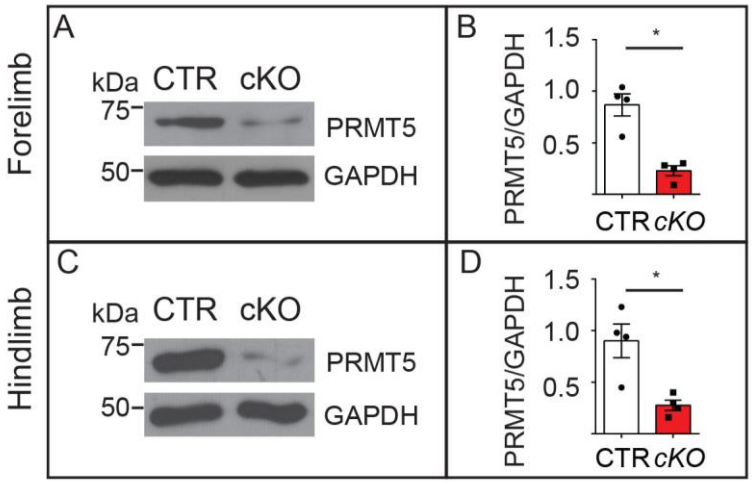

Figure 3.3: PRMT5 levels are reduced in *Prmt5cKO* limb buds. Western blots for PRMT5 and GAPDH on E11.5 limb lysate from control and *Prmt5cKO* forelimbs (A) and hindlimbs (C). (B, D) Quantification of band intensities (PRMT5 normalized to GAPDH). The asterisk indicates statistically significant changes ($P<0.05$) in *Prmt5cKO* compared with heterozygous or control siblings using a Student's t-test. Error bars indicate standard error of the mean.

At E18.5, *Prmt5cKO*s had severely truncated forelimbs (n=5/5 embryos) with the radius, ulna, and humerus each significantly shorter than those of control littermates (Fig. 3.4A-C). The deltoid tuberosity was missing from the humerus (4/5 embryos) and the forelimb autopods had substantially reduced numbers of wrist bones (2-3 total; Fig. 3.4H, H'; n=5/5). The digits on the *Prmt5cKO* were irregular, wispy and short, with little or no ossification and a complete absence of joints (Fig. 3.4G-I). Most *Prmt5cKO* limbs contained 4 severely truncated digits (n=4/5 embryos). Based on the size and position of the remaining digits, the missing digit likely corresponds to digit 1 (the thumb). Additionally, the remaining digits are fused in pairs at the base of the digits. Compared to the severe defects in the forelimbs, *Prmt5cKO* hindlimbs are normally patterned, however, the tibia, fibula, and femur were all significantly shorter than control siblings (Fig. 3.4D-F). The hindlimb autopods were also truncated and most digits were significantly shorter than control (Fig. 3.4J-L). Therefore, in both the forelimb and the hindlimb, *Prmt5* is essential for proper limb outgrowth.

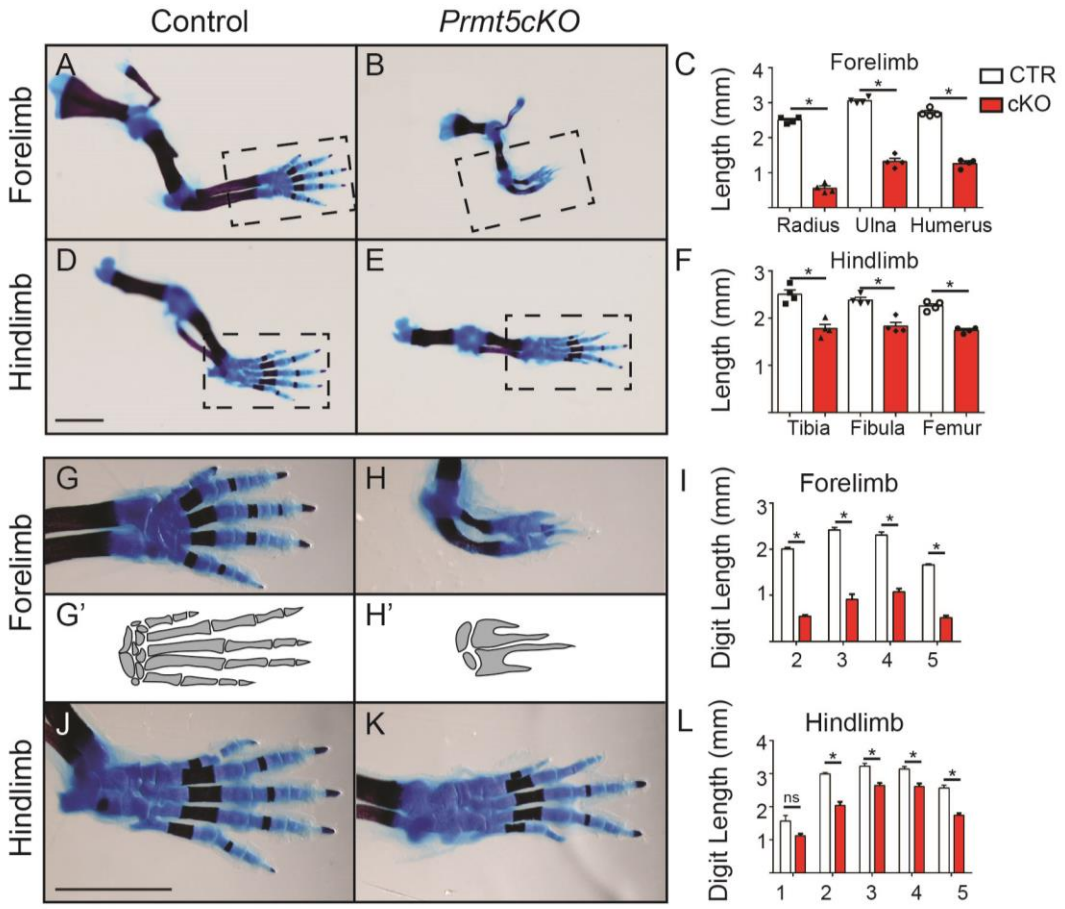

Figure 3.4: Conditional loss of *Prmt5* results in severe limb truncations and autopod defects. E18.5 skeletal preparations from control and *Prmt5cKO* forelimbs (A, B) and hindlimbs (D, E). The skeletal elements in both the forelimbs (C) and hindlimbs (F) are significantly reduced in *Prmt5cKO* embryos. (G, H, J, K) Panels show higher magnifications of the corresponding boxed regions from A, B, D and E. (G', H') Representative schematics of the autopods from control and *Prmt5cKO* forelimbs. Note the severe reduction in digit lengths (n=5) and number of digits (n=4/5). (I, L) Quantification of digit length (mm) using the right limbs from control (n=7) and *Prmt5cKO* (n=5) embryos. The asterisk indicates statistically significant changes ($P<0.005$) in *Prmt5cKO* skeletal elements compared with corresponding elements heterozygous or control siblings using a Student's t-test. Error bars indicate standard error of the mean. Scale bar indicates 2mm.

3.4: LOSS OF *PRMT5* RESULTS IN TRUNCATED DIGIT CONDENSATES THAT LACK JOINTS

Skeletal truncations can be caused by defects in either chondrogenesis or in subsequent bone formation. For example, *Indian hedgehog* null embryos have normal primary cartilage condensates but subsequent defects in subsequent bone formation that superficially resembles *Prm5cKOs* (St-Jacques et al., 1999). To determine the onset of the *Prmt5cKO* phenotype, we analyzed digit formation at E11.5 by *in-situ* hybridization for *Sox9,* the earliest known marker of chondrocytes (Akiyama et al., 2005; Bi et al., 1999; Lefebvre and Smits, 2005; Wright, 1995). At this stage, at least two distinct *Sox9*-positive digit rays could be resolved in control forelimb buds while *Prmt5cKO*s were slightly smaller, with no resolvable digit rays and a significant increase in the domain of undifferentiated, *Sox9* negative mesenchyme at the distal tip of the limb bud (Fig. 3.5A-C, J). Despite the unresolved digit rays and the increase in *Sox9* negative area, the overall SOX9 levels were unchanged (Fig. 3.5F, G). By E12.5 control embryos have five distinct *Sox9*-expressing digit rays while *Prmt5cKO* limbs are much smaller with truncated, poorly resolved digit rays (Fig. 3.5D, E, J). Because *Prmt5cKO* forelimbs lacked joints (Fig. 3.4H), we examined the expression of *Gdf5*, an early joint marker (Merino et al., 1999b; Storm and Kingsley, 1999). At E12.5 *Gdf5* expression surrounded each digit ray with additional expression traversing the digit rays, corresponding to the future joints of digits 3 and 4 (Fig. 3.5H). The *Prmt5cKO* forelimbs had comparatively reduced domains of *Gdf5* that did not extend as distally as the control and never traversed the ray (Fig. 3.5I).

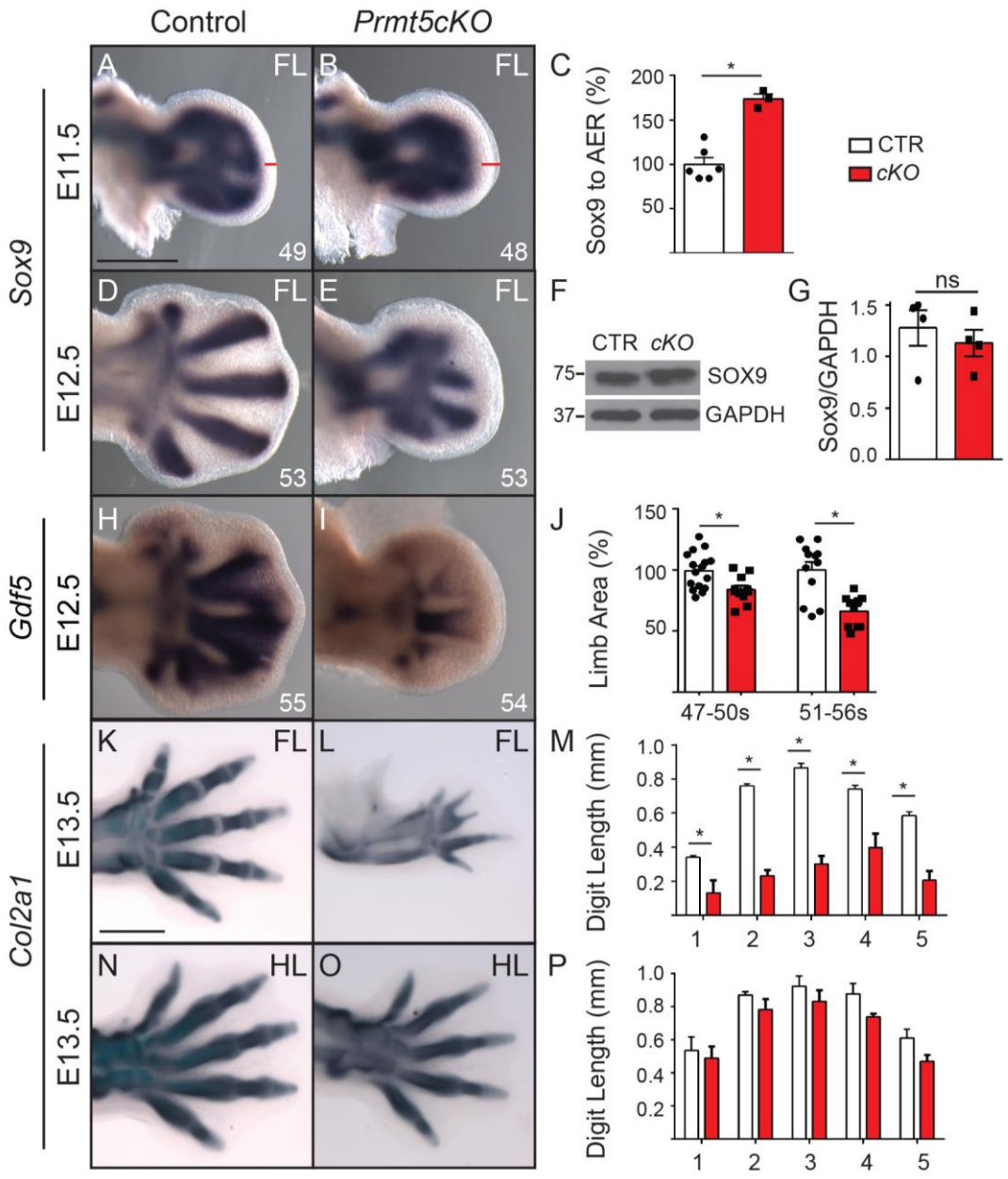

Figure 3.5: Abnormal digit ray formation and chondrogenesis.

Figure 3.5: Abnormal digit ray formation and chondrogenesis. (A-B) Whole mount *in-situ* hybridization for *Sox9* in control and *Prmt5cKO* forelimbs (FL) at E11.5. (C) Quantification of the distance from the distal boundary of *Sox9* expression to the distal tip of the forelimb as indicated by the red bars in A and B is significantly expanded in E11.5 Prmt5 embryos (control n=6; *Prmt5cKO* n=3). (D-E) *In-situ* hybridization for *Sox9* in control and *Prmt5cKO* forelimbs (FL) at E12.5 (A, B) (F) Western blot showing SOX9 and GAPDH control expression in forelimbs from individual E11.5 embryos and (G) quantification of band intensities (SOX9 normalized to GAPDH with the dots indicating biological replicates). (H, I) *In-situ* hybridization for the joint marker *Gdf5* at E12.5 in control and *Prmt5cKO* forelimbs. (J) Forelimb area (measured in image J at two different ranges of somite as indicated on the x-axis) of *Prmt5cKO* limbs smaller than controls (47-50s control n=16, *Prmt5cKO* n=11; 51-56s control n=12, *Prmt5cKO* n=10). (K, L, N, O) E13.5 whole mount in situ hybridizations cleared in benzyl alcohol:benzyl benzoate showing *Col2a1* expression control and *Prmt5cKO* forelimbs (FL) and hindlimbs (HL). The *Prmt5cKO* forelimbs have dramatic truncations in digit length (M) while the hindlimbs (P) do not have significant reductions in digit length. The asterisks (C, J, M) indicates statistically significant changes ($P<0.05$) in *Prmt5cKO* compared with corresponding elements in heterozygous or control siblings using a Student's t-test. Error bars indicate standard error of the mean. The numbers at the bottom right indicate the number of somites present in the embryo. Scale bars indicate 500μm.

We next examined expression of *Col2a1*, a marker of differentiating chondrocytes (Bi et al., 1999). At E13.5*, Prmt5cKO* forelimbs had a significant reduction in digit length with either 4 (n=1/3) or 5 (n=2/3) small, wispy digit outgrowths that tapered distally and lacked any joints (Fig. 3.5K-M). In all three cases, digit 2 was fused to digit 3 and in one case, digit 4 was fused to digit 5. Digit 1, if present, was an extremely small single piece of cartilage articulated to the anterior side of the wrist. In the forelimbs with only four digits it appeared that the anterior articulation was absent. In contrast, and consistent with the much milder phenotype at E18.5, *Prmt5cKO* hindlimbs appeared relatively normal (Fig. 3.5N, O). Although the digits were on average shorter than the control digits, it was not statistically significant at this stage (Fig. 3.5P). We conclude that the phenotypes seen in *Prmt5cKO* limb buds are the result of primary defects in early cartilage specification.

3.5: GENOMIC ANALYSIS OF *PRMT5CKO* LIMBS

To obtain insight into the genetic pathways affected by PRMT5, we performed RNA-seq on E11.5 control and *Prmt5cKO* forelimbs (Fig. 3.6A) and identified 208 differentially expressed genes using stringent conditions (fold-change > 2, an average FPKM >1 and q-value<0.01; Table S1). We then identified enriched categories using gene ontology (GO) terms (Wang et al., 2013). Top categories included upregulation of apoptotic and BMP signaling genes and the downregulation of genes involved in chondrogenic differentiation (Table S2). In addition, several of the significantly downregulated genes cause human syndromes with short digits (brachydactyly),

including *Gdf5*, *Bmpr1b* and *Noggin* (Al-Qattan et al., 2015; Byrnes et al., 2010; Lehmann et al., 2007; Lehmann et al., 2003; Ploger et al., 2008).

As PRMT5 regulates the formation of the spliceosomal complex, we also examined the frequency of intron retention in transcripts. We fit a logistic regression model of the ratio of intron to exon counts for genes in control and *Prmt5cKOs* and estimated the odds ratio between the groups. Genes in *Prmt5cKOs* have 1.3 times higher odds of a read coming from intron than the same genes in control, indicating that the number of retained introns is significantly elevated compared to controls (Fig. 3.6B). Consistent with this result, there is also a difference in the probability distribution of the intron retention rate (Fig. 3.6C). Because the differences are small, the biological significance of this finding is presently unclear.

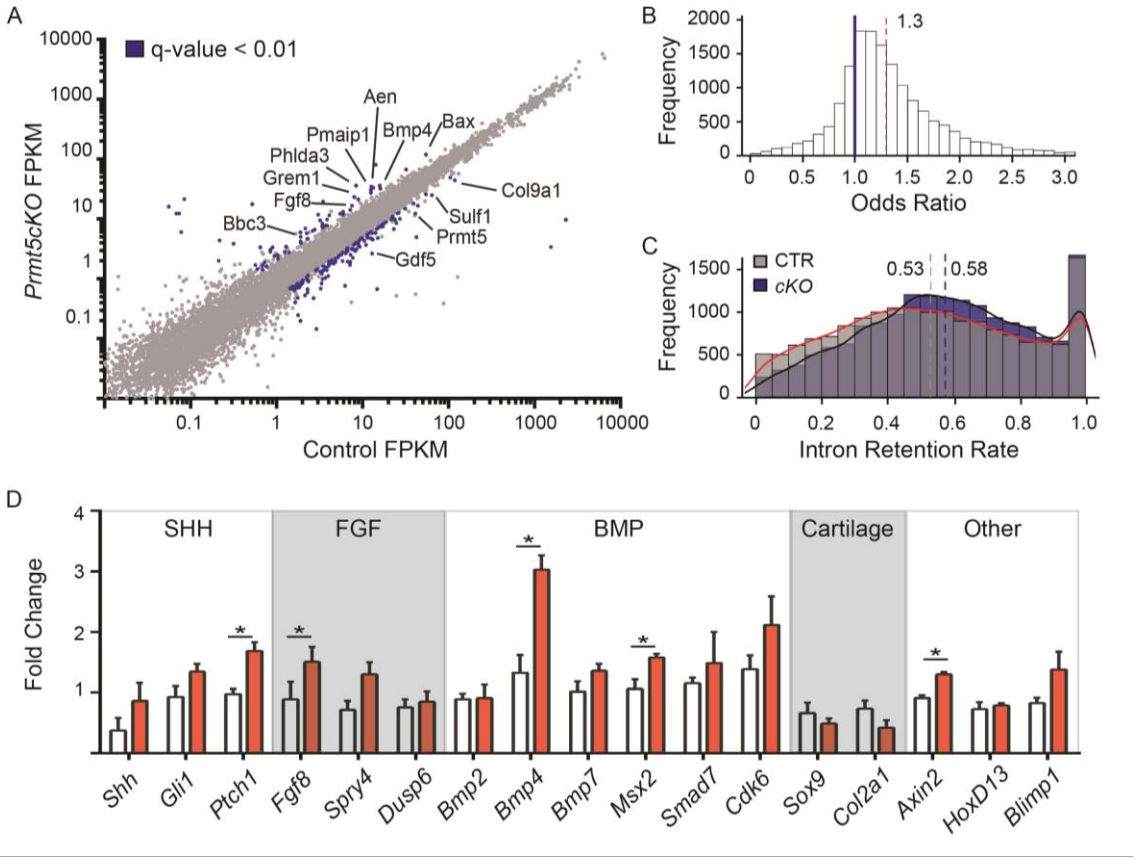

Figure 3.6: *Prmt5cKO* limb buds have elevated expression levels for apoptotic pathway genes. (A) Scatterplot of gene expression (FPKMs) for *Prmt5cKO* and control RNA-seq data. The blue data points indicate significantly changed genes using a stringent cutoff (B) Histogram showing the odds ratio $((\text{intron/exon})_{Prmt5cKO}/(\text{intron/exon})_{\text{Control}})$ acquired from logistic regression analysis. The odds ratio was 1.30 (95%CI (1.22, 1.38)). (C) Frequency of intron retention rate (intron/gene read count) of all genes for control (grey) and *Prmt5cKOs* (blue), average rates are indicated by the dashed lines (Control=0.53, *cKO*=0.58). (D) qRT-PCR validation of genes in known signaling pathways involved in limb development. Abbreviation: FPKM, Fragments Per Kilobase of Exon Per Million Fragments Mapped.

3.6: THE SHH-FGF LOOP IS UNAFFECTED IN *PRMT5CKOS*

Due to the severe limb truncations and high levels of apoptosis observed in limb buds deficient in SHH or AER-derived FGFs, we first considered the breakdown of the SHH-FGF feedback loop as a potential cause of the *Prmt5cKO* phenotype. (Chiang, 2001; Sun et al., 2002; Zhu et al., 2008). However, several lines of evidence suggest that neither of these pathways is reduced in *Prmt5cKO* limb buds. *Shh, Fgf8, Spry4* and *HoxD13* expression levels were either unchanged or slightly upregulated in *Prmt5cKO* forelimbs both in the RNA-seq data as well as in independent qRT-PCR experiments (Fig. 3.6A, D). Moreover, their gene expression domains are also unaltered (Fig. 3.7). Finally, limb buds lacking expression of SHH and FGF have greater reductions in digit number compared to *Prmt5cKO* forelimbs while the remaining digits do not have the brachydactyly or absence of joints observed in *Prmt5cKO* forelimbs (Chiang, 2001; Kraus et al., 2001; Sun et al., 2002; Zhu et al., 2008). We conclude that the SHH-FGF loop is intact and largely unaltered.

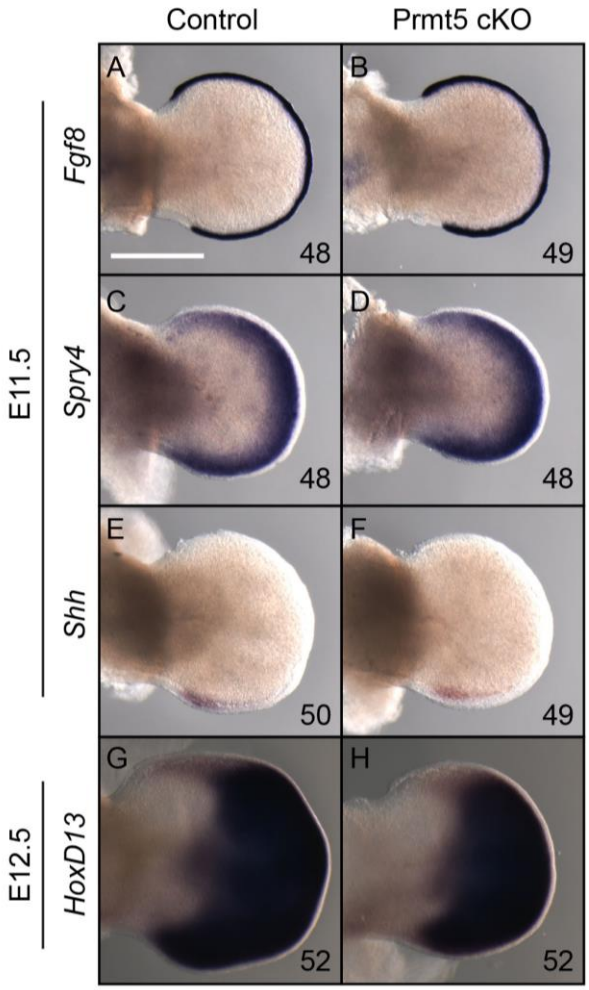

Figure 3.7: *Fgf* and *Shh* signaling are spatially unchanged. *In-situ* hybridization on E11.5 control and *Prmt5cKO* forelimbs for the indicated genes. The numbers within the panel indicate the somite stage of the embryo. Scale bar indicates 500μm.

3.7: PRMT5 PREVENTS APOPTOSIS IN THE DISTAL LIMB BUD

Prmt5cKO limbs had a significant increase in expression of genes involved in apoptosis. Therefore, we next determined the extent of apoptosis in the developing limb. Consistent with the RNA-seq findings, there was a substantial increase in apoptotic cells in E11.5 *Prmt5cKO* forelimbs (Figs. 3.8A, D; 3.9).

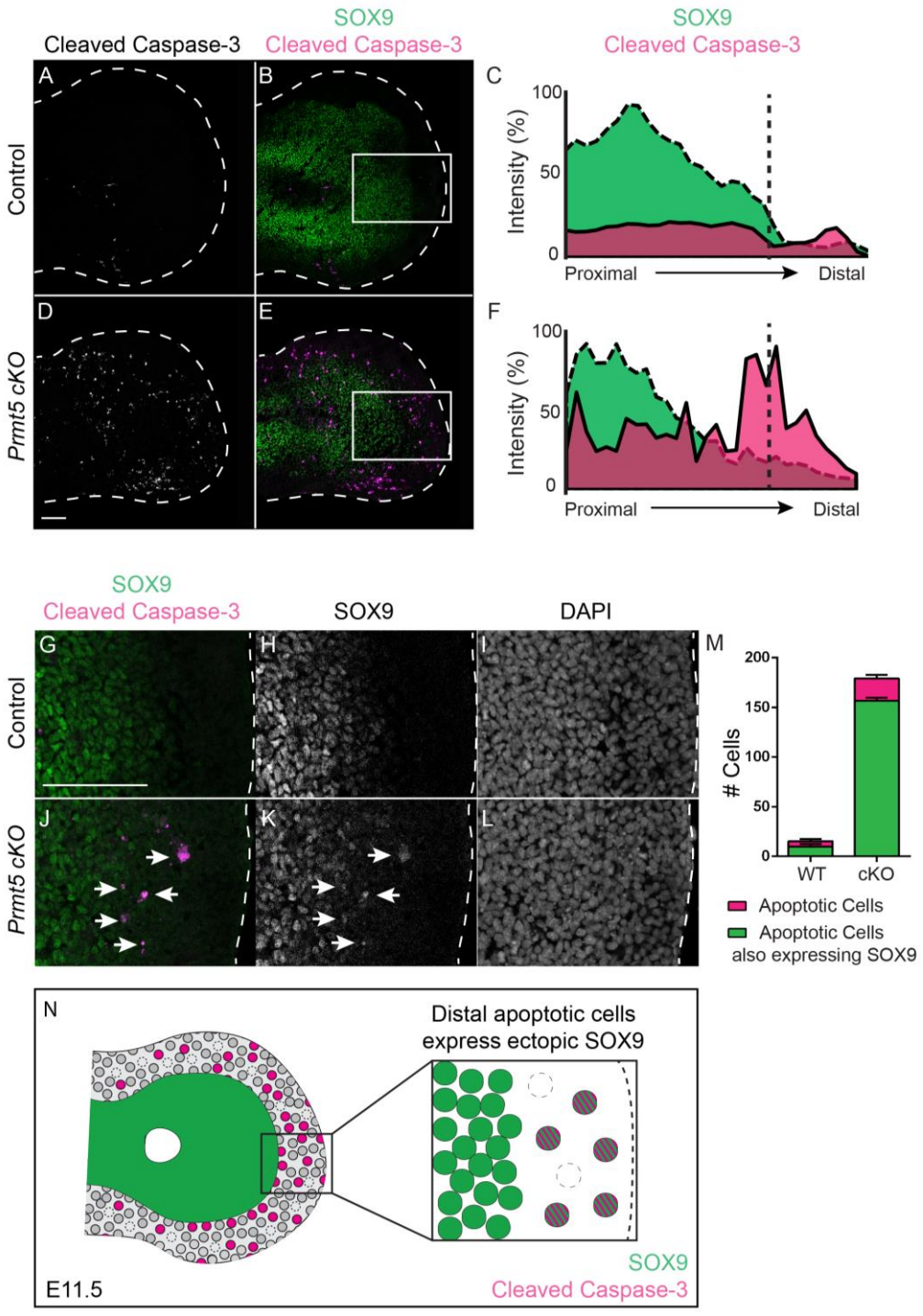

Figure 3.8: Prmt5cKO limb buds have elevated apoptosis and precocious differentiation in the distal limb bud.

Figure 3.8: Prmt5cKO limb buds have elevated apoptosis and precocious differentiation in the distal limb bud. Immunostaining for Cleaved Caspase-3 (A, D) and double staining for Cleaved Caspase-3 (pink) and SOX9 (green) (B, E) in control and Prmt5cKOs. (C, F) Quantification of fluorescent intensity for Cleaved Caspase-3 (pink) and SOX9 (green) in control (C) and Prmt5cKOs (F) from the distal region demarcated by the white boxes in panels B and E, respectively. Dashed lines indicate distal boundary where SOX9 expression drops below 20% intensity in the control embryo. (G, J) SOX9 (green) and Cleaved Caspase-3 (pink) double staining (also see controls in Fig. 3.11). Arrows indicate Cleaved Caspase-3 positive cells that are also expressing SOX9. (H, K) SOX9 and (I, L) DAPI only staining. (M) Quantification of Cleaved Caspase-3 positive cells co-expressing SOX9 in autopod regions of control and Prmt5cKO limbs. Maximum intensity projections of 3 biological replicates were quantified for control and Prmt5cKOs. (N) Cartoon indicating the widespread apoptosis in the distal region of Prmt5cKO limb buds. Cells currently undergoing apoptosis co-express SOX9 (green) and Cleaved Caspase-3 (pink) while the previous locations of cells that have undergone apoptosis are indicated with dashed outlines. Note the lack of apoptosis in differentiating chondrocytes. Scale bars indicate 50μm.

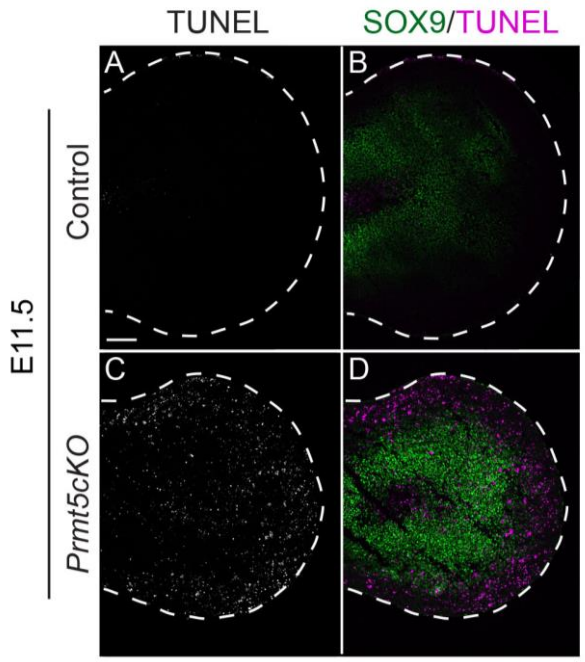

Figure 3.9: Apoptosis is upregulated in the *Prmt5cKOs* at E11.5. Immunostaining in sections from E11.5 control and *Prmt5cKO* forelimbs for TUNEL (A, C) and TUNEL (pink) and SOX9 (green) double staining (B, D). Scale bar indicates 100µm.

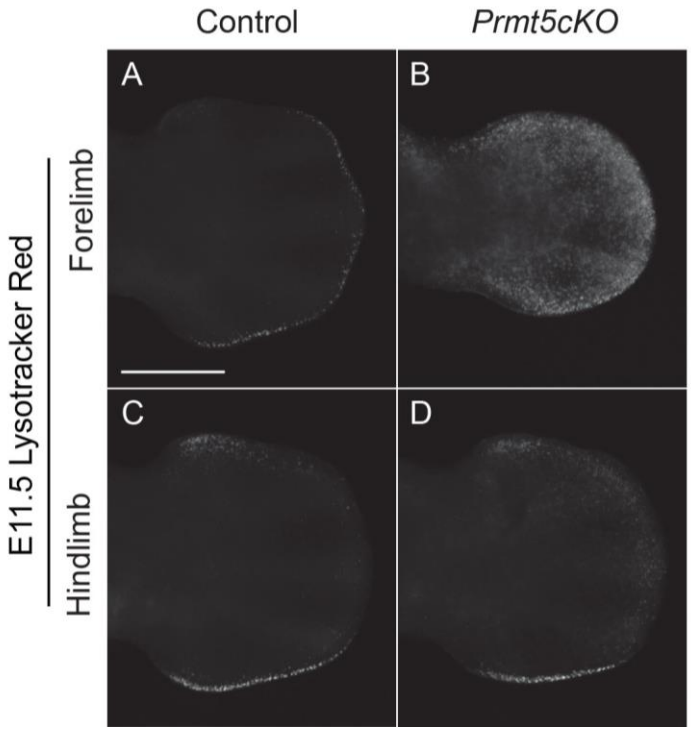

Figure 3.10: Apoptosis is upregulated in the *Prmt5cKOs* at E12.5. Whole mount limb buds stained for Lysotracker red in control and *Prmt5cKO* forelimbs (A, B) and hindlimbs (C, D) at E12.5. Scale bar indicates 500µm.

High levels of apoptosis were sustained at least through E12.5 (Fig. 3.10). Compared to the forelimb, the hindlimb had fewer apoptotic cells (Fig. 3.10B, D), perhaps explaining the milder phenotype. To determine which cells were dying, we examined sections that were co-stained for Cleaved Caspase-3 and SOX9 (Fig. 3.8B, E). Consistent with the gene expression data (Fig. 3.5A-C), the SOX9 domain was proximally truncated. The expanded region of distal mesenchyme contained the majority of apoptotic cells with the apoptotic domain located outside the SOX9-expressing

cartilage condensates (Fig. 3.8C, F). While control embryos rarely expressed SOX9 in the distal limb (an average of 4 cells per section; n=3) (Fig. 3.8G-I, M), the large majority of apoptotic cells express low levels of SOX9 (Figs. 3.8J-N; 3.11). The presence of SOX9 in apoptotic cells lying outside the normal condensate domain suggests that the mesodermal progenitor cells undergoing apoptosis may also be in the process of precociously differentiating into chondrocytes.

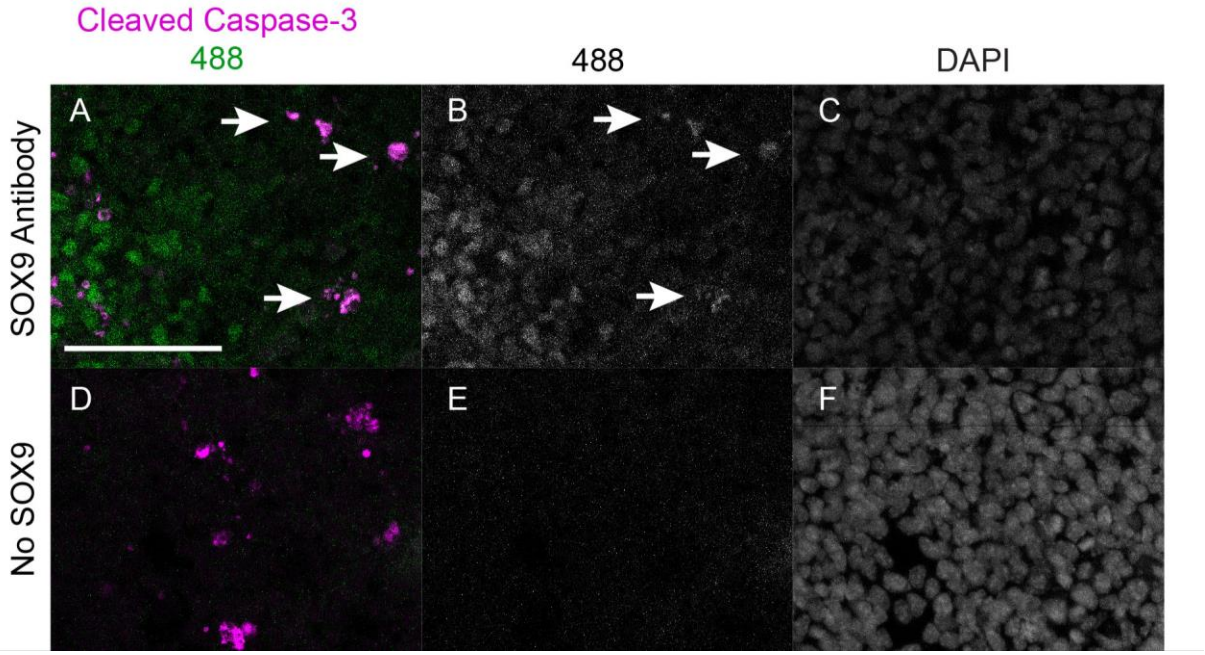

Figure 3.11: Control for apoptotic cells co-express Cleaved Caspase-3 and SOX9. Sections were stained for SOX9 and Cleaved Caspase-3 (A-C) or Cleaved Caspase-3 alone (D-F) and imaged with the 568nm laser (Cleaved Caspase-3 primary and AlexaFluor 568-conjugated anti-rabbit) and the 488nm laser (SOX9 directly conjugated to AlexaFluor 488) to ensure that SOX9 expressing cells did not have bleed-through fluorescence caused by Cleaved Caspase-3 staining. Scale bar indicates 50µm.

3.8: *PRMT5CKOS* HAVE INCREASED NON-CANONICAL BMP SIGNALING

The most upregulated limb-patterning gene in the *Prmt5cKO* forelimbs was *Bmp4,* while *Bmp2* and *Bmp7* were not significantly altered (Fig. 3.6D). Consistent with the increased expression levels indicated by RNA-seq and qPCR, there was also a substantial increase in the spatial domain of *Bmp4* in *Prmt5cKO* forelimbs as well as hindlimbs (Fig. 3.12A-D). *Msx2*, a target of canonical BMP signaling while slightly upregulated by independent qPCR (Fig. 3.6D) was unchanged by RNA-seq analysis and its spatial expression was unaltered in *in-situ hybridization* (Fig. 3.12E, F). In addition, the spatial domain and overall levels of phosphorylated SMAD 1,5,8, a direct readout of BMP signaling, were unchanged (Fig. 3.12G, H; S7). Together, these results suggest that there are not large alterations in responses to canonical BMP signaling.

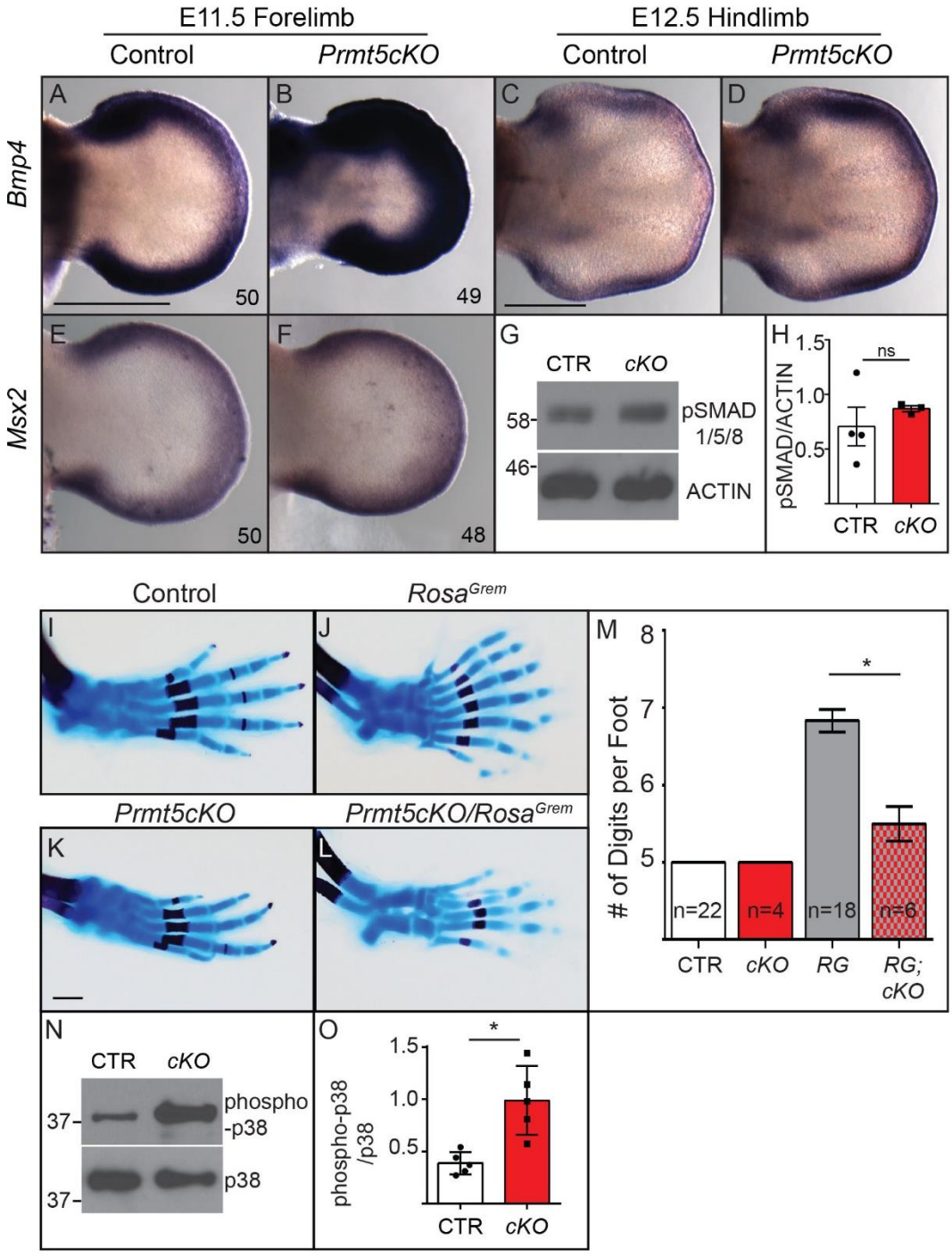

Figure 3.12: Prmt5cKO limb buds have upregulated BMP activity and elevated levels of phosphorylated P38.

Figure 3.12: *Prmt5cKO* limb buds have upregulated BMP activity and elevated levels of phosphorylated P38. (A, B) *In-situ* hybridization of *Bmp4* in control and *Prmt5cKO* forelimbs at E11.5 (50 and 49 somites) and (C, D) hindlimbs at E12.5. (E, F) *In-situ* hybridization of *Msx2* in control and *Prmt5cKO* forelimbs at E11.5 (50 and 49 somites). (G) Western blot showing pSMAD1/5/8 and ACTIN control in forelimbs from individual E11.5 embryos and (H) quantification of band intensities (pSMAD1/5/8 normalized to ACTIN) (control n=4; *Prmt5cKO* n=4). (I-L) E18.5 skeletal preparations of hindlimbs from the specified genotypes. (M) Bar graph indicating digit number for each hindlimb of embryos from the specified genotypes (Control n= 22; *Prmt5cKO* n=4; $Rosa^{Gremlin}$ n=18; *Prmt5cKO/* $Rosa^{Gremlin}$ n=6). (N) Western blot showing phospho-p38 and pan-p38 control (blot was stripped and reprobed with pan-p38) in forelimbs from individual E12.5 embryos and (O) quantification of band intensities (phospho-p38 normalized to pan-p38) (control n=5; *Prmt5cKO* n=5). The asterisk indicates statistically significant changes ($P<0.01$) in *Prmt5cKO* compared with heterozygous or control siblings using a Student's t-test. Error bars indicate standard error of the mean. The scale bars indicate 500µm Abbreviations: CTR, control; pSMAD1/5/8, phosphorylated SMAD1/5/8; phospho-p38, phosphorylated p38; p38, pan-p38

As BMP4 activity is regulated on several levels, including negative transcriptional feedback by GREM1 and proteolytic processing of the pro-protein, the increased *Bmp4* expression does not imply an increase in BMP activity (Benazet et al., 2009; Bragdon et al., 2011; Capdevila et al., 1999a; Michos et al., 2004; Norrie et al., 2014). To establish if there is a biologically relevant increase in BMP activity in the *Prmt5cKO* hindlimbs, we crossed *Prmt5cKOs* into $Rosa^{Gremlin/+}$, a Cre-inducible line that reduces BMP activity by over 50% (Norrie et al., 2014). As a consequence of reduced BMP activity, there is an early failure of forelimb initiation while the hindlimbs have fully penetrant polydactyly (Norrie et al., 2014). We reasoned that if BMP4 activity was increased in *Prmt5cKO* hindlimb buds, it might rescue the hindlimb polydactyly caused by reduced BMP levels. We did not expect to rescue the forelimb outgrowth defect in $Prx1Cre^{+/-};Rosa^{Gremlin/+}$ embryos, as this is likely due to an early defect in AER specification that precedes limb bud outgrowth (Norrie et al., 2014). As expected, control and *Prmt5cKO* littermates had 5 hindlimb digits while $Rosa^{Gremlin/+}$ embryos had polydactyly with an average of 6.8 digits. Compared to $Prx1Cre^{+/-};Rosa^{Gremlin/+}$ embryos, $Prx1Cre^{+/-};Rosa^{Gremlin/+};Prmt5cKO$ embryos had a significant rescue in digit number (5.5 digits, n=6) (Fig. 3.12I-M). We conclude that the increased *Bmp4* expression results in increased BMP4 activity that can offset hindlimb polydactyly caused by reductions in BMP activity.

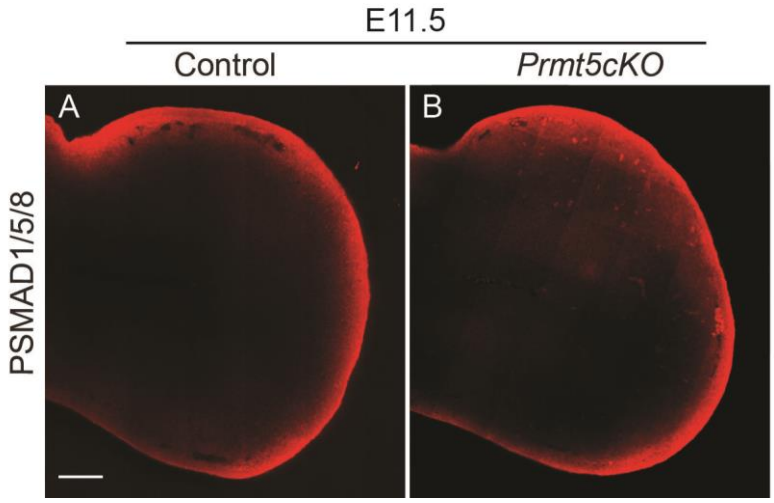

Figure 3.13. pSmad1,5,8 expression is spatially unchanged. (A, B) Immunostaining for phosphorylated Smad 1,5,8 in control and *Prmt5cKO* forelimbs at E11.5. Embryos were fixed for 3 hours then transferred into 70% EtOH and vibratome sectioned (100 μm). Sections were incubated with primary (1:100) overnight at 4 degrees, and subsequently incubated with secondary Alexa Fluor-488 (1:250) for 4 hours at room temperature. Images were taken on a Zeiss LSM 710 confocal at 63x magnification, stitched and processed to indicate maximum intensity projections.

Increased BMP activity has been shown to cause apoptosis in embryonic limb buds (Macias et al., 1997) and consequently the increased BMP activity in *Prmt5cKO* hindlimbs likely drives apoptosis. As canonical BMP signaling was not noticeably upregulated, we analyzed levels of phosphorylated p38 (phospho-p38), which mediate non-canonical BMP signaling (Derynck and Zhang, 2003; Kondo et al., 2014; Kuroyanagi et al., 2015). There was a significant upregulation of phospho-p38 in *Prmt5cKO* limb buds (Fig. 3.12N, O), suggesting that the upregulation of BMP4 may activate apoptosis through non-canonical p38 signaling.

3.9: DISCUSSION

The conditional deletion of *Prmt5* confers a striking limb phenotype. All skeletal elements in the forelimbs are truncated with wispy digits that lack joints while the hindlimbs are less severely affected. Underlying the phenotype is widespread apoptosis throughout the undifferentiated mesenchyme that occurs without obvious perturbations to the SHH-FGF loop. The majority of the apoptotic cells are located distal to the SOX9-expressing cartilage condensates but nonetheless precociously express low levels of SOX9. This suggests that they have begun to precociously differentiate into chondrocytes, perhaps because of heightened BMP activity. We conclude that PRMT5 has an intrinsic role for maintaining progenitor cells in the limb bud.

Initially, we considered that a breakdown in the SHH-FGF signaling loop caused the truncation phenotype in the *Prmt5cKOs*. However, *Shh*, *Fgf8*, the FGF-responsive *Spry4* (Minowada et al., 1999a) and *Gremlin* are not reduced spatially or quantitatively in *Prmt5cKO* forelimbs, suggesting the loop is intact even shortly before its normal termination (Figs. 3.6A, D, 3.7). In addition, there are significant differences between the *Prmt5cKO* phenotype and those reported for *Shh* or compound *Fgf* mutants (Chiang, 2001; Chiang et al., 1996; Sun et al., 2002). *Prmt5cKO* limbs, while also truncated, contain all limb elements and most of the digits but lack distinct elements due to digit fusion and loss of joints. They are also notably distinct from *Grem1*$^{-/-}$ limb buds, which have elevated BMP activity. *Grem1*$^{-/-}$ forelimbs have a disrupted SHH-FGF loop that leads to the loss of two

digits. The remaining digits, while truncated, still contain joints (Khokha et al., 2003; Michos et al., 2004).

3.9.1: Enhanced, non-canonical BMP activity in *Prmt5cKOs*

As *Bmp4* expression is negatively regulated by BMP activity, the observed increase in gene expression does not in itself imply enhanced activity (Khokha et al., 2003; Michos et al., 2004; Norrie et al., 2014). The BMP target gene *Msx2* (Lallemand et al., 2005; Pizette and Niswander, 1999), although slightly upregulated in independent qRT-PCR experiments (Fig. 3.6D), was unchanged in the RNA-seq analysis and does not have consistently expanded spatial expression (Fig. 3.12E, F). In addition, there was no detectable increase in pSMAD1,5,8 activity either quantitatively or spatially (Figs. 3.12G, H; 3.13) (see next subheading below for discussion on SOX9 induction). Nonetheless, *Prmt5cKOs* are able to rescue the polydactylous hindlimb phenotype present in a $Rosa^{Gremlin}$ background that is caused by reductions in BMP activity (Fig. 3.12I-M), suggesting that upregulation of BMP activity rescues digit number.

BMP signaling has well-established roles in driving apoptosis in the inter-digit mesenchyme (Bandyopadhyay et al., 2006; Buckland et al., 1998; Ganan et al., 1996; Kaltcheva et al., 2016; Merino et al., 1999a; Pajni-Underwood et al., 2007). The application of BMP-containing beads to limb buds causes widespread apoptosis in uncondensed mesoderm but does not affect condensed digit rays (Ganan et al., 1996; Macias et al., 1997). Consistent with this, the majority of apoptosis in *Prmt5cKO*s occurs outside the differentiating chondrocyte domain. Digit 1, the sole digit lost in mutants, is the last

condensate to form in limb buds (Zhu et al., 2008) and therefore the most vulnerable to apoptosis.

The p38 mitogen-activated protein kinase (MAPK) pathway, a mediator of non-canonical BMP response, is substantially elevated in *Prmt5cKO*s. Although the mechanisms underlying the activation of p38 by non-canonical BMPs are not completely understood, the non-canonical and canonical pathways are mutually antagonistic and, in osteoblasts, can toggle between pathways (Feng and Derynck, 2005; Kimura et al., 2000; Kua et al., 2012; Lo et al., 2001; Sapkota et al., 2007). This mutual antagonism provides an explanation for the observed lack of upregulated pSMAD signaling in embryos with upregulated p38. Our results are also consistent with recent findings that BMPs directly regulate apoptosis in inter-digit mesenchyme through an unidentified non-canonical pathway (Kaltcheva et al., 2016). In other contexts, BMPs also induce apoptosis through the p38 pathway (Cuadrado et al., 2007; Fukuda et al., 2006; Hay et al., 2001; Kendall et al., 2005; Kondo et al., 2014; Kuroyanagi et al., 2015; Lafont et al., 2015; Tian et al., 2012). These known roles for BMPs suggest that they mediate apoptosis in cartilage progenitor cells, potentially through the upregulated levels of phosphorylated p38 that are present in *Prmt5cKOs* (Fig. 3.12N, O).

3.9.2: PRMT5 is essential for the maintenance of chondrocyte progenitor cells

The majority of apoptotic cells in *Prmt5cKOs* lie within the undifferentiated, uncondensed mesoderm that is distal to the normal SOX9 expressing domains (Fig. 3.8D-F). In control embryos, there is a nearly complete absence of cells in this region that express

SOX9 above background levels. In contrast to their neighboring, non-apoptotic cells, apoptotic cells express low, but distinct levels of SOX9 (Fig. 3.8J-L). The abnormal expression of SOX9 suggests that the uncondensed mesenchymal cells are undergoing precocious differentiation. As low levels of BMP signaling are essential for activating chondrogenesis and SOX9 in the distal mesoderm (Bandyopadhyay et al., 2006; Benazet et al., 2012; Norrie et al., 2014; Pizette and Niswander, 2000), the elevated levels of BMP activity in *Prmt5cKOs* could result in the activation of precocious SOX9 in a subset of cells that either concomitantly or subsequently undergo apoptosis. A caveat to this interpretation is that SOX9 induction in this region of the limb bud requires the canonical BMP-mediator SMAD4 (Benazet et al., 2012). While we do not detect elevated pSMAD levels indicative of enhanced canonical BMP signaling, we speculate that *Prmt5cKO* limb buds nonetheless express mild and/or transient increases in canonical BMP activity that were not detectable in our experiments. Consistent with this possibility, the activation of SOX9 occurs even in conditions that substantially reduce BMP signaling activity in limb buds (Bandyopadhyay et al., 2006; Norrie et al., 2014).

We propose the following model for PRMT5-directed maintenance of progenitor cells in the forelimb. In normal conditions, PRMT5 inhibits *Bmp4*, thereby promoting survival and continued proliferation of progenitor cells, while inhibiting their differentiation into chondrocytes. In the absence of PRMT5, an upregulation of *Bmp4* triggers apoptosis through non-canonical BMP signaling. Sustained high levels of apoptosis in the progenitor population deplete progenitor cells resulting in smaller numbers

of chondrocytes that will eventually condense and differentiate into severely truncated limbs (Fig. 3.14).

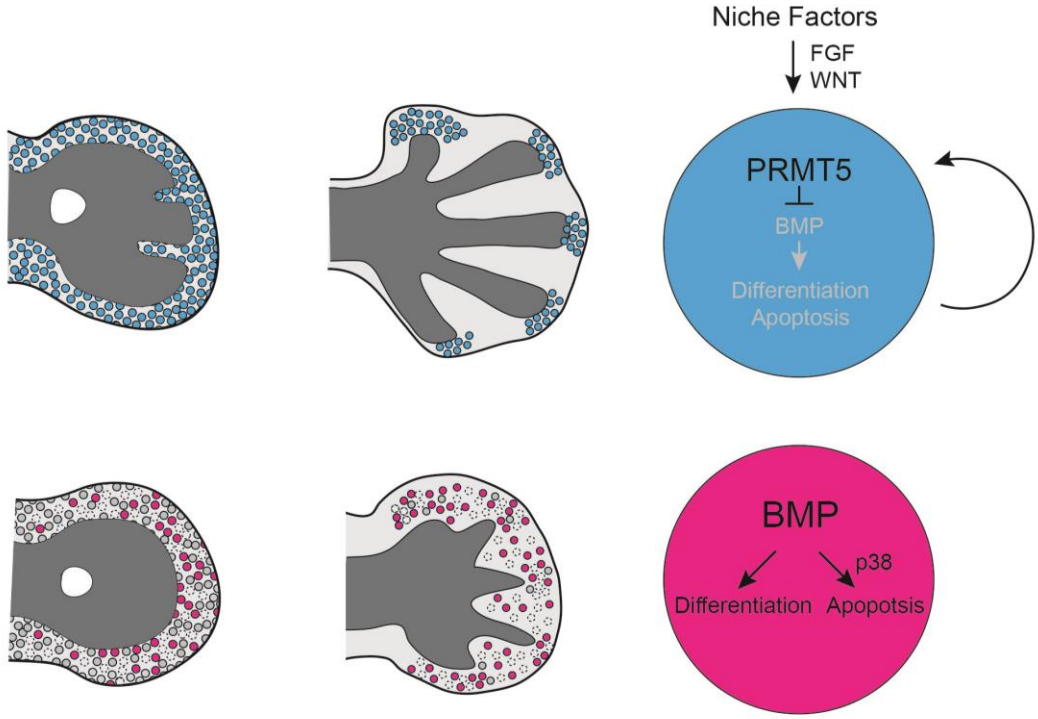

Figure 3.14: PRMT5 is essential for maintaining chondrocyte progenitor cells. During normal limb development, undifferentiated progenitor cells express PRMT5, which inhibits Bmp4, thereby promoting cell survival and limiting differentiation. Prmt5-expressing cells are progressively restricted to the distal tip of the developing digit rays where they likely continue to serve as a progenitor population to the digits. In the absence of PRMT5, widespread apoptosis depletes the chondrocyte progenitor cells, resulting in truncated skeletal elements. Without Prmt5, an upregulation of Bmp4 drives precocious differentiation and apoptosis.

Prmt5 is expressed in both the forelimb and hindlimb (Fig. 1B-G) but *Prmt5cKO* forelimbs have more severe defects than the hindlimbs (Fig. 3.4 A, E, F). Nonetheless,

nearly all hindlimb elements are reduced in size (Fig. 3.4F, L). This difference is likely due to the differential onset of *Cre* expression in the *Prx1Cre* transgene, which has delayed activity in the hindlimb compared to the forelimb (Logan et al., 2002) resulting in a longer duration of PRMT5 activity during hindlimb development in *Prmt5cKOs*. This explanation is consistent with the comparatively reduced apoptotic domain in the hindlimbs, which is more distally restricted (Fig. 3.9). Placed in the context of our model, it suggests a transient requirement for PRMT5; the later loss of *Prmt5* results in the production of more chondrocytes before the progenitor population starts undergoing apoptosis.

The expression of *Prmt5* becomes progressively restricted to undifferentiated limb mesoderm, and is finally expressed the uncondensed mesoderm distal to the digit ray (arrowheads in Fig. 1D). This region corresponds to the phalanx-forming region (PFR), an uncondensed progenitor region expressing SOX9 gives rise to progressively more distal digit elements (Suzuki et al., 2008; Witte et al., 2010). The loss of this region could contribute to the truncated, unarticulated digits in *Prmt5cKOs*. Alternatively, digit truncation could be occurring analogously to *Noggin*$^{-/-}$ embryos, in which BMP levels are elevated (Brunet et al., 1998). Both *Prmt5cKO* and *Noggin*$^{-/-}$ embryos have truncated digits that lack joints. However, *Noggin*$^{-/-}$ embryos have normal numbers of digits (and even occasionally ectopic cartilage elements) that are thick and stubby, contrasting the wispy digits in *Prmt5cKO*. It is presently unknown whether *Noggin*$^{-/-}$ autopods undergo apoptosis, and future studies will be required to clarify whether the truncated digits are primarily caused by an inability to form articulated phalanges or the depletion of a progenitor pool.

3.9.3: PRMT5-mediated mechanisms for maintaining progenitor cells

How is *Prmt5* itself regulated? The co-administration of FGF8 and WNT3a is sufficient to maintain cultured limb bud mesenchyme in a distal, undifferentiated state, likely reflecting their endogenous role (Cooper et al., 2011; ten Berge et al., 2008). It is tempting to speculate that they could maintain the expression of *Prmt5*, which would then act as a downstream effector. Interestingly, *Prmt5* also mimics the later expression pattern of *Fgf8,* which becomes restricted to the distal tip of the digit rays during later development (Lu, 2006). Another potential interacting factor is WNT5a, whose loss leads to truncated limbs that have similarities to Prmt5cKOs, although without apoptosis (Gros et al., 2010b; Wyngaarden et al., 2010; Yamaguchi et al., 1999; Yang et al., 2003). Alternatively, differentiation factors might repress *Prmt5*, restricting its expression and subsequent activity to progenitor cell populations. Although we favor the first model, additional experiments will be necessary to determine if and how external signaling factors regulate *Prmt5*.

Our results indicate that PRMT5 maintains chondrocyte progenitor cells at least in part by inhibiting BMP4-mediated differentiation. Interestingly, an *in-vivo* population of *Grem1*-expressing mesenchymal skeletal stem cells was recently identified that has the potential to give rise to bone and cartilage in postnatal animals (Worthley et al., 2015). While this population is not active in embryos, it highlights a central role for BMP suppression in both embryonic and adult progenitor populations. In several stem cell populations, *Prmt5* helps maintain pluripotency by inhibiting differentiation factors, suggesting a similar mechanism with limb bud progenitors (Nagamatsu et al., 2011; Tee et

al., 2010). PRMT5 directly interacts with several different repressor complexes including SKI and BLIMP1 (Ancelin et al., 2006; Bedford and Clarke, 2009). *Blimp1* is required for the posterior limb bud, however the *Blimp1* null limb phenotype is quite different and cell death is not affected (Robertson et al., 2007). In addition, PRMT5 symmetrically dimethylates arginines on a variety of histones, including histones H2A, H3 and H4, which affects the binding ability of repressor complexes (Tee et al., 2010; Zhao et al., 2009). Finally, PRMT5 also has the ability to methylate other proteins that could directly or indirectly inhibit differentiation. Regardless of the mechanism, the dynamic expression of *Prmt5* in multiple embryonic tissues suggests that it has a central role in maintaining embryonic progenitor cells and regulating their differentiation.

Chapter 4: Future direction and concluding remarks

In this work, we uncover specific mechanisms controlling chondrogenesis during limb development. First, I show that BMPs are necessary between E10.5 and E11.5 to negatively regulate digit number and that FGFs can inhibit BMP driven chondrogenesis, (Chapter 2). Additionally, I show that PRMT5 plays an essential role maintaining chondro-progenitor cells in the developing limb and loss of *Prmt5* results in upregulation of BMPs, apoptosis, and severe limb truncations (Chapter 3). These studies significantly advance our understanding of how chondrogenic differentiation takes place in the developing limb. However, there are still some important questions that need to be addressed: How is FGF regulating BMP-mediated chondrogenesis? How is *Prmt5* expression regulated? And how is *Prmt5* regulating factors such as BMPs?

4.1: What are the mechanism of FGF inhibition of BMP-mediated chondrogenesis?

In Chapter 2, we show that while addition of BMP to limb mesenchymal cultures promotes chondrogenesis, adding both BMP and FGFs significantly reduces differentiation. These data suggest that FGFs can inhibit BMP-mediated chondrogenesis. I hypothesize that FGFs may act through a repressor to counteract BMP-mediated chondrogenesis, and we speculated that HOX family genes may serve as this repressor. However, based on the data presented in Chapter 3, showing that PRMT5 is able to repress *Bmp4*, it is possible that PRMT5 could be the factor downstream of FGFs that inhibits BMPs. Using limb bud cultures, we could inhibit *Fgf* signaling and determine whether

Prmt5 expression is reduced. Furthermore, if we found that BMP driven chondrogenesis was no longer inhibited by the addition of FGF in the absence of *PRMT5* we could conclude that PRMT5 likely mediates FGF-mediated BMP inhibition in the limb. Crucially, these experiments could provide evidence for a direct link between the opposing roles we known for BMPs and FGFs during limb development.

4.2: FURTHER DEFINING *PRMT5* REGULATION OF CHONDROPROGENITOR CELLS

Knockout of *Prmt5* is embryonic lethal due to its essential roles in embryonic stem cell and primordial germ cell survival and pluripotency (Branscombe et al., 2001; Kim et al., 2014; Tee et al., 2010; Wang et al., 2015a). Therefore, the role of *Prmt5* in later embryonic development has never been explored. In Chapter 3 we show that *Prmt5* is expressed in discrete progenitor cell populations during development and that it is essential in limbs for the maintenance of chondroprogenitor cells (Fig. 3.1). This new role for *Prmt5* during embryogenesis leads us to wonder what are there other tissue specific roles for Prmt5 during embryogenesis? It is strongly expressed in the brain and presomitic mesoderm at E11.5, where conditional inhibition could be used to study its functions. Furthermore, while we know PRMT5 can methylate both proteins and histones to regulate cellular processes, how it is controlling gene expression within the limb is still unclear. To determine if PRMT5 globally or specifically methylates histones to repress expression, ChIP-seq for repressive histone methylation, H4R3me2s and H3R8me2s, could be combined with our *Prmt5cKO* RNA-seq data to determine direct regulation of regulatory regions around mis-expressed genes.

These studies have uncovered important events contributing to proper chondrogenic differentiation. We now have a more complete understanding of how limb buds regulate size and initiate chondrogenesis. Additionally, we now have evidence of how chondroprogentior cells in the distal limb are maintained and how they contribute to the growth of differentiating skeletal elements in the proximal limb. Furthering this research will bring us closer to a complete model of limb development.

Chapter 5: Materials and Methods

5.1: CREATION OF MOUSE STRAINS AND MANIPULATION OF EMBRYOS

Experiments involving mice were approved by the Institutional Animal Care and Use Committee at the University of Texas at Austin (protocol AUP-2013-00168).

5.1.1: *RosaGremlin* mice

A mouse *Grem1* cDNA was subcloned into pBigT and targeted to the *Rosa26* locus under control of the *Rosa26* promoter in CJ7 ES cells (Srinivas et al., 2001; Swiatek and Gridley, 1993). ES cells were then injected to generate a Cre-inducible *Gremlin*, *RosaGremlin*, (official name is Gt(ROSA)26Sor<tm1(Grem1)Svok>; Accession ID: MGI:5561086). Embryos were genotyped for the presence of the *Rosa26* knock-in allele using the following primers that generated a 315bp amplicon: 5'GCGAAG AGTTTGTCCTCAACC3' and 5' AAAGTCGCTCTGAGTTGTTAT3'. *RosaGremlin* mice were crossed to PrxCre (Logan et al., 2002), *HoxB6CreER* (Nguyen et al., 2009), *ShhCre* (Harfe et al., 2004) and RosaCreER^{T2} (Ventura et al., 2007) lines. Pregnant mice containing *HoxB6CreER* embryos were intraperitoneally injected with 3mg of Tamoxifen per 40g at specified times.

5.1.2: *Prmt5* mice

A *Prmt5* conditional mouse line, *Prmt5*$^{tm2c(EUCOMM)Wtsi}$, (hereafter referred to as *Prmt5*^{c}) was crossed with *Prx1Cre1*$^{+/-}$ males (Logan et al., 2002) to generate *Prx1Cre*$^{+/-}$

;Prmt5$^{c/+}$ males. These were crossed with *Prmt5*$^{c/c}$ females to generate *Prx1Cre*$^{+/-}$*; Prmt5*$^{c/c}$ embryos (*Prmt5cKOs*). *Prmt5* alleles were detected with the primers: 5'-TGGAACTGCAGGCATATGCC-3' and 5'-TTCTGGCCTCCATGGGGGAA-3', generating a 465 base-pair fragment for the conditional allele and a 247 base pair fragment for the wildtype allele. *Prmt5*$^{c/c}$ females were crossed with *Gt(ROSA)26Sor*$^{tm1(Grem1)Svok}$ mice (referred to as *Rosa*^{Gremlin}) (Norrie et al., 2014) to generate *Prmt5*$^{c/+}$*;Rosa*$^{Gremlin/+}$ mice that were subsequently crossed to *Prx1Cre*$^{+/-}$*;Prmt5*$^{c/+}$ mice to generate *Prx1Cre*$^{+/-}$;*Prmt5*$^{c/c}$;*Rosa*$^{Gremlin/+}$ embryos.

5.1.3: Embryonic manipulations

Skeletal preparations were performed as previously described (Allen et al., 2011). Limb skeletal elements were imaged with a Canon EOS Rebel T2i with macro lens or on a Leica M165 stereo microscope and quantified using Image J.

In cell proliferation experiments, pregnant females were intraperitoneally injected with 2mg BrdU and embryos were collected 1 hour later. Lysotracker Red staining was visualized using 1:2 benzyl alcohol:benzyl benzoate using established protocols except that limb buds were stained for 5 minutes in Lysotracker Red (Fogel et al., 2012; Zhu et al., 2008).

In-situ hybridizations were performed using standard protocols and visualized in glycerol, the exception being Col2a1 in-situs, which were visualized after 1:2 benzyl alcohol:benzyl benzoate clearing.

5.2: WESTERN BLOTS

Limb buds from E11.5, E12.5 or E16.5 limb buds (ectoderm was removed in Fig. 2.1) were homogenized in RIPA buffer (5mM Tris 7.5, 150mM NaCl, 0.1% SDS, 0.5% sodium deoxycholate, 1% Triton-X100) containing complete mini EDTA free protease inhibitors and PhosphoSTOP (Roche). Approximately 10-20µg of each sample was run on a 8% SDS PAGE gels (15% for SDMA), transferred onto PVDF membranes (nitrocellulose for pSMAD) and incubated with primary antibodies. Primary antibodies include; anti-PRMT5 (Cell signaling 07-405 1:500), anti-pSMAD 1,5,8 (Cell signaling #9511 1:500), anti-P38 (Abcam ab170099 1:2500), anti-phospho-P38 (Cell signaling #4511 1:1000), anti-GAPDH (Cell Signaling #2118 1:1000), anti-ACTIN (Sigma #A2066 1:2000), anti-SDMA (2C3D6) (Dhar et al., 2013). Membranes were then incubated in Donkey anti-rabbit secondary (Jackson Immunoresearch 711-035-152 1:2000) and developed using ECL Prime Western Blotting Detection Reagent (GE Healthcare). Band intensities were quantified (ImageQuant Chapter 2, Image J Chapter 3).

5.3: IMMUNOSTAINING

Figures 2.13 A, E were imaged on a Zeiss Axiovert Fluorescent light microscope. All other immunostaining images were taken on a Zeiss confocal (710 or LSM 700). Limb buds were fixed in 4% paraformaldehyde for 20 minutes at room temperature. Cryosections were incubated with primary. Primaries used include anti-phosphohistone H3 (1:200; Millipore #06-570), anti-Cleaved Caspase 3 (Cell signaling #9664 1:250), anti-SOX9

Alexa Fluor 488 conjugate (Millipore AB5535-AF488 1:250), anti-SOX9 (Millipore AB5535 1:250), Alexa Fluor 568 goat anti-rabbit secondary (Life technologies A11036 1:250), and DAPI (Life technologies D1306). Tunnel staining was accomplished using an *in-situ* cell death detection kit, Fluorescein (Roche 11684795910). Unless noted otherwise, confocal images collected as tiled scans and processed using ZEN (Zeiss) to obtain maximum intensity projections. The total number of phosphohistone H3-expressing cells and DAPI expressing cells were counted using CellProfiler 2.0 (r11710) as described previously (Ljosa and Carpenter, 2009). Flourescent intensity was quantified using Image J. Limb buds used for visualizing BrdU/Sox9 expression were cryosectioned prior to fixation in acetone for 2 min. Sections were then incubated for 30 minutes in 2M HCl, 5 minutes in Tris base, blocked for 15 minute at room temperature in TNB buffer (0.1M Tris pH 3.5, 0.15M NaCl, 0.5% Blocking solution (Roche #11096176001)) and incubated with primary antibodies (Sox9 1:500 - Millipore #AB5535; Biotin-conjugated BrdU 1:50 - Abcam #ab74547) and either Alexa Flour 568-conjugated goat anti-rabbit (1:250) or streptavidin-conjugated Dylight 488 (1:200) followed by DAPI. The fluorescence intensity of anit-Sox9 immunostaining was analyzed using MetaMorph.

5.4: FLOW CYTOMETRY ANALYSIS

Hindlimb autopods at E11.75 (45-49 somites, 1 litter per experiment containing hindlimbs from a minimum of 3 embryos per genotype) or E12.5 (hindlimbs from 2-3 embryos per genotype per experiment) were dissected as previously described (Lopez-Rios

et al., 2012). Cells were prepared for analysis using the FITC BrdU Flow Kit (BD Biosciences) and sorted on an LSRII Fortessa FCM (BD Biosciences). Data was analyzed using FlowJo software.

5.5: LIMB MESENCHYMAL CULTURE

We used Hindlimbs from E11.5 (45-49 somites) Prx-RG and sibling controls ($PrxCre^{+/-}$). Five separate experiments were performed, and per experiment, we pooled both hindlimbs from approximately three embryos. Limb cell cultures were performed as described in (Lewandowski et al., 2014). Briefly, for each respective genotype, limb buds were trypsinized and cells were passed through a 40uM nylon filter. Dissociated limb cells were plated at approximately 150,000 cells per well on 96-well half area plates. Limb cells were cultured for 24 hours in either control media or media supplemented with 150ng/mL FGF8b (R&D Systems,), 50ng/mL BMP4 (R&D Systems), or both. At 24 hours cells were harvested, RNA was extracted using PureLink RNA mini kit (Ambion) and treated with DNAse I. cDNA was synthesized using SuperScript II with random hexamers (Invitrogen) from 250ng of total RNA.

5.6: QUANTITATIVE RT-PCR

RNA was extracted from limb buds using Trizol Reagent (Life Technologies;15596-026) and cDNA was synthesized using SuperScript II with random hexamers (Invitrogen; 18064-014) from 500ng of DNAse 1 treated total RNA. Gene

expression experiments were performed on a Viia7 (ABI) platform using SensiFast SYBR Lo-Rox (Bioline). Unless specified otherwise in the figure legends, values were normalized to beta-actin. Fold-changes in gene expression was calculated using the delta-CT method (Livak and Schmittgen, 2001). Primers used in this study are listed in Table 1.

Acctb	F	GCTGTATTCCCCTCCATCGTG
	R	CACGGTTGGCCTTAGGGTTCAG
Agc1	F	AGGACTGAAATCAGCGGAGA
	R	AGGGACATGGTTGTTTCTGC
Axin2	F	GAGGAGATCGAGGCAGAAGC
	R	CACCTCTGCTGCCACAAAAC
Bmp2	F	CAAAGCAGGACCAGTGGGAA
	R	AGCCCCCTGGAAGGGATTAT
Bmp4	F	ACGTACTCCCAAGCATCACC
	R	GCACAATGGCATGGTTGGTT
Bmp7	F	CGCACTCTCCCTCACAGTAG
	R	AAGACGCCAAAGAACCAAGA
Cdk6	F	TCCCAGGAGAGGAAGACTGG
	R	GCCGTAGGCGGATATCCTTT
Col2a1	F	GATGGCTGGAGGGTATGACG
	R	CAGGTTCACCAGGATTGCCT
Dusp6	F	CGGAAATGGCGATCTGCAAG
	R	GACGACTCGTACAGCTCCTG
Fgf8	F	CCGGACCTACCAGCTCTACA
	R	GGCAATTAGCTTCCCCTTCT
Gapdh	F	GGTGAAGGTCGGTGTGAACG
	R	CTCGCTCCTGGAAGATGGTG
Gli1	F	CCCAGCTCGCTCCGCAAACA
	R	CTGCTGCGGCATGGCACTCT

Table 5.1: qRT-PCR primer sequences.

HoxD13	F	TGTCCACTTTTGGATCCGG
	R	TTCTTCCTTCCCCGTCGGTA
Msx2	F	CAAGTGAAGGGGGAGGTGTA
	R	CAGGGACCTGACATGGAGTT
Prdm1	F	ATCCAGCTTCCCTACCGAGT
	R	GGGGGACTACTCTCGTCCTT
Ptch1	F	GACCGGCCTTGCCTCAACCC
	R	CAGGGCGTGAGCGCTGACAA
Shh	F	TCTCGAGACCCAACTCCGAT
	R	GACTTGTCTCCGATCCCCAC
Smad7	F	CCTTCCCTTTGGATCAGCGT
	R	CACTATGAGCCTCTCAGCCG
Sox9	F	TAAGTTCCCCGTGTGCATCC
	R	TTGCCCAGAGTCTTGCTGAG
Spry4	F	GACCCACTCGGGTTCGGGGA
	R	GGGGCGCTCTGCTGTCAAGG

Table 5.1 Continued.

5.7: RNA-SEQ

RNA from three control and two *Prmt5cKO* forelimbs were pair-end sequenced on the Illumina HiSeq 2500 platform. On average we obtained over 26 million aligned pairs per sample. Reads were analyzed using FastQC and sequences were trimmed to 100bp using FASTX-Toolkit. Trimmed sequences were aligned to the mouse mm10 genome using Tophat/2.0.10 (with Bowtie/2.1.0) (Trapnell et al., 2012). Aligned reads were assembled, merged, and tested for differential expression using Cufflinks/2.1.1 (Trapnell et al., 2012). Differential expression data was analyzed in R using

CummeRbund (RStudioTeam, 2015; Trapnell et al., 2012). We chose genes with a fold-change>2, an average FPKM >1, and a q-value<0.01 (Storey and Tibshirani, 2003) in expression between control and *Prmt5cKO* (208 genes) for GO analysis. The RNA-seq datasets were deposited in GEO (accession #GSE79487).

To identify retained introns, we first identified genes with two or more exons and mapped sequencing reads to their defined exonic and intronic regions using mouse mm10 "TxDb.Mmusculus.UCSC.mm10.knownGene" (R package version 3.2.2). For each gene, we assumed the read count of intron X followed a binomial distribution with parameters n and p. We then calculated X~B(n,p), where n was the total read count of the gene, and p was the probability a read came from an intron. We fit this to a logistic regression model to estimate the coefficient β_1:

log(p/(1-p))= β_0+β_1*group, where group was 0 for control and 1 for *Prmt5cKO*

Based on this model, changing the genetic background from control to *Prmt5cKO* would increase the odds of a read coming from intron by e^{β_1} fold. The mean of estimated $e^{\hat{\beta}_1}$ across all genes was 1.30, and the 95% confidence interval was (1.22, 1.38). Across all analyzed genes, the average of β_1 is significantly different from 0 (One Sample t-test, $p < 0.001$).

Appendix A: RosaGrem digit phenotype quantification

This appendix contains tables quantifying digit phenotypes in various RosaGremlin crosses.

PrxCre		
	WT	RG
	Hindlimb	
Polydactyly	0	10
Normal	15	0
Total	15	10
	Forelimb	
Polydactyly	0	1
Digit Reduction	0	2
No Forelimb	0	7
Normal	15	0
Total	15	10

Table A.1: PrxCre E18.5 digit phenotypes. Polydactyly is the presence of an ectopic digit. Digit reductions refer to embryos with less than 5 digits. Embryos with no forelimbs had only small pieces of cartilage attached to the scapula.

ShhGFPCre		
	WT	RG
	Hindlimb	
Polydactyly	0	3
Distal Bifurcations	0	1
Normal	4	0
Total	4	4
	Forelimb	
Polydactyly	0	1
Nubs	0	3
Normal	4	0
Total	4	4

Table A.2: ShhCre E18.5 digit phenotypes. Polydactyly is the presence of an ectopic posterior digit. Distal bifurcations refer to ectopic pieces of cartilage attached to the distal phalanges. Nubs refer to ectopic pieces of cartilage on the outside of the anterior or posterior most digit.

HoxB6CreER															
	Hindlimb														
	9.5			10			10.5			11			11.5		
	WT	RG	RGG	WT	RG	RGG	WT	RG	RGG	WT	RG	RGG	WT	RG	RGG
Polydactyly	-	-	-	-	-	8	-	3	3	-	-	-	-	-	-
Distal Bifurcation	-	-	-	-	-	-	-	1	-	-	1	3	-	-	-
Nubs	-	-	-	-	1	-	-	2	-	-	5	-	-	2	3
No Hindlimb	-	1	3	-	-	-	-	-	-	-	-	-	-	-	-
Normal	4	3	2	8	-	-	7		-	5	-	1	2		
Total	4	4	5	8	1	8	7	6	3	5	6	4	2	2	3
	Forelimb														
Nubs	-	-	-	-	1	8	-	6	3	-	4	4	-	-	-
Digit Reduction	-	1	3	-	-	-	-	-	-	-	-	-	-	-	-
Normal	4	3	2	8	-	-	7	-	-	5	2	-	2	2	3
Total	4	4	5	8	1	8	7	6	3	5	6	4	2	2	3

Table A3: HoxB6Cre E18.5 digit phenotypes. Polydactyly is the presence of an ectopic posterior digit. Distal bifurcations refer to ectopic pieces of cartilage attached to the distal phalanges. Nubs refer to ectopic pieces of cartilage on the outside of the anterior or posterior most digit. Embryos without hindlimbs had only ectopic pieces of cartilage on their pelvic gurdle. Digit reductions refer to embryos with less than 5 digits.

RosaCreER								
	Hindlimb							
	9.5		10.5		11.5		12.5	
	WT	RG	WT	RG	WT	RG	WT	RG
Polydactyly	-	5	-	-	-	-	-	-
Nubs	-	7	-	5	-	-	-	-
Normal	6	-	6	-	7	5	4	4
Total	6	12	6	5	7	5	4	4
	Forelimbs							
Nubs	-	12	-	5	-	3	-	-
Normal	6	-	6	-	7	2	4	4
Total	6	12	6	5	7	5	4	4

Table A4: RosaCreER E18.5 digit phenotypes. Polydactyly is the presence of an ectopic posterior digit. Nubs refer to ectopic pieces of cartilage on the outside of the anterior or posterior most digit.

Appendix B: Prmt5cKO RNA-seq data

This appendix contains a table of differentially expressed genes in *Prmt5cKO* from RNA-seq analysis and a table of GO terms associated with those genes.

Table B1

Gene Name	Control FPKM	*Prmt5cKO* FPKM	log2 fold_change	q_value
Kdm5d	0.055	16.370	8.206	0.00E+00
Ddx3y	0.084	21.779	8.018	0.00E+00
Uty	0.068	12.509	7.522	0.00E+00
Eif2s3y	0.073	12.526	7.422	1.95E-09
Ano3	0.077	6.145	6.316	2.18E-13
Eda2r	0.520	17.887	5.105	0.00E+00
Mir34a	0.217	4.439	4.357	0.00E+00
Ptprv	0.315	3.927	3.642	0.00E+00
Pvt1	0.211	2.022	3.260	1.22E-13
Ccng1	14.217	82.207	2.532	0.00E+00
Cdkn1a	3.450	19.893	2.528	0.00E+00
Fam212b	0.643	3.413	2.408	0.00E+00
Phlda3	8.356	36.502	2.127	0.00E+00
Zmat3	3.036	11.958	1.978	0.00E+00
Cgref1	0.896	3.424	1.934	2.65E-06
9230114K14Rik	0.847	3.117	1.880	4.25E-06
Mpeg1	0.844	2.880	1.770	1.57E-08
Zfp365	2.140	7.047	1.720	2.13E-14
Ddit4l	1.886	6.031	1.677	4.19E-09
C030034I22Rik	0.564	1.733	1.620	1.82E-05
Sesn2	3.204	9.622	1.586	2.13E-14
Grem1	7.996	23.527	1.557	0.00E+00
Slc19a2	4.097	11.704	1.514	0.00E+00
Aen	12.552	35.395	1.496	0.00E+00
Gria3	1.287	3.502	1.444	1.87E-10
Bbc3	1.903	5.072	1.414	2.35E-07
C3ar1	0.722	1.897	1.393	1.00E-04
Mapkapk3	2.229	5.837	1.389	1.47E-12
Klk14	0.936	2.432	1.377	7.06E-03
Tnfrsf10b	3.834	9.939	1.374	0.00E+00
Gtse1	13.245	33.535	1.340	0.00E+00
Gm11974	12.439	31.146	1.324	0.00E+00
Abcb1b	1.019	2.527	1.311	2.96E-04
Styk1	0.682	1.687	1.307	4.35E-05
Tyrobp	3.406	8.416	1.305	3.64E-03
Cd36	0.596	1.467	1.300	1.19E-04
Ass1	2.616	6.399	1.291	8.61E-08
Pvt1	2.765	6.747	1.287	1.39E-03
Snhg4	8.863	21.559	1.282	1.44E-07

Table B1 continued

Gene Name	Control FPKM	*Prmt5cKO* FPKM	log2 fold_change	q_value
Snord104	15.793	36.317	1.201	8.65E-10
Fgfbp3	1.235	2.827	1.195	4.45E-03
Def6	3.388	7.739	1.192	4.23E-06
9030025P20Rik	5.929	13.429	1.179	1.04E-07
Emr1	1.898	4.290	1.177	1.58E-07
4632434I11Rik	7.482	16.900	1.175	0.00E+00
C1qb	5.491	12.373	1.172	1.14E-04
Bax	54.153	120.684	1.156	0.00E+00
Pmaip1	12.480	27.748	1.153	3.87E-13
Arap2	0.760	1.626	1.099	8.81E-10
Rab26os	32.080	68.314	1.091	1.26E-07
Btbd19	1.032	2.194	1.088	2.39E-04
Mybl1	3.720	7.901	1.087	0.00E+00
1500015A07Rik	3.430	7.246	1.079	2.30E-07
Myo1f	0.684	1.441	1.075	6.94E-03
Fcgr3	1.917	4.033	1.073	6.38E-03
Tfap2c	2.259	4.722	1.064	1.96E-08
Pidd1	3.846	7.894	1.037	0.00E+00
Polk	5.911	12.050	1.028	0.00E+00
Bmp4	16.058	32.429	1.014	0.00E+00
Prrg4	0.690	1.393	1.013	7.26E-04
Rhbdf2	1.391	2.791	1.005	1.51E-03
Fgf8	7.170	14.368	1.003	1.19E-10
Kptn	9.782	4.877	-1.004	5.35E-05
Dnah7b	2.954	1.473	-1.004	4.37E-07
Tmem163	2.305	1.148	-1.006	2.80E-03
Nbl1	25.501	12.690	-1.007	1.59E-07
Fibin	22.320	11.090	-1.009	1.09E-12
Adamts12	2.843	1.412	-1.009	0.00E+00
Postn	9.461	4.698	-1.010	0.00E+00
Prob1,Spata24	11.269	5.579	-1.014	5.22E-06
Gpr153	4.040	1.993	-1.020	2.46E-08
Id4	6.666	3.283	-1.022	2.50E-07
Mir6901	12.460	6.133	-1.023	0.00E+00
Rnf182	1.527	0.751	-1.024	3.87E-03
2700069I18Rik	8.058	3.958	-1.026	7.66E-03
Gsap	1.428	0.700	-1.027	1.54E-03
Mir1193	11.620	5.691	-1.030	5.61E-03
Mmp11	17.369	8.487	-1.033	1.25E-08
Olfml3	26.134	12.756	-1.035	4.11E-10
Nek8	6.483	3.154	-1.039	1.81E-10
Rasa4	1.797	0.874	-1.040	3.73E-04
Pde1c	1.545	0.751	-1.042	4.35E-05
Matn4	8.340	4.036	-1.047	6.05E-11
Sfmbt2	1.447	0.699	-1.049	1.63E-03
Rarb	2.843	1.372	-1.051	1.40E-04
Foxc1	8.987	4.335	-1.052	3.38E-10
BC002163	18.550	8.918	-1.057	1.63E-03

Table B1 continued

Gene Name	Control FPKM	*Prmt5cKO* FPKM	log2 fold_change	q_value
Spag4	1.749	0.838	-1.061	9.53E-03
Ttc38	3.441	1.649	-1.061	2.77E-06
Hs3st3a1	8.019	3.843	-1.061	1.24E-07
Carkd	31.306	14.968	-1.065	0.00E+00
Mpnd	54.487	26.040	-1.065	4.69E-12
Adcy4	5.829	2.783	-1.066	1.57E-11
Rnaseh2c	104.536	49.797	-1.070	3.99E-10
Flot1	15.314	7.295	-1.070	3.61E-08
Cpq	16.314	7.770	-1.070	3.50E-08
Ino80b	104.315	49.634	-1.072	0.00E+00
Dpyd	4.855	2.309	-1.072	4.05E-07
Bves	7.876	3.733	-1.077	1.41E-10
Nxph3	2.218	1.051	-1.078	8.54E-03
Hpse2	14.662	6.928	-1.082	0.00E+00
1600016N20Rik	2.024	0.956	-1.083	9.58E-03
Emp2	4.369	2.059	-1.086	8.62E-05
Scrn1	5.262	2.476	-1.087	1.24E-07
Shisa2	39.067	18.354	-1.090	4.14E-14
Mycbpap	1.689	0.788	-1.100	2.33E-04
Abca8b	2.382	1.110	-1.101	2.18E-13
Flywch2	21.386	9.957	-1.103	2.25E-08
Abca9	1.538	0.711	-1.113	2.18E-06
Pisd-ps1	16.392	7.563	-1.116	0.00E+00
Zcwpw1	4.839	2.229	-1.118	3.91E-08
Rnasel	5.349	2.462	-1.120	1.42E-13
Glb1l2	1.941	0.892	-1.121	4.66E-05
Chrdl1	12.794	5.876	-1.123	0.00E+00
Cadps2	5.443	2.498	-1.124	0.00E+00
Csgalnact1	1.624	0.741	-1.131	1.92E-04
Sat2	5.628	2.569	-1.131	3.11E-04
Lmbr1	5.426	2.468	-1.137	3.63E-04
Tubb4a	1.764	0.802	-1.138	7.61E-03
Hpse	1.699	0.770	-1.142	1.09E-03
Samd12	4.149	1.872	-1.148	5.60E-03
Fdxr	6.799	3.063	-1.151	1.15E-06
Zcchc12	5.053	2.270	-1.154	9.37E-09
Isoc2a	11.321	5.033	-1.169	3.11E-05
Ebf2	6.693	2.971	-1.172	3.05E-09
Pgm5	17.130	7.596	-1.173	2.84E-11
Prss35	4.013	1.776	-1.176	2.53E-09
Osr2	6.565	2.887	-1.185	5.56E-09
Vill	15.089	6.608	-1.191	0.00E+00
Strip2	1.557	0.681	-1.192	2.47E-04
Nqo1	8.849	3.851	-1.200	1.04E-05
Slc2a13	1.616	0.703	-1.202	1.00E-04
Dpf3	2.004	0.869	-1.206	1.68E-03
Glis3	2.249	0.972	-1.211	1.89E-05
Acss2	5.489	2.368	-1.213	4.72E-08

Table B1 continued

Gene Name	Control FPKM	*Prmt5cKO* FPKM	log2 fold_change	q_value
Fam101a	6.332	2.716	-1.221	2.77E-06
Pcdhb22	3.661	1.570	-1.221	9.51E-09
Hacl1	4.481	1.914	-1.227	1.43E-08
Gfra3	1.923	0.820	-1.230	3.60E-03
Sdpr	3.386	1.442	-1.231	7.14E-05
Cdh8	1.693	0.721	-1.231	2.59E-03
Dcn	7.447	3.170	-1.232	1.08E-09
Adamts5	5.174	2.198	-1.235	1.00E-09
Serhl	7.769	3.298	-1.236	5.39E-05
Svopl	4.386	1.862	-1.236	3.58E-05
Nlrp5-ps	14.036	5.929	-1.243	0.00E+00
Kera	10.395	4.380	-1.247	0.00E+00
Ift43	23.670	9.869	-1.262	2.60E-12
Wfikkn2	7.616	3.167	-1.266	0.00E+00
Hyi	3.996	1.647	-1.279	3.01E-03
Tle6	1.851	0.758	-1.288	7.47E-04
Pak7	1.605	0.656	-1.290	3.65E-04
Pycr1	4.804	1.962	-1.292	1.08E-05
D030045P18Rik	2.082	0.848	-1.295	3.76E-03
Rab3d	3.219	1.311	-1.296	5.91E-04
Gprin2	1.710	0.688	-1.314	2.52E-06
Snta1	3.494	1.401	-1.318	1.06E-04
Tcp11l2	3.374	1.351	-1.320	8.12E-05
Fuz	4.065	1.625	-1.323	1.65E-04
Col8a2	3.264	1.304	-1.324	1.07E-06
Hkdc1	1.833	0.730	-1.327	2.04E-04
9430076C15Rik,Creb5	8.925	3.553	-1.329	0.00E+00
Pnck	4.601	1.823	-1.335	6.45E-06
Sulf1	63.851	25.164	-1.343	0.00E+00
Mansc4	1.658	0.653	-1.344	2.27E-03
Atp1a2	2.333	0.916	-1.348	1.63E-08
H2-Ke6	12.356	4.798	-1.365	3.75E-06
Gas2	43.764	16.934	-1.370	0.00E+00
Ndrg2	8.127	3.124	-1.379	0.00E+00
Gsc	9.216	3.489	-1.401	7.80E-08
Col9a1	118.337	44.694	-1.405	0.00E+00
Col9a2	27.036	10.185	-1.409	0.00E+00
Egfl6	3.821	1.419	-1.429	4.04E-07
Nkx3-2	3.337	1.232	-1.438	2.77E-06
Csad	8.509	3.125	-1.445	1.86E-08
Pde9a	8.179	2.960	-1.466	0.00E+00
Haghl	24.555	8.680	-1.500	0.00E+00
Aplp1	7.240	2.556	-1.502	9.51E-09
Rdm1	13.017	4.575	-1.509	7.80E-08
Col16a1	5.828	2.001	-1.542	0.00E+00
Athl1	10.940	3.746	-1.546	2.18E-13
Gstm7	15.019	4.878	-1.622	0.00E+00
Prmt5	40.900	12.518	-1.708	0.00E+00

Table B1 continued

Gene Name	Control FPKM	*Prmt5cKO* FPKM	log2 fold_change	q_value
Gulo	2.281	0.684	-1.738	1.92E-06
Col9a3	22.962	6.857	-1.744	0.00E+00
Mid1	7.679	2.274	-1.755	0.00E+00
Mturn	6.668	1.971	-1.758	0.00E+00
Pamr1	3.397	1.003	-1.760	3.05E-09
Miat	3.683	1.057	-1.800	0.00E+00
Acss3	3.968	1.132	-1.809	4.14E-14
Trpm5	1.761	0.484	-1.862	3.14E-11
Loxl1	7.136	1.929	-1.888	0.00E+00
Eps8l1	2.290	0.602	-1.928	1.89E-09
Fxyd1	3.329	0.847	-1.974	5.87E-03
Isoc2b	1.646	0.411	-2.003	5.08E-03
Eomes	2.133	0.532	-2.003	2.36E-10
Cpa4	7.112	1.729	-2.040	8.28E-09
Irx1	3.251	0.694	-2.227	1.43E-09
Gdf5	12.863	2.666	-2.271	0.00E+00
Gstm6	2.672	0.483	-2.468	3.38E-05
BC006965	1.768	0.250	-2.819	4.23E-06
G530011O06Rik	6.231	0.771	-3.015	0.00E+00
Erdr1	42.128	5.028	-3.067	0.00E+00
Gm13154	1.889	0.200	-3.242	5.68E-03
Klk1b22	2.902	0.148	-4.295	3.32E-03
Erdr1	14.787	0.677	-4.449	0.00E+00
Rprl3	2301.320	9.878	-7.864	0.00E+00
BC107364	1540.270	3.433	-8.809	0.00E+00

Table B1. Differentially expressed genes in *Prmt5cKOs*. Results from RNA-seq analysis from control and *Prmt5cKO* E11.5 forelimb buds. Genes listed have an average FPKM > 1, a log2 fold change > 1, and a q-value < 0.01. Abbreviation: FPKM, Fragments Per Kilobase of Exon Per Million Fragments Mapped.

Table B2

GO Term	Gene Names	p-value
Signal transduction by p53 class mediator genes	*Bbc3, Tnfrsf10b, Bax, Pmaip1, Phlda3, Aen*	1.00E-04
Negative regulation of cellular processes	*Mid1, Id4, Tfap2c, Prmt5, Aplp1, Osr2, Nbl1, Gsc, Phlda3, Bmp4, 4632434I11Rik, Bax, Uty, Bbc3, Ccng1, Fgf8, Vill, Eomes, Rarb, Cd36, Zmat3, Pde1c, Ddit4l, Sesn2, Foxc1, Klk14, Gas2, Glis3, Ndrg2, Sulf1, Pak7, Erdr1, Grem1, Cdkn1a, Cgref1, Myo1f, Gdf5, Pmaip1, Rhbdf2, Ptprv, Nkx3-2*	2.00E-04
Embryonic hindlimb morphogenesis	*Fgf8, Lmbr1, Rarb, Osr2, Bmp4*	2.00E-04
Chondrocyte differentiation	*Gdf5, Sulf1, Rarb, Nkx3-2, Osr2, Bmp4*	4.00E-04
Sensory organ development	*Fgf8, Gsc, C1qb, Chrdl1, Rarb, Miat, Bmp4, Bax, Nkx3-2, Osr2, Foxc1, Kera, Col8a2*	7.00E-04
Telencephalon development	*Fgf8, Id4, Tfap2c, Bax, Rarb, Eomes, Bmp4*	1.40E-03
Extracellular matrix organization	*Csgalnact1, Aplp1, Postn, Egfl6, Sulf1, Grem1, Foxc1*	1.40E-03
Intrinsic apoptotic signaling pathway	*Cdkn1a, Bbc3, Pmaip1, Ptprv, Phlda3, Grem1, Aen*	1.40E-03
Bone morphogenesis	*Csgalnact1, Rarb, Osr2, Col9a1, Bmp4*	1.40E-03
Kidney development	*Fgf8, Bax, Sulf1, Grem1, Osr2, Foxc1, Bmp4*	2.40E-03
BMP signaling pathway	*Fgf8, Zcchc12, Sulf1, Grem1, Nbl1, Bmp4*	2.40E-03
Embryonic skeletal system development	*Gsc, Fuz, Sulf1, Nkx3-2, Osr2, Bmp4*	2.40E-03

Table B2. GO terms of differentially expressed genes. GO analysis of the 208 differentially expressed genes. GO terms are listed with the gene names for each category and the associated p-value.

Glossary

BMP- Bone morphogenetic protein

SHH- Sonic hedgehog

FGF- Fibroblast growth factor

PRMT5- Protein arginine methyltransferase

GREM1- Gremlin1

FPKM- Fragments Per Kilobase of transcript per Million mapped reads

Prx-RG- $Prx1Cre^{+/-};Rosa^{Gremlin/+}$

HoxB6CreER-RG- $HoxB6CreER^{+/-};Rosa^{Gremlin/+}$

HoxB6CreER-RG- $HoxB6CreER^{+/-};Rosa^{Gremlin/Gremlin}$

Prmt5cKO- $Prx1Cre^{+/-};Prmt5^{c/c}$

References

Ahn, K., Mishina, Y., Hanks, M.C., Behringer, R.R., Crenshaw, E.B., 2001. BMPR-IA signaling is required for the formation of the apical ectodermal ridge and dorsal-ventral patterning of the limb. Development (Cambridge, England) 128, 4449-4461.

Akiyama, H., Kim, J.E., Nakashima, K., Balmes, G., Iwai, N., Deng, J.M., Zhang, Z., Martin, J.F., Behringer, R.R., Nakamura, T., de Crombrugghe, B., 2005. Osteo-chondroprogenitor cells are derived from Sox9 expressing precursors. Proc Natl Acad Sci U S A 102, 14665-14670.

Al-Qattan, M.M., Al-Motairi, M.I., Al Balwi, M.A., 2015. Two novel homozygous missense mutations in the GDF5 gene cause brachydactyly type C. American journal of medical genetics. Part A 167, 1621-1626.

Allen, Benjamin L., Song, Jane Y., Izzi, L., Althaus, Irene W., Kang, J.-S., Charron, F., Krauss, Robert S., McMahon, Andrew P., 2011. Overlapping Roles and Collective Requirement for the Coreceptors GAS1, CDO, and BOC in SHH Pathway Function. Developmental Cell 20, 775-787.

Ancelin, K., Lange, U.C., Hajkova, P., Schneider, R., Bannister, A.J., Kouzarides, T., Surani, M.A., 2006. Blimp1 associates with Prmt5 and directs histone arginine methylation in mouse germ cells. Nature Cell Biology 8, 623-630.

Antonysamy, S., Bonday, Z., Campbell, R.M., Doyle, B., Druzina, Z., Gheyi, T., Han, B., Jungheim, L.N., Qian, Y., Rauch, C., Russell, M., Sauder, J.M., Wasserman, S.R., Weichert, K., Willard, F.S., Zhang, A., Emtage, S., 2012. Crystal structure of the human PRMT5:MEP50 complex. Proceedings of the National Academy of Sciences of the United States of America 109, 17960-17965.

Badugu, A., Kraemer, C., Germann, P., Menshykau, D., Iber, D., 2012. Digit patterning during limb development as a result of the BMP-receptor interaction. Scientific Reports 2.

Bandyopadhyay, A., Tsuji, K., Cox, K., Harfe, B.D., Rosen, V., Tabin, C.J., 2006. Genetic Analysis of the Roles of BMP2, BMP4, and BMP7 in Limb Patterning and Skeletogenesis. PLoS Genetics 2, e216-e216.

Barna, M., Niswander, L., 2007. Visualization of Cartilage Formation: Insight into Cellular Properties of Skeletal Progenitors and Chondrodysplasia Syndromes. Developmental Cell 12, 931-941.

Barrow, J.R., 2003. Ectodermal Wnt3/beta -catenin signaling is required for the establishment and maintenance of the apical ectodermal ridge. Genes & Development 17, 394-409.

Bastida, M.F., Sheth, R., Ros, M.A., 2009. A BMP-Shh negative-feedback loop restricts Shh expression during limb development. Development 136, 3779-3789.

Bedford, M.T., Clarke, S.G., 2009. Protein arginine methylation in mammals: who, what, and why. Mol Cell 33, 1-13.

Bell, D.M., Leung, K.K.H., Wheatley, S.C., Ng, L.J., Zhou, S., Wing Ling, K., Har Sham, M., Koopman, P., Tam, P.P.L., Cheah, K.S.E., 1997. SOX9 directly regulates the type-ll collagen gene. Nature Genetics 16, 174-178.

Bénazet, J.-D., Bischofberger, M., Tiecke, E., Gonçalves, A., Martin, J.F., Zuniga, A., Naef, F., Zeller, R., 2009. A self-regulatory system of interlinked signaling feedback loops controls mouse limb patterning. Science (New York, N.Y.) 323, 1050-1053.
Benazet, J.-D., Zeller, R., 2013. Dual requirement of ectodermal Smad4 during AER formation and termination of feedback signaling in mouse limb buds. genesis, 1-7.
Benazet, J.D., Bischofberger, M., Tiecke, E., Goncalves, A., Martin, J.F., Zuniga, A., Naef, F., Zeller, R., 2009. A Self-Regulatory System of Interlinked Signaling Feedback Loops Controls Mouse Limb Patterning. Science 323, 1050-1053.
Benazet, J.D., Pignatti, E., Nugent, A., Unal, E., Laurent, F., Zeller, R., 2012. Smad4 is required to induce digit ray primordia and to initiate the aggregation and differentiation of chondrogenic progenitors in mouse limb buds. Development 139, 4250-4260.
Bi, W., Deng, J.M., Zhang, Z., Behringer, R.R., de Crombrugghe, B., 1999. Sox9 is required for cartilage formation. Nature genetics 22, 85-89.
Biesecker, L.G., 2011. Polydactyly: How many disorders and how many genes? 2010 update. Developmental Dynamics 240, 931-942.
Boehm, B., Westerberg, H., Lesnicar-Pucko, G., Raja, S., Rautschka, M., Cotterell, J., Swoger, J., Sharpe, J., 2010. The Role of Spatially Controlled Cell Proliferation in Limb Bud Morphogenesis. PLoS Biology 8, e1000420-e1000420.
Bragdon, B., Moseychuk, O., Saldanha, S., King, D., Julian, J., Nohe, A., 2011. Bone morphogenetic proteins: a critical review. Cellular signalling 23, 609-620.
Branscombe, T.L., Frankel, A., Lee, J.H., Cook, J.R., Yang, Z.h., Pestka, S., Clarke, S., 2001. PRMT5 (Janus Kinase-binding Protein 1) Catalyzes the Formation of Symmetric Dimethylarginine Residues in Proteins. Journal of Biological Chemistry 276, 32971-32976.
Brunet, L.J., McMahon, J.A., McMahon, A.P., Harland, R.M., 1998. Noggin, cartilage morphogenesis, and joint formation in the mammalian skeleton. Science 280, 1455-1457.
Buckland, R.A., Collinson, J.M., Graham, E., Davidson, D.R., Hill, R.E., 1998. Antagonistic effects of FGF4 on BMP induction of apoptosis and chondrogenesis in the chick limb bud. Mechanisms of development 71, 143-150.
Burgos, E.S., Wilczek, C., Onikubo, T., Bonanno, J.B., Jansong, J., Reimer, U., Shechter, D., 2015. Histone H2A and H4 N-terminal Tails Are Positioned by the MEP50 WD Repeat Protein for Efficient Methylation by the PRMT5 Arginine Methyltransferase. Journal of Biological Chemistry 290, 9674-9689.
Byrnes, A.M., Racacho, L., Nikkel, S.M., Xiao, F., MacDonald, H., Underhill, T.M., Bulman, D.E., 2010. Mutations in GDF5 presenting as semidominant brachydactyly A1. Human mutation 31, 1155-1162.
Capdevila, J., Tsukui, T., Rodriquez Esteban, C., Zappavigna, V., Izpisua Belmonte, J.C., 1999a. Control of vertebrate limb outgrowth by the proximal factor Meis2 and distal antagonism of BMPs by Gremlin. Mol. Cell 4, 839-849.
Capdevila, J., Tsukui, T., Rodríquez Esteban, C., Zappavigna, V., Izpisúa Belmonte, J.C., 1999b. Control of vertebrate limb outgrowth by the proximal factor Meis2 and distal antagonism of BMPs by Gremlin. Molecular cell 4, 839-849.

Chari, A., Golas, M.M., Klingenhager, M., Neuenkirchen, N., Sander, B., Englbrecht, C., Sickmann, A., Stark, H., Fischer, U., 2008. An assembly chaperone collaborates with the SMN complex to generate spliceosomal SnRNPs. Cell 135, 497-509.
Chiang, C., 2001. Manifestation of the limb prepattern: limb development in the absence of Sonic hedgehog function. Dev. Biol. 236, 421-435.
Chiang, C., Litingtung, Y., Lee, E., Young, K.E., Corden, J.L., Westphal, H., Beachy, P.A., 1996. Cyclopia and defective axial patterning in mice lacking Sonic hedgehog gene function. Nature 383, 407-413.
Choi, K.-S., Lee, C., Maatouk, D.M., Harfe, B.D., 2012. Bmp2, Bmp4 and Bmp7 Are Co-Required in the Mouse AER for Normal Digit Patterning but Not Limb Outgrowth. PLoS ONE 7, e37826-e37826.
Cooper, K.L., Hu, J.K.H., ten Berge, D., Fernandez-Teran, M., Ros, M.A., Tabin, C.J., 2011. Initiation of Proximal-Distal Patterning in the Vertebrate Limb by Signals and Growth. Science 332, 1083-1086.
Cuadrado, A., Lafarga, V., Cheung, P.C., Dolado, I., Llanos, S., Cohen, P., Nebreda, A.R., 2007. A new p38 MAP kinase-regulated transcriptional coactivator that stimulates p53-dependent apoptosis. Embo j 26, 2115-2126.
Derynck, R., Zhang, Y.E., 2003. Smad-dependent and Smad-independent pathways in TGF-β family signalling. Nature 425, 577-584.
Dhar, S., Vemulapalli, V., Patananan, A.N., Huang, G.L., Di Lorenzo, A., Richard, S., Comb, M.J., Guo, A., Clarke, S.G., Bedford, M.T., 2013. Loss of the major Type I arginine methyltransferase PRMT1 causes substrate scavenging by other PRMTs. Sci Rep 3, 1311.
Di Lorenzo, A., Bedford, M.T., 2011. Histone arginine methylation. FEBS letters 585, 2024-2031.
Dudley, A.T., Ros, M.A., Tabin, C.J., 2002. A re-examination of proximodistal patterning during vertebrate limb development. Nature 418, 539-544.
Dunn, N.R., Winnier, G.E., Hargett, L.K., Schrick, J.J., Fogo, A.B., Hogan, B.L.M., 1997. Haploinsufficient Phenotypes inBmp4Heterozygous Null Mice and Modification by Mutations inGli3andAlx4. Developmental Biology 188, 235-247.
Eimon, P.M., Harland, R.M., 1999. In Xenopus Embryos, BMP Heterodimers Are Not Required for Mesoderm Induction, but BMP Activity Is Necessary for Dorsal/Ventral Patterning. Developmental Biology 216, 29-40.
Fallon, J., 1994. FGF-2: Apical ectodermal ridge growth signal for chick limb development. Science 264, 104-107.
Farin, H.F., Lüdtke, T.H.W., Schmidt, M.K., Placzko, S., Schuster-Gossler, K., Petry, M., Christoffels, V.M., Kispert, A., 2013. Tbx2 Terminates Shh/Fgf Signaling in the Developing Mouse Limb Bud by Direct Repression of Gremlin1. PLoS Genetics 9, e1003467-e1003467.
Feng, X.H., Derynck, R., 2005. Specificity and versatility in tgf-beta signaling through Smads. Annual review of cell and developmental biology 21, 659-693.
Fogel, J.L., Thein, T.Z.T., Mariani, F.V., 2012. Use of LysoTracker to detect programmed cell death in embryos and differentiating embryonic stem cells. Journal of visualized experiments : JoVE.

Fromental-Ramain, C., Warot, X., Messadecq, N., LeMeur, M., Dollé, P., Chambon, P., 1996. HOXA-13 and HOXD-13 play a crucial role in the patterning of the limb autopod. Development 122, 2997-3011.
Fukuda, N., Saitoh, M., Kobayashi, N., Miyazono, K., 2006. Execution of BMP-4-induced apoptosis by p53-dependent ER dysfunction in myeloma and B-cell hybridoma cells. Oncogene 25, 3509-3517.
Ganan, Y., Macias, D., Duterque-Coquillaud, M., Ros, M.A., Hurle, J.M., 1996. Role of TGF beta s and BMPs as signals controlling the position of the digits and the areas of interdigital cell death in the developing chick limb autopod. Development 122, 2349-2357.
Goldring, M.B., 2012. Chondrogenesis, chondrocyte differentiation, and articular cartilage metabolism in health and osteoarthritis. Therapeutic Advances in Musculoskeletal Disease 4, 269-285.
Gros, J., Hu, J.K.-H., Vinegoni, C., Feruglio, P.F., Weissleder, R., Tabin, C.J., 2010a. WNT5A/JNK and FGF/MAPK Pathways Regulate the Cellular Events Shaping the Vertebrate Limb Bud. Current Biology 20, 1993-2002.
Gros, J., Hu, J.K., Vinegoni, C., Feruglio, P.F., Weissleder, R., Tabin, C.J., 2010b. WNT5A/JNK and FGF/MAPK pathways regulate the cellular events shaping the vertebrate limb bud. Current biology : CB 20, 1993-2002.
Harfe, B.D., Scherz, P.J., Nissim, S., Tian, H., McMahon, A.P., Tabin, C.J., 2004. Evidence for an Expansion-Based Temporal Shh Gradient in Specifying Vertebrate Digit Identities. Cell 118, 517-528.
Hay, E., Lemonnier, J., Fromigue, O., Marie, P.J., 2001. Bone morphogenetic protein-2 promotes osteoblast apoptosis through a Smad-independent, protein kinase C-dependent signaling pathway. J Biol Chem 276, 29028-29036.
Hendzel, M.J., Wei, Y., Mancini, M.A., Van Hooser, A., Ranalli, T., Brinkley, B.R., Bazett-Jones, D.P., Allis, C.D., 1997. Mitosis-specific phosphorylation of histone H3 initiates primarily within pericentromeric heterochromatin during G2 and spreads in an ordered fashion coincident with mitotic chromosome condensation. Chromosoma 106, 348-360.
Hsu, D.R., Economides, A.N., Wang, X., Eimon, P.M., Harland, R.M., 1998. The Xenopus Dorsalizing Factor Gremlin Identifies a Novel Family of Secreted Proteins that Antagonize BMP Activities. Molecular Cell 1, 673-683.
Kaltcheva, M.M., Anderson, M.J., Harfe, B.D., Lewandoski, M., 2016. BMPs are direct triggers of interdigital programmed cell death. Developmental biology.
Kawakami, Y., Rodríguez-León, J., Koth, C.M., Büscher, D., Itoh, T., Raya, Á., Ng, J.K., Esteban, C.R., Takahashi, S., Henrique, D., Schwarz, M.-F., Asahara, H., Izpisúa Belmonte, J.C., 2003. MKP3 mediates the cellular response to FGF8 signalling in the vertebrate limb. Nature Cell Biology 5, 513-519.
Kendall, S.E., Battelli, C., Irwin, S., Mitchell, J.G., Glackin, C.A., Verdi, J.M., 2005. NRAGE Mediates p38 Activation and Neural Progenitor Apoptosis via the Bone Morphogenetic Protein Signaling Cascade. Molecular and Cellular Biology 25, 7711-7724.

Khokha, M.K., Hsu, D., Brunet, L.J., Dionne, M.S., Harland, R.M., 2003. Gremlin is the BMP antagonist required for maintenance of Shh and Fgf signals during limb patterning. Nature Genetics 34, 303-307.
Kim, S., Günesdogan, U., Zylicz, Jan J., Hackett, Jamie A., Cougot, D., Bao, S., Lee, C., Dietmann, S., Allen, George E., Sengupta, R., Surani, M.A., 2014. PRMT5 Protects Genomic Integrity during Global DNA Demethylation in Primordial Germ Cells and Preimplantation Embryos. Molecular Cell 56, 564-579.
Kimura, N., Matsuo, R., Shibuya, H., Nakashima, K., Taga, T., 2000. BMP2-induced apoptosis is mediated by activation of the TAK1-p38 kinase pathway that is negatively regulated by Smad6. J Biol Chem 275, 17647-17652.
Kimura, S., Shiota, K., 1996. Sequential changes of programmed cell death in developing fetal mouse limbs and its possible roles in limb morphogenesis. Journal of Morphology 229, 337-346.
Kondo, A., Tokuda, H., Matsushima-Nishiwaki, R., Kuroyanagi, G., Yamamoto, N., Mizutani, J., Kozawa, O., Otsuka, T., 2014. Rho-kinase limits BMP-4-stimulated osteocalcin synthesis in osteoblasts: regulation of the p38 MAP kinase pathway. Life sciences 96, 18-25.
Kraus, P., Fraidenraich, D., Loomis, C.A., 2001. Some distal limb structures develop in mice lacking Sonic hedgehog signalling. Mech. Dev. 100, 45-58.
Kua, H.Y., Liu, H., Leong, W.F., Li, L., Jia, D., Ma, G., Hu, Y., Wang, X., Chau, J.F., Chen, Y.G., Mishina, Y., Boast, S., Yeh, J., Xia, L., Chen, G.Q., He, L., Goff, S.P., Li, B., 2012. c-Abl promotes osteoblast expansion by differentially regulating canonical and non-canonical BMP pathways and p16INK4a expression. Nat Cell Biol 14, 727-737.
Kuroyanagi, G., Tokuda, H., Yamamoto, N., Matsushima-Nishiwaki, R., Mizutani, J., Kozawa, O., Otsuka, T., 2015. Resveratrol amplifies BMP-4-stimulated osteoprotegerin synthesis via p38 MAP kinase in osteoblasts. Molecular medicine reports 12, 3849-3854.
Kuss, P., Villavicencio-Lorini, P., Witte, F., Klose, J., Albrecht, A.N., Seemann, P., Hecht, J., Mundlos, S., 2008. Mutant Hoxd13 induces extra digits in a mouse model of synpolydactyly directly and by decreasing retinoic acid synthesis. Journal of Clinical Investigation.
Lafont, J.E., Poujade, F.A., Pasdeloup, M., Neyret, P., Mallein-Gerin, F., 2015. Hypoxia potentiates the BMP-2 driven COL2A1 stimulation in human articular chondrocytes via p38 MAPK. Osteoarthritis and cartilage / OARS, Osteoarthritis Research Society.
Lallemand, Y., 2005. Analysis of Msx1; Msx2 double mutants reveals multiple roles for Msx genes in limb development. Development 132, 3003-3014.
Lallemand, Y., Nicola, M.A., Ramos, C., Bach, A., Clement, C.S., Robert, B., 2005. Analysis of Msx1; Msx2 double mutants reveals multiple roles for Msx genes in limb development. Development 132, 3003-3014.
Lee, J., Bedford, M.T., 2002. PABP1 identified as an arginine methyltransferase substrate using high-density protein arrays. EMBO reports 3, 268-273.
Lefebvre, V., Smits, P., 2005. Transcriptional control of chondrocyte fate and differentiation. Birth defects research. Part C, Embryo today : reviews 75, 200-212.

Lehmann, K., Seemann, P., Silan, F., Goecke, T.O., Irgang, S., Kjaer, K.W., Kjaergaard, S., Mahoney, M.J., Morlot, S., Reissner, C., Kerr, B., Wilkie, A.O., Mundlos, S., 2007. A new subtype of brachydactyly type B caused by point mutations in the bone morphogenetic protein antagonist NOGGIN. Am J Hum Genet 81, 388-396.
Lehmann, K., Seemann, P., Stricker, S., Sammar, M., Meyer, B., Suring, K., Majewski, F., Tinschert, S., Grzeschik, K.H., Muller, D., Knaus, P., Nurnberg, P., Mundlos, S., 2003. Mutations in bone morphogenetic protein receptor 1B cause brachydactyly type A2. Proc Natl Acad Sci U S A 100, 12277-12282.
Lewandoski, M., Sun, X., Martin, G.R., 2000. Fgf8 signalling from the AER is essential for normal limb development. Nature genetics 26, 460-463.
Lewandowski, J.P., Pursell, T.A., Rabinowitz, A.H., Vokes, S.A., 2014. Manipulating gene expression and signaling activity in cultured mouse limb bud cells. Developmental Dynamics 243, 928-936.
Li, Q., Lewandowski, J.P., Powell, M.B., Norrie, J.L., Cho, S.H., Vokes, S.A., 2014. A Gli silencer is required for robust repression of gremlin in the vertebrate limb bud. Development 141, 1906-1914.
Litingtung, Y., Dahn, R.D., Li, Y., Fallon, J.F., Chiang, C., 2002. Shh and Gli3 are dispensable for limb skeleton formation but regulate digit number and identity. Nature 418, 979-983.
Liu, F., Cheng, G., Hamard, P.-J., Greenblatt, S., Wang, L., Man, N., Perna, F., Xu, H., Tadi, M., Luciani, L., Nimer, S.D., 2015. Arginine methyltransferase PRMT5 is essential for sustaining normal adult hematopoiesis. Journal of Clinical Investigation 125, 3532-3544.
Livak, K.J., Schmittgen, T.D., 2001. Analysis of Relative Gene Expression Data Using Real-Time Quantitative PCR and the $2^{-\Delta\Delta CT}$ Method. Methods 25, 402-408.
Ljosa, V., Carpenter, A.E., 2009. Introduction to the Quantitative Analysis of Two-Dimensional Fluorescence Microscopy Images for Cell-Based Screening. PLoS Computational Biology 5, e1000603-e1000603.
Lo, R.S., Wotton, D., Massague, J., 2001. Epidermal growth factor signaling via Ras controls the Smad transcriptional co-repressor TGIF. The EMBO journal 20, 128-136.
Logan, M., Martin, J.F., Nagy, A., Lobe, C., Olson, E.N., Tabin, C.J., 2002. Expression of Cre Recombinase in the developing mouse limb bud driven by a Prxl enhancer. Genesis 33, 77-80.
Lopez-Rios, J., Speziale, D., Robay, D., Scotti, M., Osterwalder, M., Nusspaumer, G., Galli, A., Holländer, Georg A., Kmita, M., Zeller, R., 2012. GLI3 Constrains Digit Number by Controlling Both Progenitor Proliferation and BMP-Dependent Exit to Chondrogenesis. Developmental Cell 22, 837-848.
Lu, P., 2006. Increasing Fgf4 expression in the mouse limb bud causes polysyndactyly and rescues the skeletal defects that result from loss of Fgf8 function. Development 133, 33-42.
Macias, D., Ganan, Y., Sampath, T.K., Piedra, M.E., Ros, M.A., Hurle, J.M., 1997. Role of BMP-2 and OP-1 (BMP-7) in programmed cell death and skeletogenesis during chick limb development. Development 124, 1109-1117.

Mariani, F.V., Ahn, C.P., Martin, G.R., 2008. Genetic evidence that FGFs have an instructive role in limb proximal–distal patterning. Nature 453, 401-405.
Martin, G.R., 1998. The roles of FGFs in the early development of vertebrate limbs. Genes Dev. 12, 1571-1586.
Martin, J.F., Olson, E.N., 2000. Identification of a prx1 limb enhancer. Genesis 26, 225-229.
Meister, G., Fischer, U., 2002. Assisted RNP assembly: SMN and PRMT5 complexes cooperate in the formation of spliceosomal UsnRNPs. Embo j 21, 5853-5863.
Merino, R., Ganan, Y., Macias, D., Rodriguez-Leon, J., Hurle, J.M., 1999a. Bone morphogenetic proteins regulate interdigital cell death in the avian embryo. Annals of the New York Academy of Sciences 887, 120-132.
Merino, R., Macias, D., Ganan, Y., Economides, A.N., Wang, X., Wu, Q., Stahl, N., Sampath, K.T., Varona, P., Hurle, J.M., 1999b. Expression and function of Gdf-5 during digit skeletogenesis in the embryonic chick leg bud. Dev Biol 206, 33-45.
Michos, O., Panman, L., Vintersten, K., Beier, K., Zeller, R., Zuniga, A., 2004. Gremlin-mediated BMP antagonism induces the epithelial-mesenchymal feedback signaling controlling metanephric kidney and limb organogenesis. Development 131, 3401-3410.
Milaire, J., Rooze, M., 1983. Hereditary and induced modifications of the normal necrotic patterns in the developing limb buds of the rat and mouse: Facts and hypotheses, pp. 459-490.
Minowada, G., Jarvis, L.A., Chi, C.L., Neubuser, A., Sun, X., Hacohen, N., Krasnow, M.A., Martin, G.R., 1999a. Vertebrate Sprouty genes are induced by FGF signaling and can cause chondrodysplasia when overexpressed. Development 126, 4465-4475.
Minowada, G., Jarvis, L.A., Chi, C.L., Neubüser, A., Sun, X., Hacohen, N., Krasnow, M.A., Martin, G.R., 1999b. Vertebrate Sprouty genes are induced by FGF signaling and can cause chondrodysplasia when overexpressed. Development (Cambridge, England) 126, 4465-4475.
Nagamatsu, G., Kosaka, T., Kawasumi, M., Kinoshita, T., Takubo, K., Akiyama, H., Sudo, T., Kobayashi, T., Oya, M., Suda, T., 2011. A germ cell-specific gene, Prmt5, works in somatic cell reprogramming. The Journal of biological chemistry 286, 10641-10648.
Neuenkirchen, N., Englbrecht, C., Ohmer, J., Ziegenhals, T., Chari, A., Fischer, U., 2015. Reconstitution of the human U snRNP assembly machinery reveals stepwise Sm protein organization. The EMBO Journal 34, 1925-1941.
Nguyen, M.-T., Zhu, J., Nakamura, E., Bao, X., Mackem, S., 2009. Tamoxifen-dependent, inducible Hoxb6CreERT recombinase function in lateral plate and limb mesoderm, CNS isthmic organizer, posterior trunk neural crest, hindgut, and tailbud. Developmental Dynamics 238, 467-474.
Norrie, J.L., Lewandowski, J.P., Bouldin, C.M., Amarnath, S., Li, Q., Vokes, M.S., Ehrlich, L.I., Harfe, B.D., Vokes, S.A., 2014. Dynamics of BMP signaling in limb bud mesenchyme and polydactyly. Dev Biol 393, 270-281.
Oh, C.-d., Maity, S.N., Lu, J.-F., Zhang, J., Liang, S., Coustry, F., de Crombrugghe, B., Yasuda, H., 2010. Identification of SOX9 Interaction Sites in the Genome of Chondrocytes. PLoS ONE 5, e10113-e10113.

Ovchinnikov, D.A., Selever, J., Wang, Y., Chen, Y.-T., Mishina, Y., Martin, J.F., Behringer, R.R., 2006. BMP receptor type IA in limb bud mesenchyme regulates distal outgrowth and patterning. Developmental Biology 295, 103-115.
Pajni-Underwood, S., Wilson, C.P., Elder, C., Mishina, Y., Lewandoski, M., 2007. BMP signals control limb bud interdigital programmed cell death by regulating FGF signaling. Development 134, 2359-2368.
Pal, S., Baiocchi, R.A., Byrd, J.C., Grever, M.R., Jacob, S.T., Sif, S., 2007. Low levels of miR-92b/96 induce PRMT5 translation and H3R8/H4R3 methylation in mantle cell lymphoma. Embo j 26, 3558-3569.
Pelz, J.-P., Schindelin, H., van Pee, K., Kuper, J., Kisker, C., Diederichs, K., Fischer, U., Grimm, C., 2015. Crystallizing the 6S and 8S spliceosomal assembly intermediates: a complex project. Acta Crystallographica Section D Biological Crystallography 71, 2040-2053.
Perez, W.D., Weller, C.R., Shou, S., Stadler, H.S., 2010. Survival of Hoxa13 homozygous mutants reveals a novel role in digit patterning and appendicular skeletal development. Developmental Dynamics 239, 446-457.
Pignatti, E., Zeller, R., Zuniga, A., 2014. To BMP or not to BMP during vertebrate limb bud development. Seminars in cell & developmental biology 32, 119-127.
Pizette, S., Abate-Shen, C., Niswander, L., 2001. BMP controls proximodistal outgrowth, via induction of the apical ectodermal ridge, and dorsoventral patterning in the vertebrate limb. Development (Cambridge, England) 128, 4463-4474.
Pizette, S., Niswander, L., 1999. BMPs negatively regulate structure and function of the limb apical ectodermal ridge. Development.
Pizette, S., Niswander, L., 2000. BMPs are required at two steps of limb chondrogenesis: formation of prechondrogenic condensations and their differentiation into chondrocytes. Dev Biol 219, 237-249.
Ploger, F., Seemann, P., Schmidt-von Kegler, M., Lehmann, K., Seidel, J., Kjaer, K.W., Pohl, J., Mundlos, S., 2008. Brachydactyly type A2 associated with a defect in proGDF5 processing. Human molecular genetics 17, 1222-1233.
Rabinowitz, A.H., Vokes, S.A., 2012. Integration of the transcriptional networks regulating limb morphogenesis. Developmental Biology 368, 165-180.
Robert, B., 2007. Bone morphogenetic protein signaling in limb outgrowth and patterning. Dev Growth Differ 49, 455-468.
Robertson, E.J., Charatsi, I., Joyner, C.J., Koonce, C.H., Morgan, M., Islam, A., Paterson, C., Lejsek, E., Arnold, S.J., Kallies, A., Nutt, S.L., Bikoff, E.K., 2007. Blimp1 regulates development of the posterior forelimb, caudal pharyngeal arches, heart and sensory vibrissae in mice. Development 134, 4335-4345.
Rosello-Diez, A., Arques, C.G., Delgado, I., Giovinazzo, G., Torres, M., 2014. Diffusible signals and epigenetic timing cooperate in late proximo-distal limb patterning. Development 141, 1534-1543.
Rowe, D.A., Fallon, J.F., 1982. The proximodistal determination of skeletal parts in the developing chick leg. J. Embryol. Exp. Morphol. 68, 1-7.

RStudioTeam, 2015. RStudio: Integrated Development for R., RStudio, Inc.,Boston, MA URL http://www.rstudio.com/.
Saha, K., Adhikary, G., Eckert, R.L., 2016. MEP50/PRMT5 Reduces Gene Expression by Histone Arginine Methylation and this Is Reversed by PKCδ/p38δ Signaling. The Journal of investigative dermatology 136, 214-224.
Sapkota, G., Alarcon, C., Spagnoli, F.M., Brivanlou, A.H., Massague, J., 2007. Balancing BMP signaling through integrated inputs into the Smad1 linker. Mol Cell 25, 441-454.
Sekiya, I., 2000. SOX9 Enhances Aggrecan Gene Promoter/Enhancer Activity and Is Up-regulated by Retinoic Acid in a Cartilage-derived Cell Line, TC6. Journal of Biological Chemistry 275, 10738-10744.
Selever, J., Liu, W., Lu, M.-F., Behringer, R.R., Martin, J.F., 2004. Bmp4 in limb bud mesoderm regulates digit pattern by controlling AER development. Developmental Biology 276, 268-279.
Sheth, R., Marcon, L., Bastida, M.F., Junco, M., Quintana, L., Dahn, R., Kmita, M., Sharpe, J., Ros, M.A., 2012. Hox Genes Regulate Digit Patterning by Controlling the Wavelength of a Turing-Type Mechanism. Science 338, 1476-1480.
Shubin, N.H., Alberch, P., 1986. A Morphogenetic Approach to the Origin and Basic Organization of the Tetrapod Limb, in: Hecht, M.K., Wallace, B., Prance, G.T. (Eds.), Evolutionary Biology: Volume 20. Springer US, Boston, MA, pp. 319-387.
Srinivas, S., Watanabe, T., Lin, C.S., William, C.M., Tanabe, Y., Jessell, T.M., Costantini, F., 2001. Cre reporter strains produced by targeted insertion of EYFP and ECFP into the ROSA26 locus. BMC developmental biology 1, 4-4.
St-Jacques, B., Hammerschmidt, M., McMahon, A.P., 1999. Indian hedgehog signaling regulates proliferation and differentiation of chondrocytes and is essential for bone formation. Genes Dev 13, 2072-2086.
Stadler, H.S., Higgins, K.M., Capecchi, M.R., 2001. Loss of Eph-receptor expression correlates with loss of cell adhesion and chondrogenic capacity in Hoxa13 mutant limbs. Development (Cambridge, England) 128, 4177-4188.
Stark, R.J., Searls, R.L., 1973. A description of chick wing bud development and a model of limb morphogenesis. Dev Biol 33, 138-153.
Stopa, N., Krebs, J.E., Shechter, D., 2015. The PRMT5 arginine methyltransferase: many roles in development, cancer and beyond. Cellular and molecular life sciences : CMLS 72, 2041-2059.
Storey, J.D., Tibshirani, R., 2003. Statistical significance for genomewide studies. Proc Natl Acad Sci U S A 100, 9440-9445.
Storm, E.E., Kingsley, D.M., 1999. GDF5 coordinates bone and joint formation during digit development. Dev Biol 209, 11-27.
Sun, X., Mariani, F.V., Martin, G.R., 2002. Functions of FGF signalling from the apical ectodermal ridge in limb development. Nature 418, 501-508.
Suzuki, T., Hasso, S.M., Fallon, J.F., 2008. Unique SMAD1/5/8 activity at the phalanx-forming region determines digit identity. Proceedings of the National Academy of Sciences of the United States of America 105, 4185-4190.

Swiatek, P.J., Gridley, T., 1993. Perinatal lethality and defects in hindbrain development in mice homozygous for a targeted mutation of the zinc finger gene Krox20. Genes & Development 7, 2071-2084.
Tarighat, S.S., Santhanam, R., Frankhouser, D., Radomska, H.S., Lai, H., Anghelina, M., Wang, H., Huang, X., Alinari, L., Walker, A., Caligiuri, M.A., Croce, C.M., Li, L., Garzon, R., Li, C., Baiocchi, R.A., Marcucci, G., 2015. The dual epigenetic role of PRMT5 in acute myeloid leukemia: gene activation and repression via histone arginine methylation. Leukemia.
te Welscher, P., 2002. Progression of Vertebrate Limb Development Through SHH-Mediated Counteraction of GLI3. Science 298, 827-830.
Tee, W.W., Pardo, M., Theunissen, T.W., Yu, L., Choudhary, J.S., Hajkova, P., Surani, M.A., 2010. Prmt5 is essential for early mouse development and acts in the cytoplasm to maintain ES cell pluripotency. Genes & Development 24, 2772-2777.
ten Berge, D., Brugmann, S.A., Helms, J.A., Nusse, R., 2008. Wnt and FGF signals interact to coordinate growth with cell fate specification during limb development. Development 135, 3247-3257.
Thorogood, P.V., Hinchliffe, J.R., 1975. An analysis of the condensation process during chondrogenesis in the embryonic chick hind limb. Journal of embryology and experimental morphology 33, 581-606.
Tian, X.Y., Yung, L.H., Wong, W.T., Liu, J., Leung, F.P., Liu, L., Chen, Y., Kong, S.K., Kwan, K.M., Ng, S.M., Lai, P.B., Yung, L.M., Yao, X., Huang, Y., 2012. Bone morphogenic protein-4 induces endothelial cell apoptosis through oxidative stress-dependent p38MAPK and JNK pathway. Journal of molecular and cellular cardiology 52, 237-244.
Towers, M., Mahood, R., Yin, Y., Tickle, C., 2008. Integration of growth and specification in chick wing digit-patterning. Nature 452, 882-886.
Trapnell, C., Roberts, A., Goff, L., Pertea, G., Kim, D., Kelley, D.R., Pimentel, H., Salzberg, S.L., Rinn, J.L., Pachter, L., 2012. Differential gene and transcript expression analysis of RNA-seq experiments with TopHat and Cufflinks. Nature protocols 7, 562-578.
Vargesson, N., Kostakopoulou, K., Drossopoulou, G., Papageorgiou, S., Tickle, C., 2001. Characterisation ofHoxa gene expression in the chick limb bud in response to FGF. Developmental Dynamics 220, 87-90.
Ventura, A., Kirsch, D.G., McLaughlin, M.E., Tuveson, D.A., Grimm, J., Lintault, L., Newman, J., Reczek, E.E., Weissleder, R., Jacks, T., 2007. Restoration of p53 function leads to tumour regression in vivo. Nature 445, 661-665.
Verheyden, J.M., 2005. Conditional inactivation of Fgfr1 in mouse defines its role in limb bud establishment, outgrowth and digit patterning. Development 132, 4235-4245.
Verheyden, J.M., Sun, X., 2008. An Fgf/Gremlin inhibitory feedback loop triggers termination of limb bud outgrowth. Nature 454, 638-641.
Vokes, S.A., Ji, H., Wong, W.H., McMahon, A.P., 2008. A genome-scale analysis of the cis-regulatory circuitry underlying sonic hedgehog-mediated patterning of the mammalian limb. Genes & Development 22, 2651-2663.

Wang, J., Duncan, D., Shi, Z., Zhang, B., 2013. WEB-based GEne SeT AnaLysis Toolkit (WebGestalt): update 2013. Nucleic Acids Research 41, W77-W83.
Wang, Y., Li, Q., Liu, C., Han, F., Chen, M., Zhang, L., Cui, X., Qin, Y., Bao, S., Gao, F., 2015a. Protein arginine methyltransferase 5 (Prmt5) is required for germ cell survival during mouse embryonic development. Biology of reproduction 92, 104-104.
Wang, Y., Zhu, T., Li, Q., Liu, C., Han, F., Chen, M., Zhang, L., Cui, X., Qin, Y., Bao, S., Gao, F., 2015b. Prmt5 is required for germ cell survival during spermatogenesis in mice. Scientific Reports 5, 11031-11031.
Witte, F., Chan, D., Economides, A.N., Mundlos, S., Stricker, S., 2010. Receptor tyrosine kinase-like orphan receptor 2 (ROR2) and Indian hedgehog regulate digit outgrowth mediated by the phalanx-forming region. Proc Natl Acad Sci U S A 107, 14211-14216.
Worthley, D.L., Churchill, M., Compton, J.T., Tailor, Y., Rao, M., Si, Y., Levin, D., Schwartz, M.G., Uygur, A., Hayakawa, Y., Gross, S., Renz, B.W., Setlik, W., Martinez, A.N., Chen, X., Nizami, S., Lee, H.G., Kang, H.P., Caldwell, J.M., Asfaha, S., Westphalen, C.B., Graham, T., Jin, G., Nagar, K., Wang, H., Kheirbek, M.A., Kolhe, A., Carpenter, J., Glaire, M., Nair, A., Renders, S., Manieri, N., Muthupalani, S., Fox, J.G., Reichert, M., Giraud, A.S., Schwabe, R.F., Pradere, J.P., Walton, K., Prakash, A., Gumucio, D., Rustgi, A.K., Stappenbeck, T.S., Friedman, R.A., Gershon, M.D., Sims, P., Grikscheit, T., Lee, F.Y., Karsenty, G., Mukherjee, S., Wang, T.C., 2015. Gremlin 1 identifies a skeletal stem cell with bone, cartilage, and reticular stromal potential. Cell 160, 269-284.
Wright, E., 1995. The Sry-related gene Sox9 is expressed during chondrogenesis in mouse embryos. Nature Genet. 9, 15-20.
Wyngaarden, L.A., Vogeli, K.M., Ciruna, B.G., Wells, M., Hadjantonakis, A.K., Hopyan, S., 2010. Oriented cell motility and division underlie early limb bud morphogenesis. Development 137, 2551-2558.
Yamaguchi, T.P., Bradley, A., McMahon, A.P., Jones, S., 1999. A Wnt5a pathway underlies outgrowth of multiple structures in the vertebrate embryo. Development 126, 1211-1223.
Yang, Y., Topol, L., Lee, H., Wu, J., 2003. Wnt5a and Wnt5b exhibit distinct activities in coordinating chondrocyte proliferation and differentiation. Development 130, 1003-1015.
Yoon, B.S., Lyons, K.M., 2004. Multiple functions of BMPs in chondrogenesis. Journal of Cellular Biochemistry 93, 93-103.
Zhang, B., Dong, S., Zhu, R., Hu, C., Hou, J., Li, Y., Zhao, Q., Shao, X., Bu, Q., Li, H., Wu, Y., Cen, X., Zhao, Y., 2015a. Targeting protein arginine methyltransferase 5 inhibits colorectal cancer growth by decreasing arginine methylation of eIF4E and FGFR3. Oncotarget 6, 22799-22811.
Zhang, T., Günther, S., Looso, M., Künne, C., Krüger, M., Kim, J., Zhou, Y., Braun, T., 2015b. Prmt5 is a regulator of muscle stem cell expansion in adult mice. Nature Communications 6, 7140-7140.
Zhao, Q., Rank, G., Tan, Y.T., Li, H., Moritz, R.L., Simpson, R.J., Cerruti, L., Curtis, D.J., Patel, D.J., Allis, C.D., Cunningham, J.M., Jane, S.M., 2009. PRMT5-mediated methylation of histone H4R3 recruits DNMT3A, coupling histone and DNA methylation in gene silencing. Nature Structural & Molecular Biology 16, 304-311.

Zhu, J., Nakamura, E., Nguyen, M.-T., Bao, X., Akiyama, H., Mackem, S., 2008. Uncoupling Sonic Hedgehog Control of Pattern and Expansion of the Developing Limb Bud. Developmental Cell 14, 624-632.